Problem Description

In managed pressure drilling (MPD) operations, the well is sealed and mud pressure is controlled by opening/closing the valve that releases the mud at the top of the well. This technology has proven successful when drilling from stationary platforms. Managed Pressure Drilling from floaters brings about several challenges. In normal drilling, heave motion of the floater (due to waves) is compensated by the draw-works and the drill string is not affected by heave. During drill string connection, however, the drill string is disconnected from the draw-works and gets rigidly attached to the floater. Thus the drill string follows the heave motion of the floater thus moving back and forth in the well and acting like a piston. This generates large pressure fluctuations, which can damage the well. These pressure fluctuations must therefore be fully or at least partly compensated by active control of the top-side choke. Previous attempts to achieve such compensation, although successful in simulations, failed in full scale tests.

Objective

The objective of this project is to study the problem of Managed Pressure Drilling with respect to active compensation of pressure fluctuations due to heave. The project has the following sub goals:

1) Develop a model for well hydraulics that sufficiently accurately models the effect of the heave motion of the drill string. The accuracy of the model should be evaluated against relevant data from Ullrigg tests. The use of model reduction techniques to establish accuracy bounds on lower order models should be explored.

2) Develop control algorithms for active compensation of the heave-induced pressure fluctuations with top-side choke. Evaluate various control strategies: feed forward-based compensation; control algorithms taking into account delays in pressure distribution along the well; control algorithms based on the output regulation theory. Drawbacks and benefits of these control strategies should be analyzed.

3) Analyze the heave compensation tests data from Ullrigg tests in 2009. Propose explanations on the failure of heave compensation algorithms in these tests. Possible effects of the following issues should be analyzed among other possible causes: insufficient modeling / inappropriate control strategy, communication delays, low sampling frequency, hardware limitations (rate limitation of the choke), parasitic effects in the choke (backlash and friction). The analysis should be supported with simulations. Propose necessary modifications of the hardware / control system that would solve the problem.

The modeling part should be based on the results of the fall project “Advanced Modeling for Managed Pressure Drilling”. All necessary parameters for simulations and experimental data are available from the industrial partner. At the end of the project, the candidate should submit a comprehensive report covering all stages of the work and a well commented MATLAB code for simulations and data analysis.

Preface

This master's thesis was given in the spring of 2011 by the Department of Engineering Cybernetics at NTNU in cooperation with the intelligent drilling group at Statoil ASA R&D as a part of the M.Sc. program in engineering cybernetics. It is a continuation of my project work in the fall of 2010 on advanced modeling for managed pressure drilling (MPD). This project resulted in a mathematical model of the flow and pressure distribution in a drilling fluid used in the drilling of a well, and an implementation in a MATLAB simulator program for drilling operations covering both basic, but also more advanced scenarios during drilling. Using the knowledge gained from that work, the goal for this master's thesis was to shift the focus onto control of pressure fluctuations during some challenging scenarios related to heave motion.

I would like to take this opportunity to thank my supervisors: Ole Morten Aamo has been my supervisor at the university and has offered great advice on a day-to-day basis as well as encouraging and facilitating me to go in the direction I wanted. Alexey Pavlov and Glenn-Ole Kaasa have been my supervisors from Statoil and have taken the time to come see me in Trondheim as well as guiding me through extensive electronic correspondence. Statoil also provided me with substantial data from experiments made with an existing MPD control system. In addition, I would like to thank Hessam Mahdianfar, PhD candidate at the Department of Engineering Cybernetics, NTNU, who has been a great contributor to writing one of the conference papers. Also, Gerhard Niggard and Lars Shem at the International Research Institute of Stavanger have been very helpful in providing access and guidance to their drilling simulator "IRIS Drill for MATLAB". My gratitude to you all.

At last, but by absolutely no measure least, I would never have made it this far without the love and support of my family and friends. I will hopefully always remain a student, but the submission of this master thesis represents for me the culmination of a continuous education for almost the last two decades. So, the most deeply felt appreciation goes out to my parents who have always inspired me to strive for my potential and my sister who was quick to protect me when I did not. I have also been blessed with true friends, some have been with me for a long time and some are more recent, but certainly, they have all been there on both rainy and sunny days. This last year has also seen me blessed with a remarkable and supportive woman in my life: From now on, you are my inspiration Cecilie.

Ingar Skyberg Landet
Trondheim, June 2011

Abstract

Managed pressure drilling is a sophisticated pressure control method which is intended to meet increasingly high demands in drilling operations in the oil and gas industry. With this method, the well is pressurized and the drilling mud is released through a control choke which can be used to actively control/reject pressure variations. Such a control system needs to handle several disturbances, and in particular, vertical motion of the drill string causes severe pressure variations that need to be compensated by active use of the control choke. In this thesis we first analyze data from previous experiments with an existing control strategy and show that the main reason for the poor disturbance rejection is due to a control strategy based on an insufficient model of the pressure fluctuations, although practical issues like sampling time and choke friction also played a part. Then, we present several different control strategies for regulation of both top side and bottom hole pressures based on more detailed models of the well pressure dynamics. All controllers are tested in simulations and it is shown that either an output regulation controller or a controller based on the internal model principle will achieve satisfactory disturbance rejection. Lastly, some of these controllers are also tested on a high fidelity drilling simulator from IRIS, and a pressure regulation within $\pm 0.5\,bar$ is achieved for the choke pressure, and $\pm 1.5\,bar$ for the bottom hole pressure.

Contents

List of Figures

Chapter 1

Background

1.1 Motivation and Introduction to Drilling

1.1.1 Pressure Control

> "This is probably the biggest environmental disaster we have ever faced in this country. It is certainly the biggest oil spill and we are responding with the biggest environmental response."

Carol Browner, Ba rack IBM's adviser on energy and climate on the Deep water Horizon oil spill.

The ever growing human need for oil and gas to produce energy has the potential to create some of the most dire and disturbing environmental disasters ever seen. However, this is still an enormous business with exploration and drilling efforts ranging into hundreds of billions of dollars each year in the United States alone.[1] Thus, researchers and scientists need to ensure that technological advances continue to reduce the risks (and lower the costs) associated with hydrocarbon recovery. One of the important features of the safety during drilling operations is the pressure control in the well. In drilling operations, a drilling fluid called mud is pumped into the drill string and flows through the drill bit in the bottom hole of the well. (See Figure 1.1) This mud cools down the drill bit before it flows up the well annulus carrying cuttings out of the well and also works to keep the pressure in the annulus at a desired level. This pressure control is crucial in all drilling operations, as the pressure has to lie between certain boundaries. Specifically, it has to be above the pore pressure to prevent unwanted influx from the surrounding formations into the well. Also, it has to be below the fracture pressure of the surrounding formations to prevent the well from fracturing. Another issue is the possibility of the well to collapse on itself if the pressure becomes too low. All of these issues would result in costly and time consuming repair or loss of mud or, in the worst case, great environmental damage.

Conventionally this control is done by circulating in new mud with different density whenever the pressure needs to be changed, i.e. when the drilling reaches into an area with different pore or fracture pressures. This is however a very slow process. To show a numerical example, suppose the well is 2 km long, has a cross section area

[1] Data from American Petroleum Institute survey 2007.

of $0.01m^2$ and the flow rate is $1000\frac{l}{min}$. Then the propagation speed of the new mud is $1.67\frac{m}{s}$, and the change of mud will last in total close to 40 minutes. Also, this is not a very flexible and robust way to control pressure since it cannot respond to any external influences or disturbances. Thus, there is great room for improvement in making an automatic control system that actively uses the control choke and the two pumps to control the pressure quicker, more sophisticated and more accurate. This would also allow the drilling of wells that were earlier not possible due to narrow pressure margins.

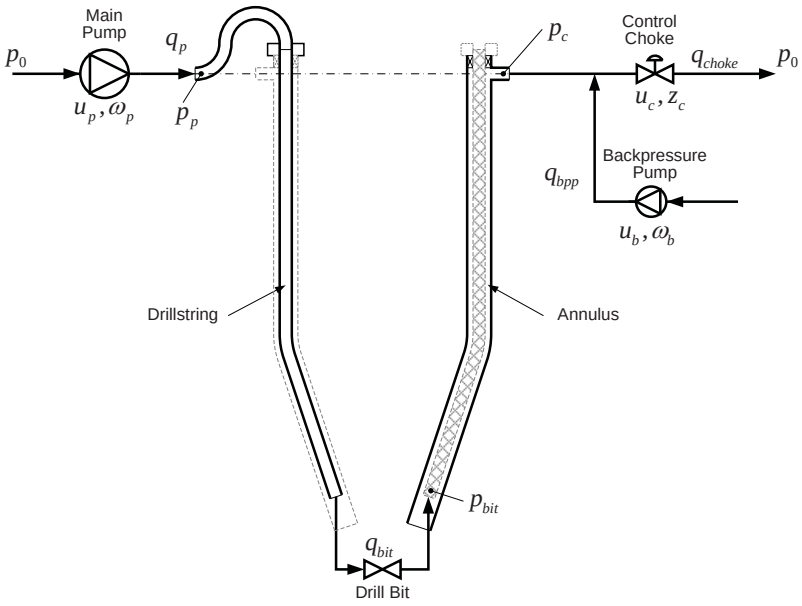

Figure 1.1: Schematic representation of drilling set up.

1.1.2 Heave Motion

> "Can ye fathom the ocean, dark and deep, where the mighty waves and the grandeur sweep?"
>
> Fanny Crosby

One of the scenarios that has proven challenging when trying to develop such a managed pressure drilling system is the situation when drilling from a floating rig. In this case, waves will affect the entire rig causing it to move vertically, so called heave motion. For most of the time spent drilling, this motion will not have a large effect on the pressure in the well, because of other heave compensation techniques decoupling the drill string from the heave motion. However, from time to time it is necessary to extend the drill string by a drill string connection, and in this case the drill string is rigidly connected to the floating vessel. This will in turn lead to the drill string acting like a piston down into the well, causing relatively large pressure fluctuations.

An attempt at making an automatic control system for this scenario was done by the Statoil research group, using a simple model of the drill string hydraulics

for controller design. This worked well in simulations, but failed in full scale testing, making it necessary to analyze these tests to find out why it failed, as well as propose improved control strategies for this challenging scenario.

1.1.3 Other Work on Managed Pressure Drilling

It seems that MPD is creating some interest, and a number of different papers have been published. Quite a lot of effort has been put into the issue of estimating the bottom hole pressure [2]. This is mostly done by using a low order model of the pressure dynamics together with the available measurements of choke and main pump pressures and adapting to unknown coefficients in the system. Recently, (maybe with reference to the Deep water Horizon accident) there has also been interest in the issue of gas kicks [3, 4], both modeling of the gas travel and control of the pressure changes. Further, one can find a few different approaches to the pressure control during more "normal" operations, with various adaptive techniques [5, 6], as well as model predictive control strategies [7]. Also, some implementational issues have been considered [8, 9], and some results from actual use of such a system can also be found [10]. However, not a lot of work has been done on the issue of rejecting the pressure variations due to heave motion. To my knowledge, the only published results are due to the mentioned attempt from the Statoil research group [11].

1.2 Scope and Emphasis

The scope of this thesis will be the design of automatic control algorithms for the attenuation of pressure fluctuations due to heave motion during drill string connection. We will focus most of the energy on the issue of bottom hole pressure regulation, but some time will also be devoted to choke pressure control. On the issues of hydraulic modeling of the well, a brief summary will be given in this thesis, but the interested reader is referred to the project report "Advanced Modeling for Managed Pressure Drilling." Also, quite some time will be invested in the analysis of existing measurement data from previous MPD system tests. We will especially be interested in assessing the influence of choke friction and insufficient modeling on the experimental results, but will also investigate other non-ideal phenomena.

1.3 Outline of Thesis

This thesis is laid out in the following way: Chapter 2 deals with the issue of analyzing the existing measurement data, acting as a further motivation to why this work is important. Chapter 3 then serves as a brief recap of the modeling effort from the fall project "Advanced Modeling for Managed Pressure Drilling." The issue of exploring model reduction techniques has been done with good results, and this can be found as a separate conference paper in the appendix. In Chapter 4, we look at the issue of choke pressure regulation before Chapter 5 dives into the bottom hole pressure regulation problem. Chapter 6 contains a simulation study with performance assessment of the different controllers from Chapter 5 and then, this performance is tested on a high fidelity drilling simulator in Chapter 7. Lastly, everything is rounded

up in the conclusion in Chapter 8. The Appendix contains different derivations and definitions needed for completeness, and also some pieces of MATLAB code for the implementation of different controllers as well as the conference papers, ready for submission.

Chapter 2

Ullrigg Data Analysis

As an additional motivation to why this work is important and necessary, we will begin the thesis with an analysis of the measurement data from the full scale tests done at Ullrigg in 2009. During 6 days, several experimental modes of a full MPD control system were tested, and among them were a version of a feedback controller designed to compensate the heave induced pressure fluctuations. On the experimental set-up, there were measurements of a large number of interesting variables, including the following:

- Pressures at the main pump, choke and, for some of the time, down hole.
- Flows at the main pump/back pressure pump and choke.
- Vertical movement of drill string.
- Controller settings and control signals.

These measurements should go a long way in determining what went wrong in the heave compensation experiments, and we will use this data together with simulations to discuss the effects of several non-ideal phenomena and their influence on the experiment, but first we will present the controller used.

2.1 Existing Control Strategy

The controller used in the full scale test of the existing MPD control system was designed by using what we will name the Kaasa model of the well hydraulics [1]. Disregarding the flow inside the drill string and adding its vertical piston motion, the Kaasa model takes on the form

$$\frac{V_a}{\beta_a}\dot{p_c} = q_{bpp} - A_d v_d(t) - q_c + q_{err} \tag{2.1}$$

$$q_c = K_c\sqrt{p_c - p_0}\,g(u) \tag{2.2}$$

Where p_c is the choke pressure, q_{err} is an unknown error term that should account for unmodeled or unknown effects, V_a is the total volume of the well annulus, β_a is the bulk modulus in the annulus, $A_d v_d$ represents the piston motion of the drill string, K_c

is a constant relating to the area of the choke, p_0 is the pressure down stream from the choke and $g(u)$ is a strictly increasing and invertible function relating the control signal to the choke opening. Using this model and a simple feedback linearization approach, one can find a controller [11]

$$\begin{aligned} u &= g^{-1}\left(\frac{q_c^*}{K_c\sqrt{p_c - p_0}}\right) \\ q_c^* &= q_{bpp} - A_d v_d(t) + \hat{q}_{err} + \frac{V_a}{\beta_a}\left(k_p\left(p_c - p_c^{ref}\right) - \dot{p}_c^{ref}\right) \\ \frac{V_a}{\beta_a}\dot{\hat{p}}_c &= q_{bpp} - A_d v_d - q_c + \hat{q}_{err} - L_p\frac{V_a}{\beta_a}\left(\hat{p}_c - p_c\right) \\ \dot{\hat{q}}_{err} &= -L_i\left(\hat{p}_c - p_c\right) \end{aligned} \tag{2.3}$$

where the two last equations correspond to an observer for the unknown error term q_{err}. This approach could be classified as a feedback linearization controller with feed forward from a measured disturbance and an observer for unknown effects. It can be shown that this results in $\hat{q}_{err}$ converging exponentially to (a constant) q_{err}, and this control input will render the closed loop system as

$$\dot{p_c} = q_{err} - \hat{q}_{err} - k_p\left(p_c - p_c^{ref}\right) + \dot{p}_c^{ref} \tag{2.4}$$

This implies that exponential tracking of p_c^{ref} is achieved.

Now, seeing that for the Kaasa model (2.1), there is no distinction between the dynamics of the choke pressure and the bottom hole pressure, this would also imply that the same controller could be used to regulate the bottom hole pressure after a translation of the bottom hole pressure set point to a choke pressure set point. It is quite obvious that the proposed controller solves the heave compensation problem as it is stated in the Kaasa model, but for future reference, a plot of the performance under the influence of a harmonic wave disturbance can be seen in Figure 2.1.
The undershoot in the regulated pressure is due to initial conditions in $\hat{p}_c, \hat{q}_{err}$ and p_c, but we can see that the controller perfectly compensates for the heave motion.
At this point, we might have a look at an example of one of the failed Ullrigg experiments which is presented in Figure 2.2. Here, the proposed controller (2.3) is implemented and control of the choke pressure is attempted under the influence of vertical motion of the drill string due to waves.

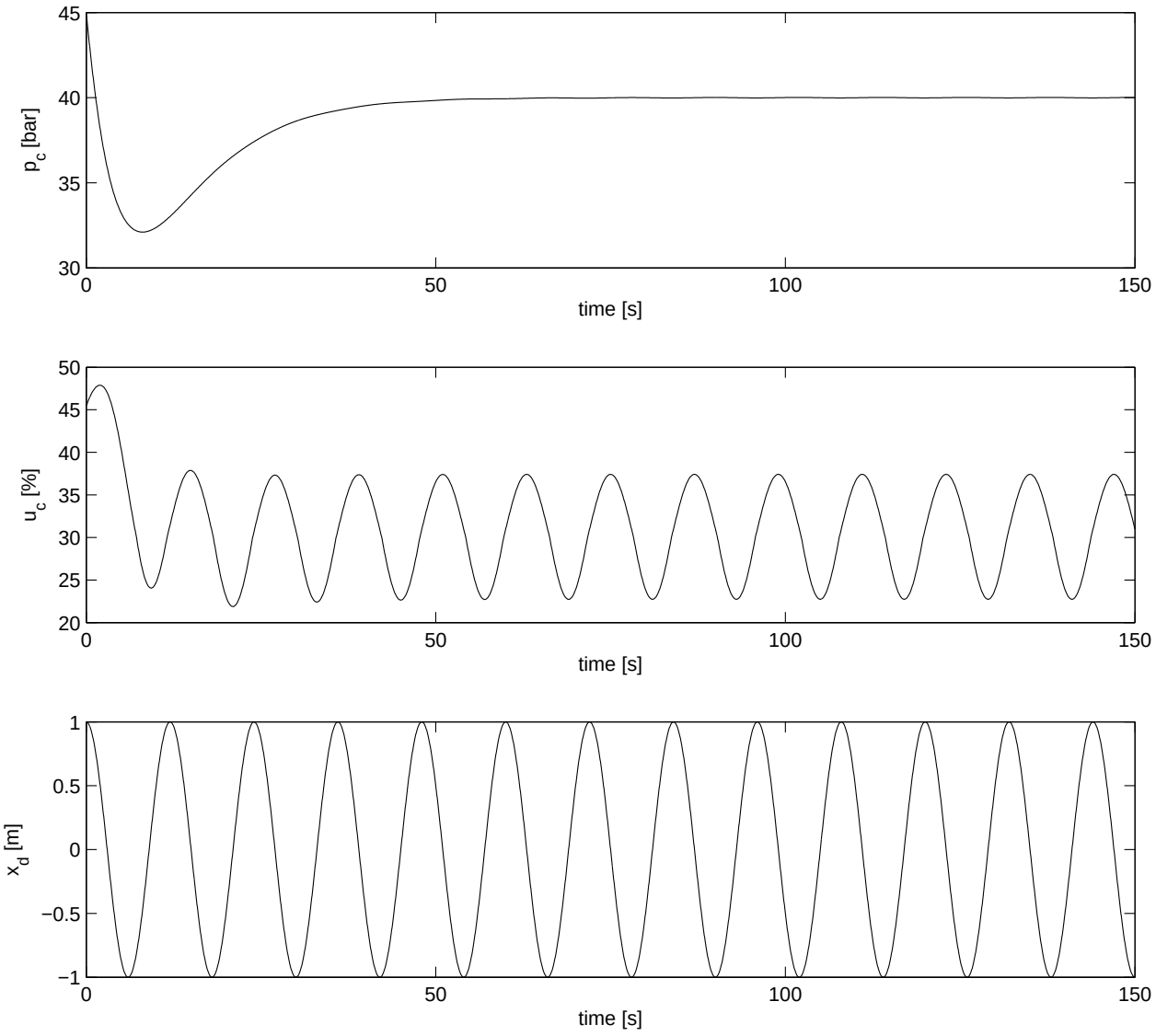

Figure 2.1: Simulation results, Kaasa model with controller. Choke pressure, choke opening and wave disturbance.

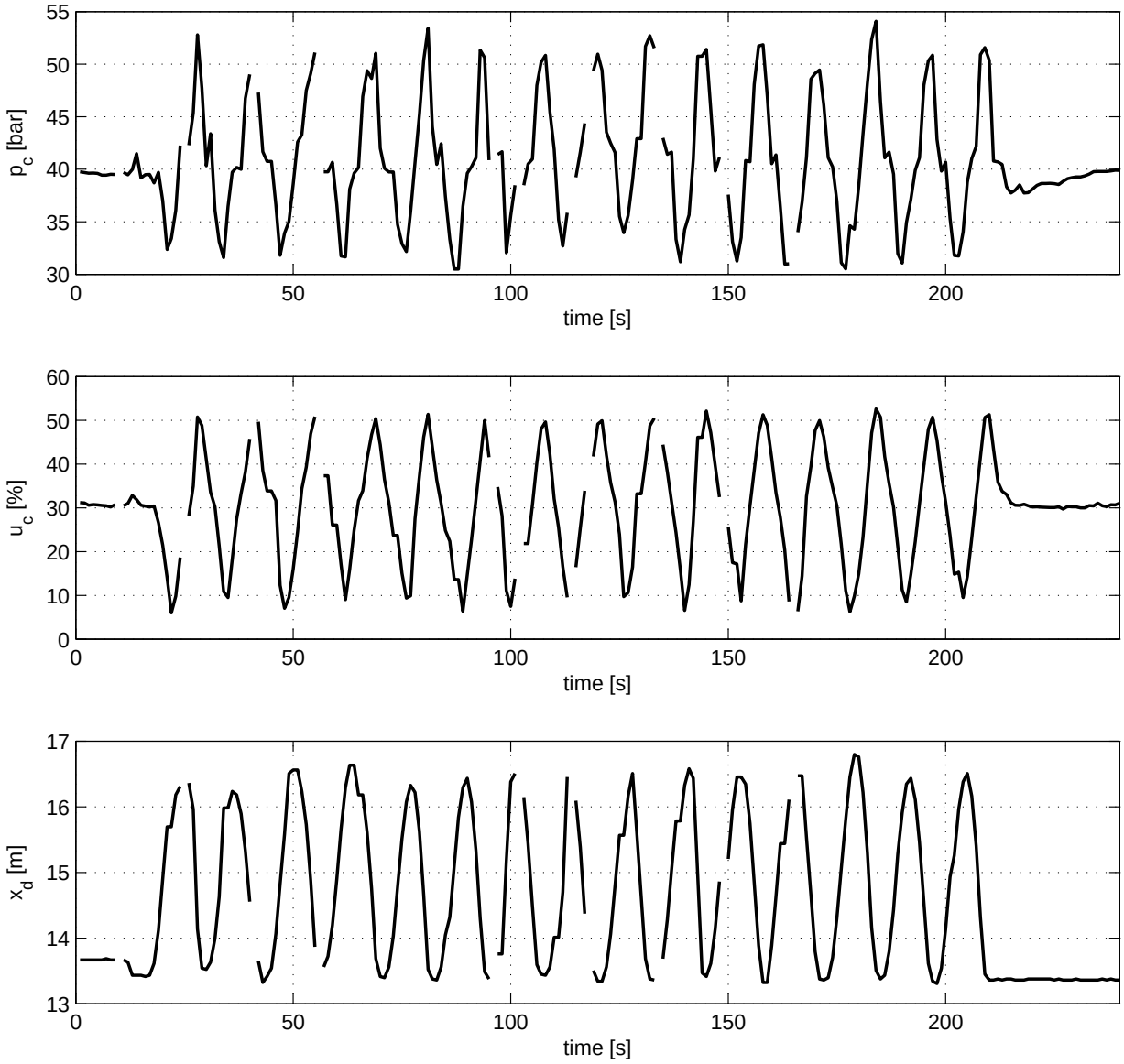

Figure 2.2: Measurement data from Ullrigg heave compensation test. Choke pressure, choke opening and wave disturbance.

We can see that the controller is not successful, and that we actually experience fluctuation of more than 10 *bar* away from the set point. This is obviously worse than hoped, and so it is necessary to try to understand which non-ideal effects are the most influential.

2.2 Insufficient Modeling/Inappropriate Control Strategy

The first non-ideal phenomenon that was examined, and also that which seems likely to be the biggest issue, is the possibility that the Kaasa model is not detailed enough and that a controller design based on this model will thus not be sufficient for the disturbance rejection. The Kaasa model is based on the idea that we treat the entire annulus region as one control volume and thus aggregate the pressure changes over the entire volume. Then, the pressure changes at the choke would equal those at the drilling bit, so it does not really matter which of these pressures we consider. This means that we lose all information regarding how pressure waves travel up and down the annulus and thus also the phase shift between the choke and bottom hole pressures. The obvious way to remedy this is to divide the annulus region into a higher number of control volumes. We will go into greater detail with regards to a more accurate model later, but for now it suffices to take a look at the performance of the proposed controller on a model that divides the annulus into several control volumes, as this will inevitably be closer to the real system. Results from such a simulation can be seen in Figure 2.3. It is quite clear that once we also start to consider the transmission of pressure waves, the proposed controller is not successful in either controlling the choke pressure or the bottom hole pressure. To further illustrate the point that a somewhat higher level of detail in the model is needed, and that controlling the choke pressure and controlling the bottom hole pressure are two different things, consider Figure 2.4. Here, we have used a different controller and a higher order model (both will be covered in great detail later, they are used here for illustrative purposes only). Control volume #1 corresponds to the bottom hole pressure, and control volume #5 corresponds to the choke pressure. As we can see, the bottom hole pressure is regulated, but in achieving this, we experience oscillations at every other point in the well profile. This is due to the phase shift between the bottom hole and choke pressures.

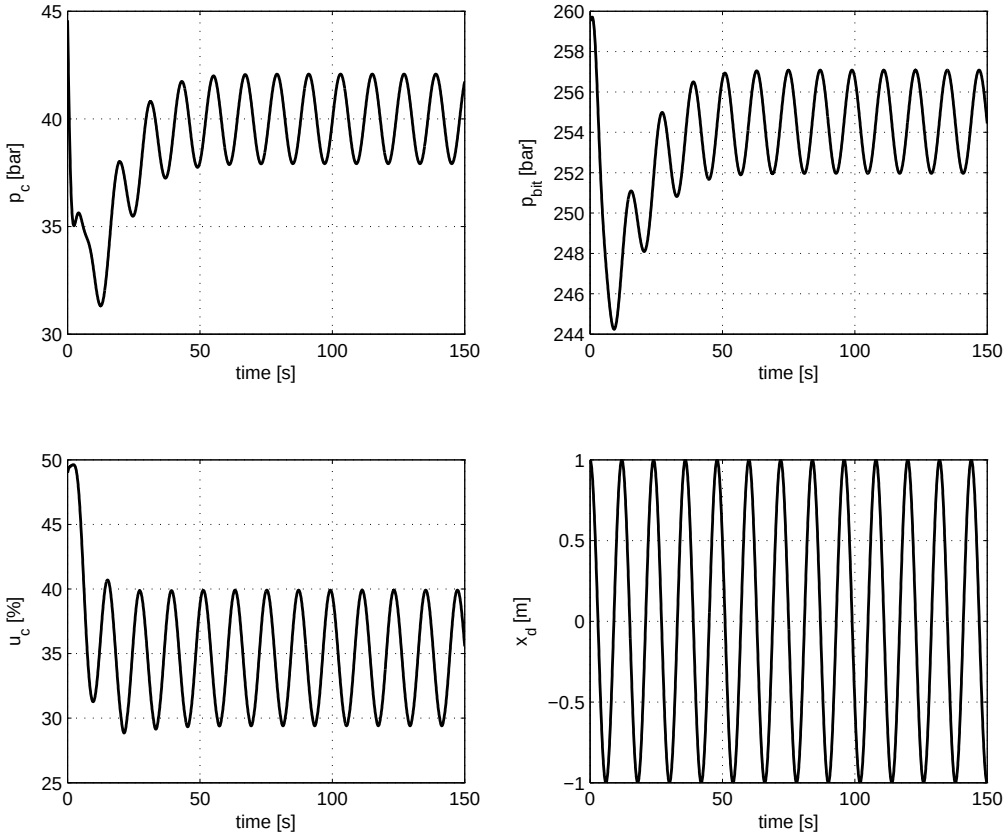

Figure 2.3: Simulation results, using the proposed controller on a higher order well model. Choke pressure, bottom hole pressure, choke opening and wave disturbance.

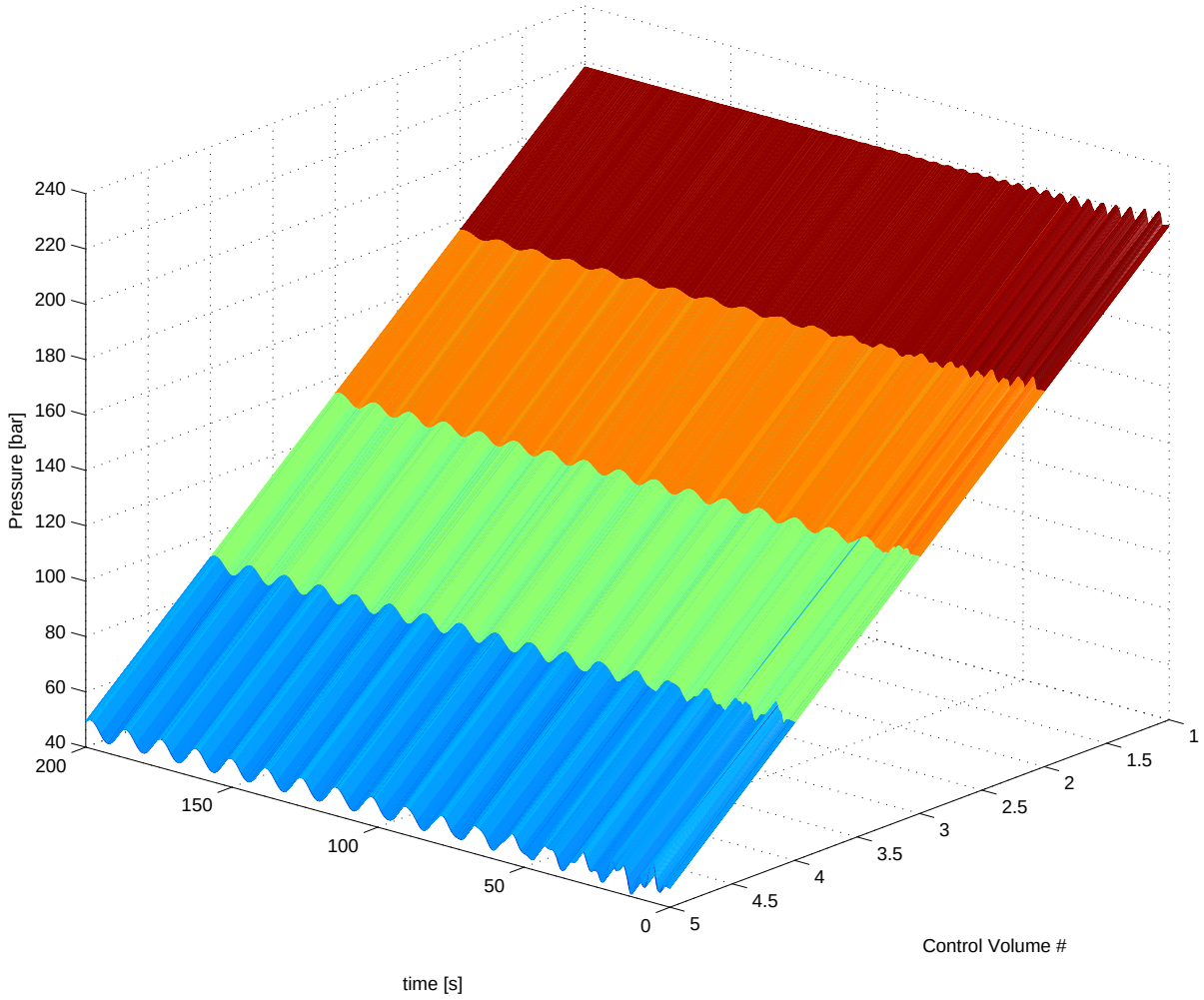

Figure 2.4: Well pressure profile, regulated bottom hole pressure. Control volume #1 is the bottom hole, #5 is choke pressure.

Finally, to show how a more detailed model could predict the failure of the control system, we will show a simulation where we have implemented the existing controller and used the measured drill string movement and back pressure pump flow from the Ullrigg test as external inputs to a higher order model, keeping everything else ideal. The simulation results compared to measurements are shown in Figure 2.5. It is quite clear that the more detailed model predicts to a large extent the pressure fluctuations where the Kaasa model would not. Thus we conclude that, for these types of periodic and relatively high frequency control objectives, it is necessary to consider the transmission time of the pressure waves and not only the aggregate pressure changes in the well annulus. However, this does not seem to completely explain the amplitude of the oscillations, so we will continue to investigate other non-ideal phenomena.

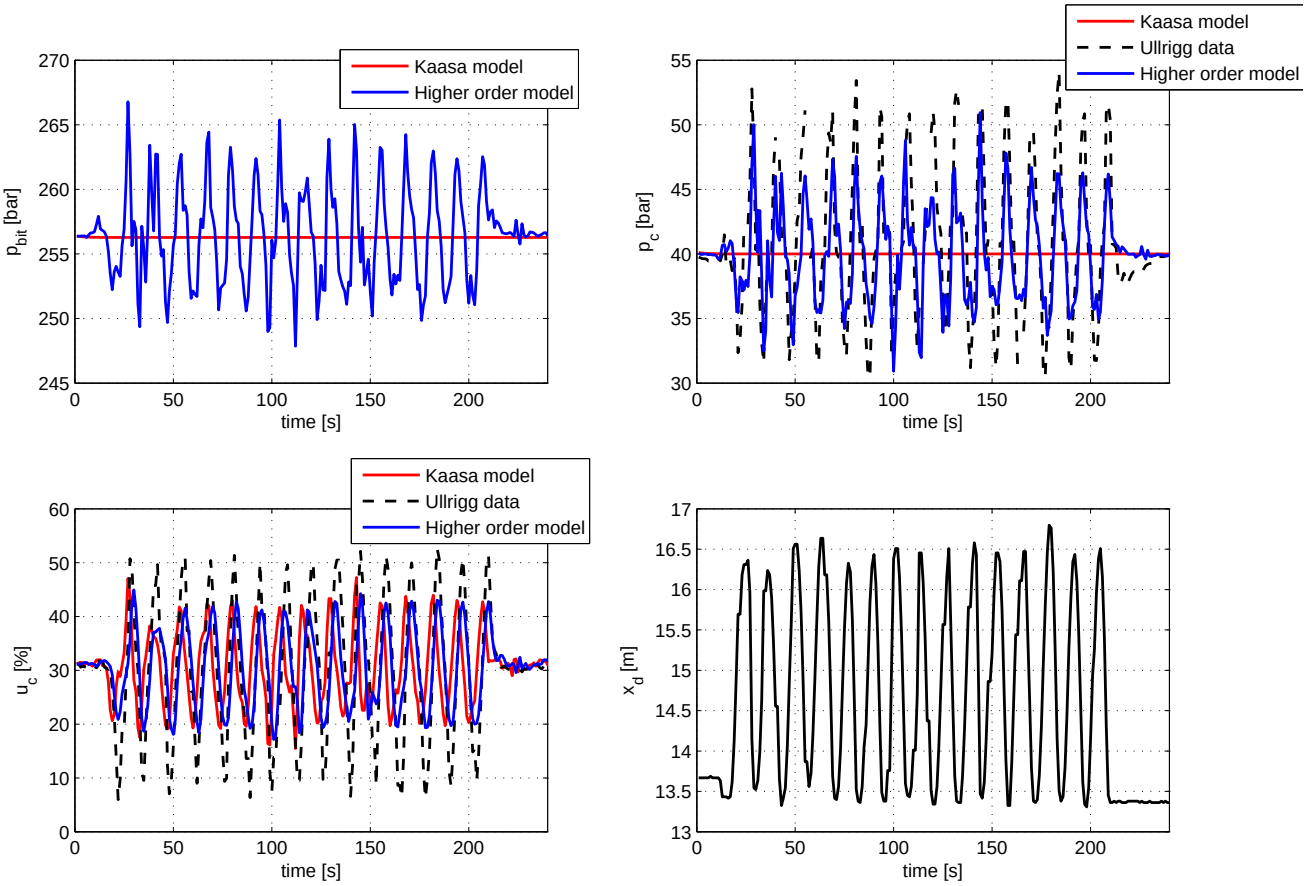

Figure 2.5: Simulation results comparing Ullrigg data to that estimated by a higher order model and Kaasa model, using the existing control strategy. Bottom hole pressure, choke pressure, control signal and drill string movement.

2.3 Time Delays/Low Sampling Frequency

Let us now consider the timing effects and take a unified look at the sampling time and other time delays in the system. Let us say that the cycle from the state of the choke pressure to the actual opening of the choke is as follows: At some point in time t_o, the choke pressure has a given value. Then, at some time later, the measurement is available at the sensor, and then at time t_1, the sensor is sampled by the PLC system and made available for the control algorithm which then computes the desired control signal for the choke. This is output to the choke at time t_2. The choke starts to move, and the correct choke opening is achieved at time t_3. See also Figure 2.6 for a time line.

Figure 2.6: Time line for delays and sampling.

These effects will together effectively cause a delay of some total time $T = t_3 - t_0$. Thus, the net effect of all delays is that the actual choke opening that is applied to the system is calculated based on the actual state of the system a time T seconds ago. To show how this might affect the performance of the proposed controller, let us consider Figure 2.7. Here, the same simulation as before is reproduced, but this time the applied choke control signal is delayed by a total time $T = 2$ seconds, and we can see that this could explain the rest of the performance issues when compared to Figure 2.5. Notice also that the time delay makes the oscillations of the applied choke opening larger than earlier. However, a total delay of 2 seconds does sound like a lot. The sampling time of the experiments was 1 second, and the implemented control algorithm used on average about 0.25 seconds for processing.[1] Thus, even though we do not know the time characteristics of the sensor or other transmission delays, it seems likely that the total delays should not be much larger than 1 second, with 2 seconds being somewhat a stretch. This is also supported by the difference in the measured choke opening to the applied choke signal. (See the next section). The choke opening lags the control signal by 1 second, but seeing how this also is the sampling time, this indicates the maximum time delay in the choke dynamics and suggests that it might be smaller. Figure 2.8 presents comparisons of simulations done with different lengths of total time delay, and we can see that, as expected, a larger time delay will cause larger fluctuations of the pressure.

[1] Recorded data from Ullrigg.

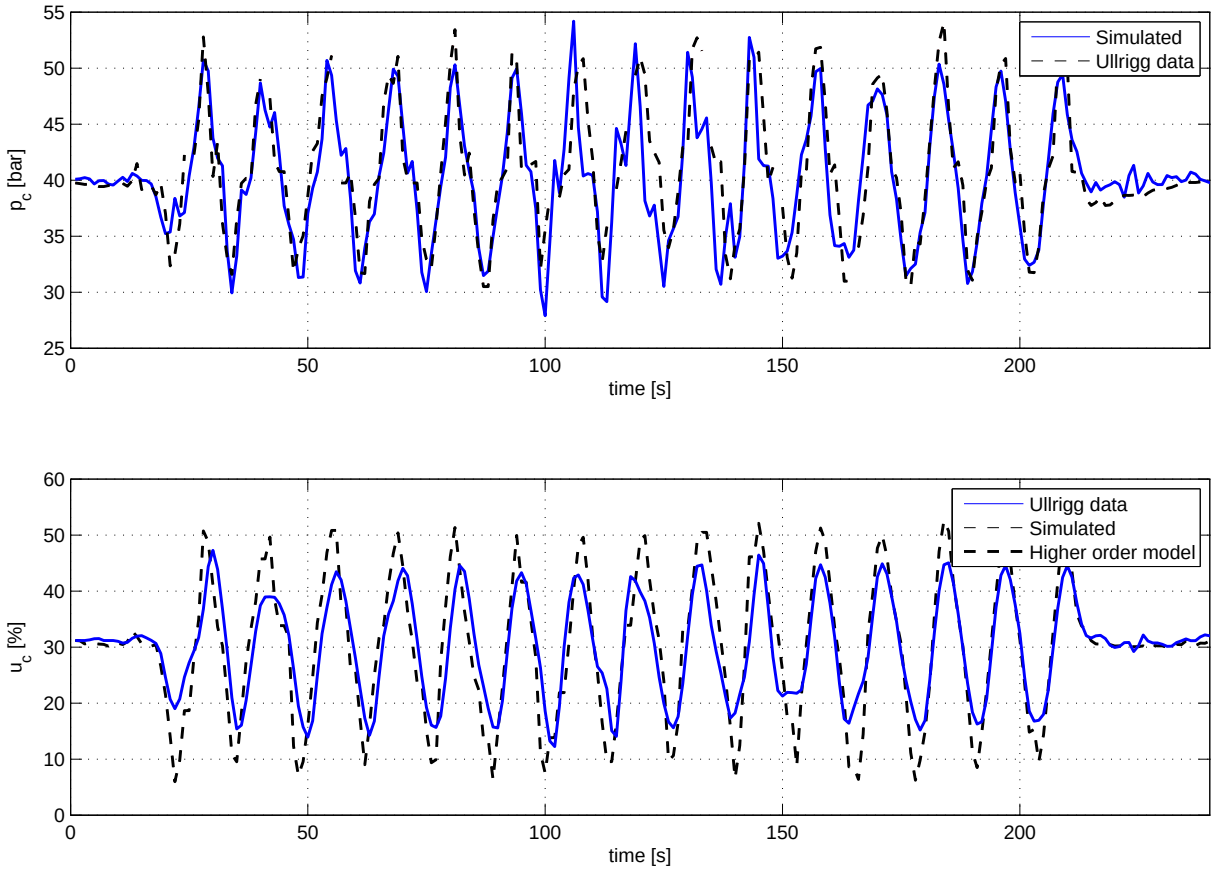

Figure 2.7: Simulation results, adding a 2 second total time delay. Choke pressure and control signal.

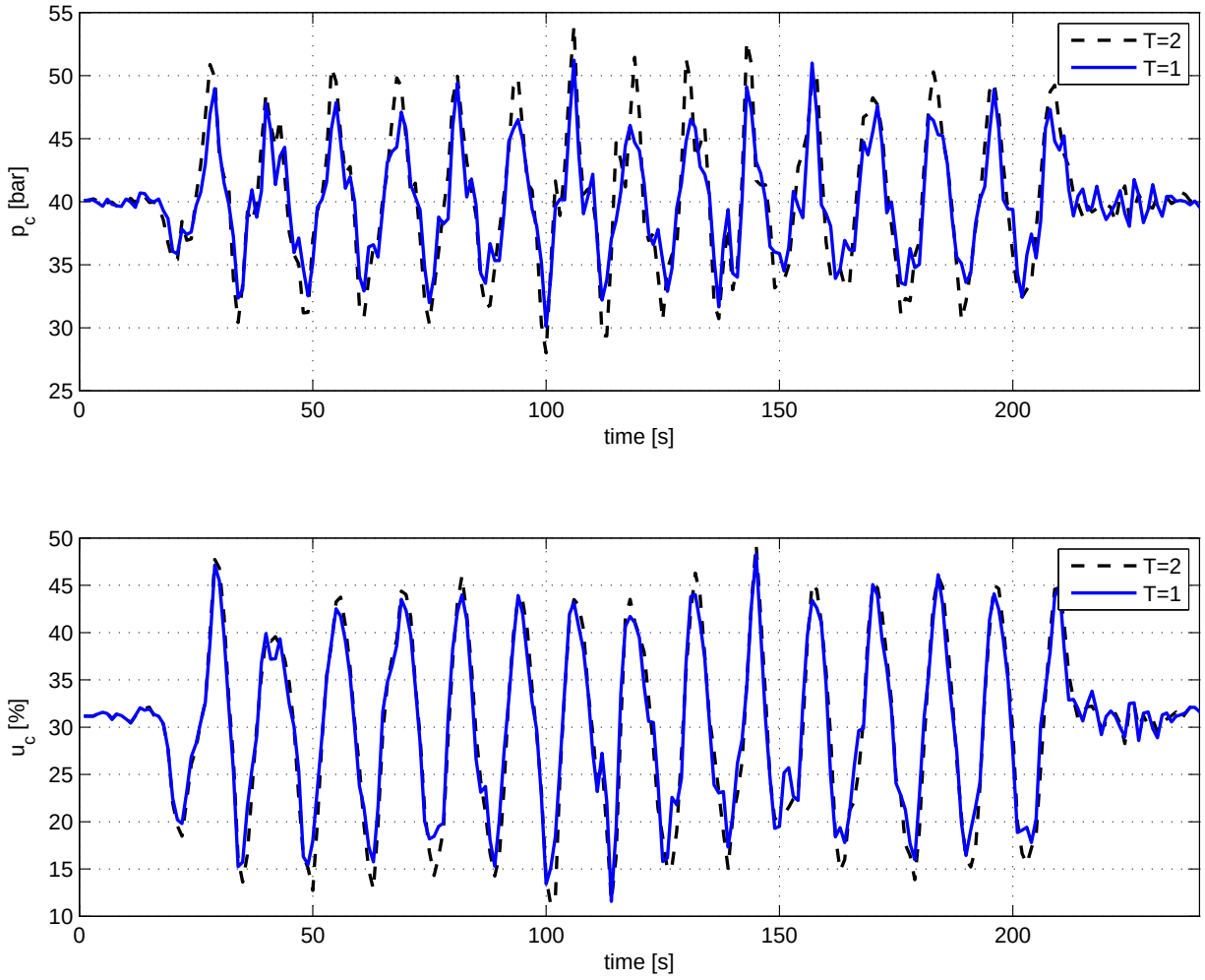

Figure 2.8: Simulation results comparing 1 second and 2 second delays. Choke pressure and control signal.

One issue regarding low sampling frequency that the previous analysis did not consider is the effect of seldom updating the control signal. The low sampling frequency might add to the time delay, but would the situation be any different if we were to update the choke opening more frequently? A simulation covering this can be seen in Figure 2.9.

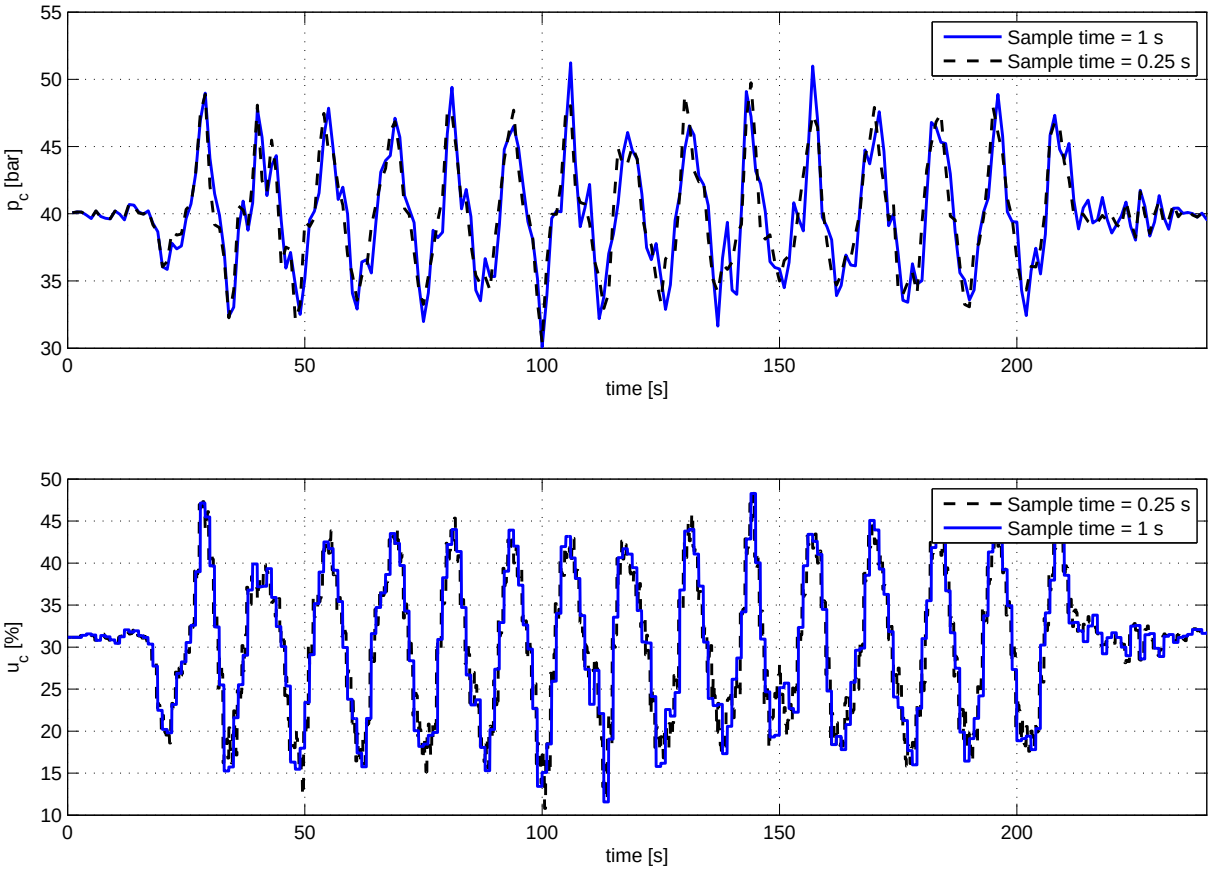

Figure 2.9: Comparison of different control update rates. Choke pressure and control signal.

Here, we isolate the effect of updating the control signal more frequently. As we can see, it does not seem like the update of the control signal is the most critical, and we should probably be more worried about the total time delay. However, this is probably a function of how fast the pressure changes are. If the frequency of the wave disturbance were to be larger, it is likely that a more frequent control update would be necessary.

To remedy the problem of long time delays, it seems that the most important changes should be to reduce the sampling time as well as implement the control algorithms on a more efficient platform suited for real-time control applications.

2.4 Rate Limitation of Control Choke

The choke is a vital piece of hardware in the MPD control system, and its performance will greatly influence the overall performance of the automated control. Thus, non-ideal phenomena in the choke are important to understand, and we will start by investigating rate limitations. This might be seen as a problem reducing the per-

formance in control valves, but in most cases, a very rapidly varying choke is not desirable due to water hammer effects.[2] Still, we will investigate how this might have affected the experiments.

The choke used in the Ullrigg tests had an opening time of about $6-8\,s$ from fully closed to fully open, which is a relatively fast choke of this dimension. That means that it should be possible to open/close the choke at a rate of somewhere between $13-17\,\frac{\%}{s}$, and this is quite well supported by the measured choke opening from the Ullrigg tests, seen in Figure 2.10.

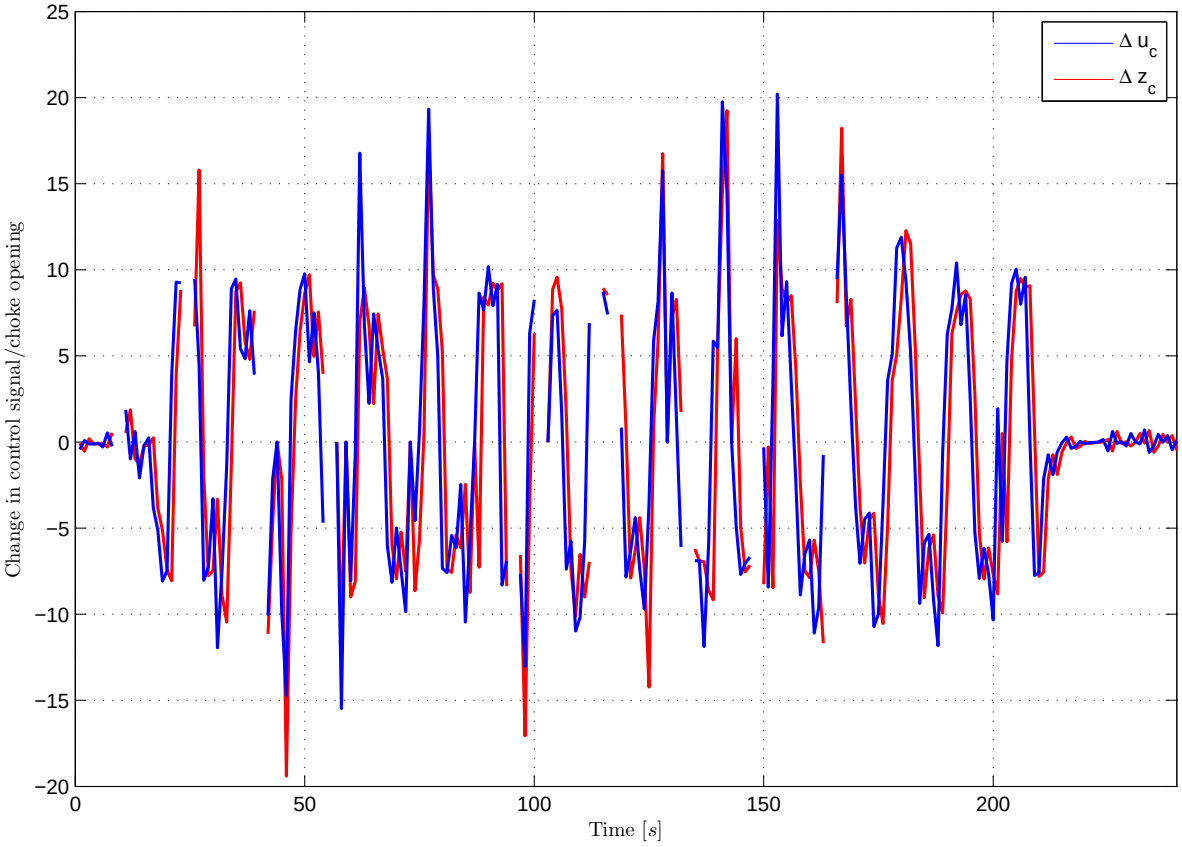

Figure 2.10: Changes in control signal, Δu_c, compared to changes in choke opening,Δz_c.

Here we can see that the maximum change in the actual choke opening, z_c, between two samples one second apart is between 15 and 20 %. Also, it is evident that the actual choke opening is not always able to follow the control signal u_c, so to assess the influence of this difference, we have simulated the system with both the control signal and the actual choke opening as inputs to see if there is a noticeable difference in the pressure outputs. Notice that there is also a time lag of the actual choke opening relative to the control signal. This lag was canceled to isolate the effect of rate limitation. The simulation results can be seen in Figure 2.11.

[2] A rapidly varying choke would cause very large pressure changes.

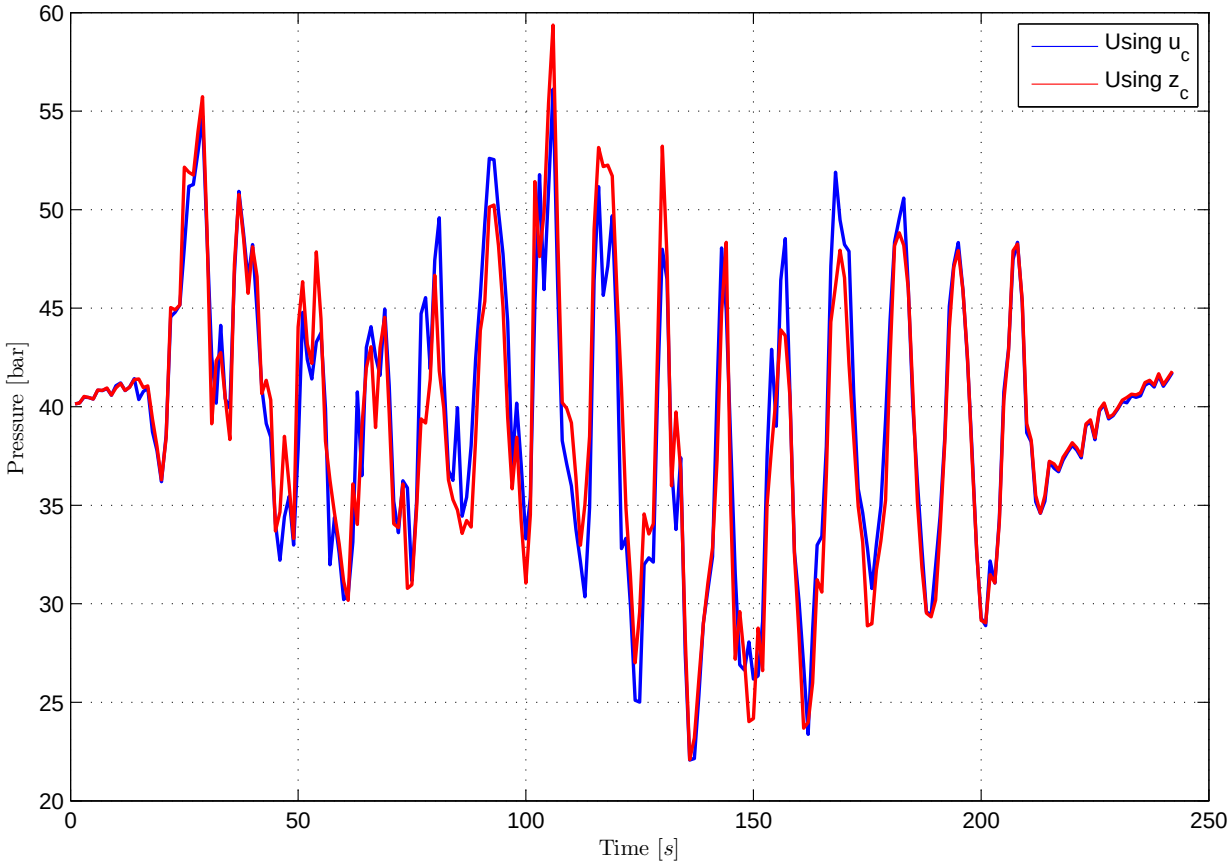

Figure 2.11: Simulation results comparing the response when using the computed control signal and using the actual choke opening.

We can see that there are noticeable differences between the two simulations, but it is difficult to get an unambiguous answer to whether this was a negative influence on the experimental results in the Ullrigg tests. In some cases, the pressure peaks are actually larger when there is no rate limitation.

To say something about the necessary opening rates for an MPD system, we can consider a harmonic wave disturbance of the type that was emulated in the Ullrigg tests. Here, the vertical drill string position followed an oscillating path

$$x_d = A cos\left(\omega_{waves} t\right) \tag{2.5}$$

Then, as will be explained in great detail later, it is necessary for the choke opening to be a scaled and phase shifted version of this sinusoid in order to compensate for the disturbance. The biggest rate of change will then be a function of almost all the parameters of the well hydraulic model. (See (5.10).) Thus, it is probably difficult to say a priori what rate is necessary to avoid saturations, but the simulations in later chapters might give an indication. The absolute largest rate

that is conceivable is found when considering a full utilization of the choke on the form $u_c = 50 + 50sin\left(\omega_{waves}t\right)$ %, so that the maximum rate of change would be $\frac{du_c}{dt}_{max} = 50\omega_{waves}\frac{\%}{s}$. However, to conclude with a rough approximation, it seems that the Ullrigg experiments were not severely affected by rate limitations.

2.5 Stiction and Backlash in Control Choke

It is well known that stiction, backlash and other nonlinear phenomena related to friction in the movement of valve positions can cause limit cycles and degrade control performance. Thus it is a question whether some of the performance issues in the Ullrigg tests can be accredited to such problems in the control choke used, and we will investigate this by modeling friction in the choke and doing simulations. First of all, the definitions of stiction and backlash are not quite clear, but we will take stiction to mean the resistance to the start of motion from an idle state, and by backlash we will mean some form of hysteresis that is the result of either a dead band or stiction.

The literature on different theories and models of friction phenomena is of course substantial, including both static and dynamic models and ranging from the very simple Coulomb model to the dynamic LuGre model which includes both stiction and the Stribeck effect. However, the problem with using these models for modeling friction forces is the fact that they often include a large number of experimental parameters and their simulation requires finding the time evolution of a second order differential equation modeling Newton's second law. This again implies that one has to estimate the mass of the moving object as well as the driving force from the valve actuator. A refreshingly simple and intuitive approach can be found in the works of Choudhury et al. [12]. They consider the specific issue of friction effects in valves and come up with a data driven friction model that encompasses all the commonly seen friction phenomena. Their approach is the following: Consider the input-output map in Figure 2.12. The input is in this case the control signal to the choke, and the output should ideally be the actual choke opening. However, since the actual choke might not be available for measurement, we can also consider the output to be the choke flow. The idea is then: Let us say that the choke is at rest at a certain opening at position A. Then, the control signal increases, but because there is a dead band where the choke is not responsive, nothing happens until point B. At this point, the dead band is overcome, but because of the sticking behavior, there is still no movement until point C. Now the applied force exceeds the static friction force, but seeing how the force required to overcome the static friction often is larger than that required to maintain movement (see Figure 2.13), there is a quick jump in the actual choke opening up to point D. Here, the viscous, linear friction force takes over and the choke can move smoothly until point E. At this point, the motion is reversed, and so the entire operation starts over in the opposite direction, causing us to follow the hysteresis path mapped out in the figure. Of course, a quite standard friction model consisting of static friction, Coulomb and viscous friction, as seen in Figure 2.13, would generate this kind of behavior, but as discussed earlier this would require quite a few parameters that are not so easy to estimate. However, if we have available measurements of the two time series required to plot Figure 2.12, we can

possibly find the two values S and J, which are the only two parameters needed in the data driven model. A copy of the flow chart for the model given in [12] can be seen in Figure 2.14.

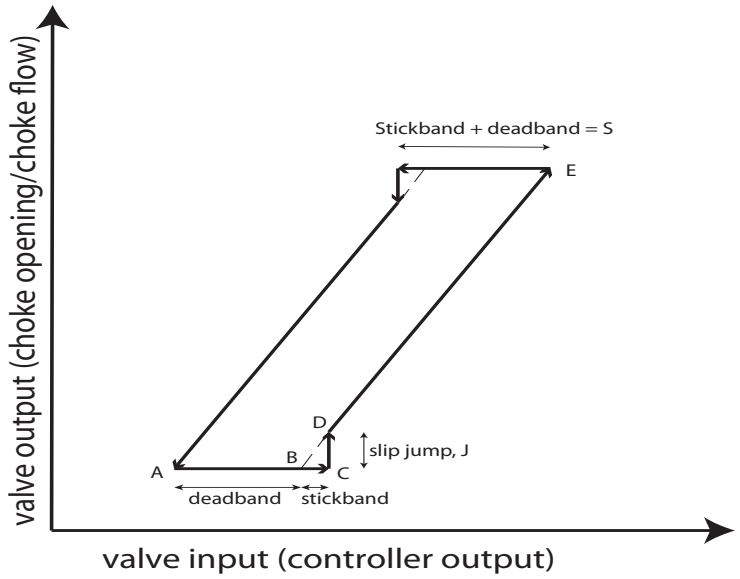

Figure 2.12: Typical input-output behavior of a sticky valve.

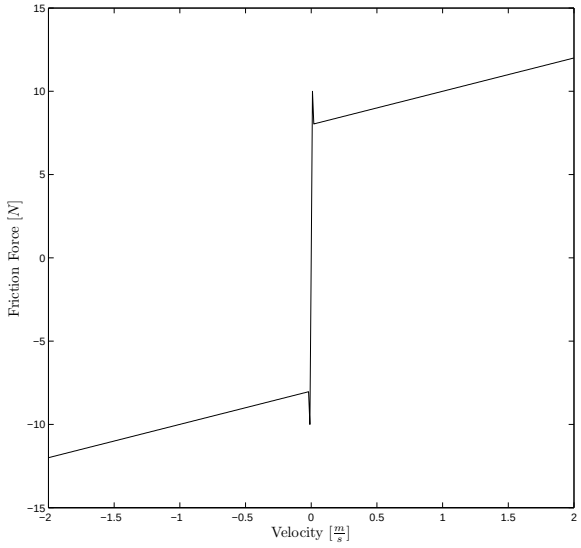

Figure 2.13: Friction force consisting of static, Coulomb and viscous friction.

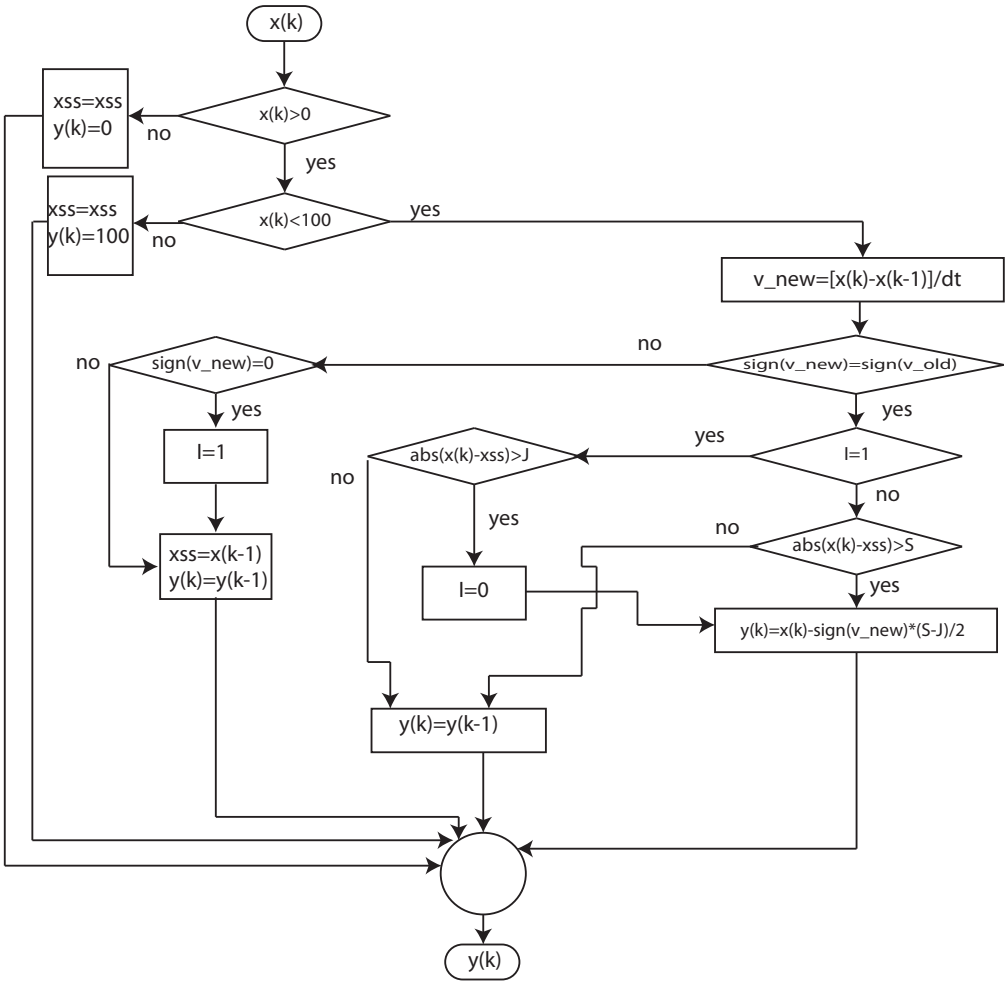

Figure 2.14: Flow chart for data driven friction model.

In this flow chart, $x(k)$ represents the control signal at time k, $y(k)$ is the actual choke opening, xss is the sticking position, v_{new}, v_{old} represent the rate of change of the control signal at the current and previous time instant and I is a Boolean variable saying whether we are stuck or not.

Using this data driven model, we can quite simply add friction to the choke opening and simulate the system with the assumption that there are significant friction issues. For example, choosing a value for dead band plus stick band, $S = 5\%$ and a value for the slip jump $J = 2\%$, we can confirm that this kind of behavior could cause some extra pressure peaks as seen in Figure 2.15. In this simulation, we combined a more realistic time delay of 1 second with friction in the choke, and it is clear that this does add to the pressure fluctuations when compared to the previous simulations.

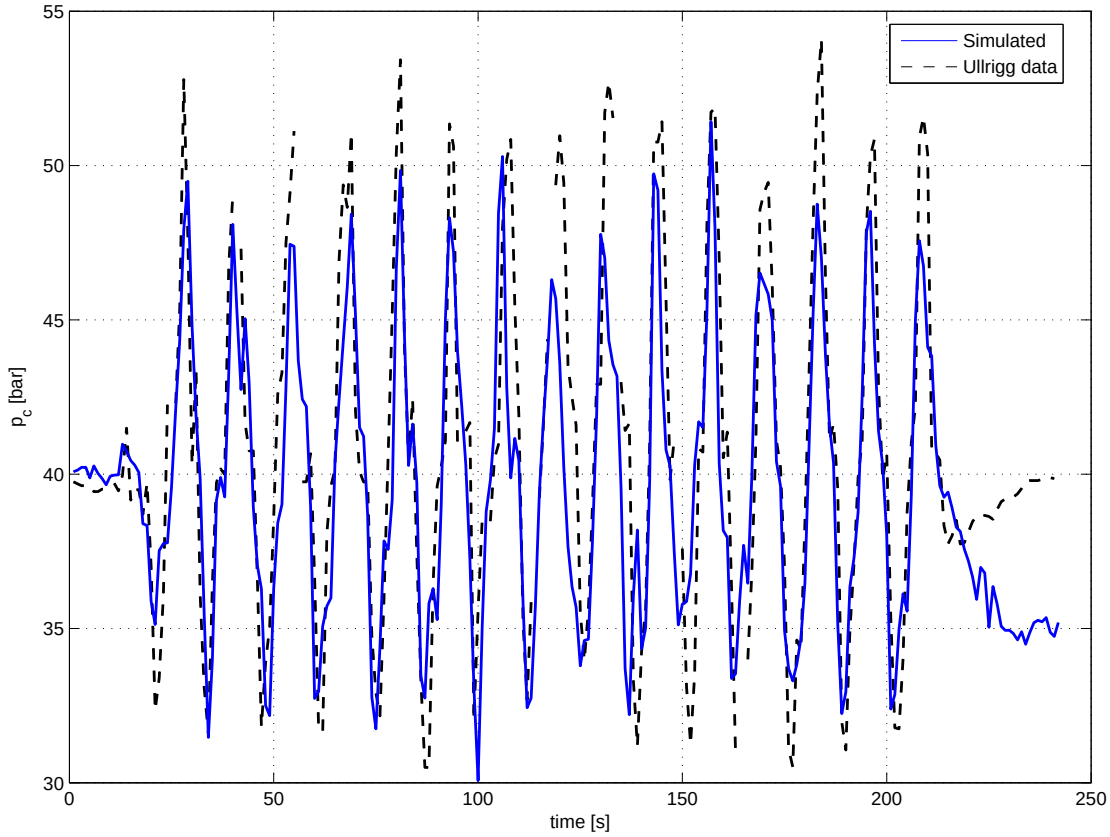

Figure 2.15: Simulation results using a 1 second time delay in addition to friction in choke. Choke pressure.

To see how this friction affects the actual choke opening, consider Figure 2.16.[3]

[3]Notice that the data driven model does not function correctly with step changes in the control signal due to the comparison of velocities between time steps. Thus, the control signal has been low pass filtered to imitate an actual current signal to the actuator.

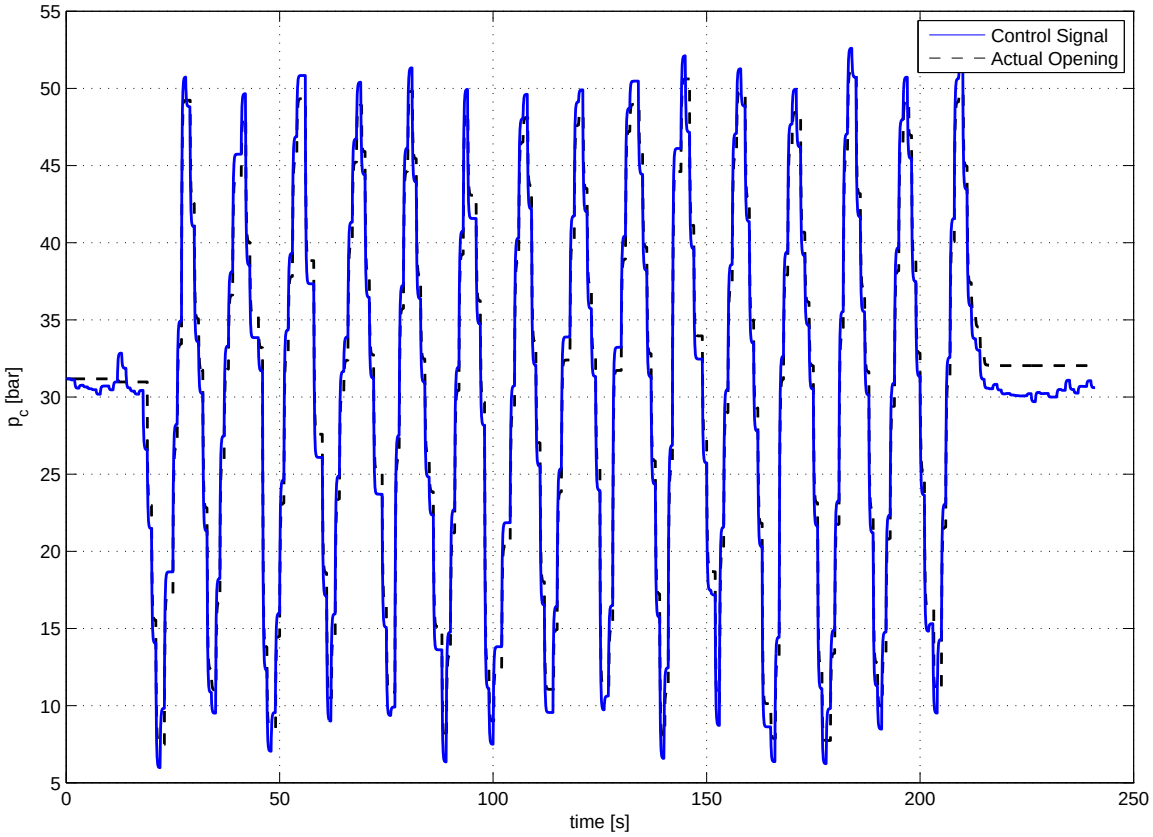

Figure 2.16: Control signal and actual choke opening when choke is subject to friction.

Here, we can see that the data driven friction model successfully implements a stick-slip motion of the actual choke opening. For every step change in the control signal, the choke has to overcome the static friction, slip and move to the new position. Because of the low sampling time of the controller, the choke comes to a rest before the new change arrives, and so the process is repeated.

We have seen that it is possible for friction in the choke to contribute to the pressure fluctuation, but we have not yet discussed whether it is likely that it did. For us to use the data driven model, we need to estimate the values S and J based on actual measurement data, so we will consider the input-output map from the control signal to the measured choke opening, seen in Figure 2.17.

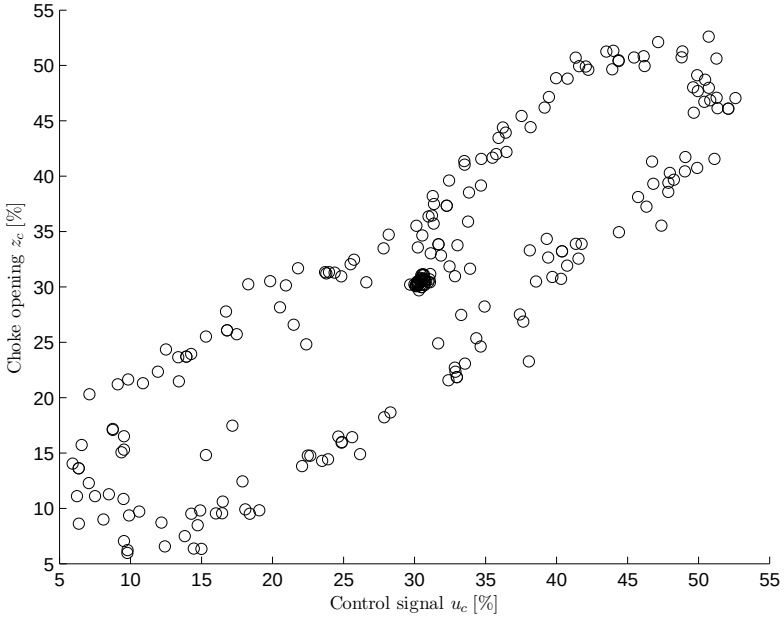

Figure 2.17: Input-output map of choke, measured Ullrigg data.

When we compare this to Figure 2.12, we see that there might be evidence of sticking and backlash in the measured data, and that the actual values of S and J used in the previous simulation are not at all impossible. We thus conclude that a one second time delay together with friction effects in the choke explain to a large extent the extra amplitude of the choke pressure oscillations of the Ullrigg data when compared to that estimated by the higher order model in Figure (2.5).

2.6 Summary

To summarize this chapter, we have seen that the main reason for the failure of the heave compensation tests at Ullrigg was the control strategy based on an insufficient model of the pressure dynamics. However, this alone cannot explain the large amplitude of the pressure oscillations, but combined with friction in the choke and time delays in the control system, it seems that we are able to explain most of the problems seen in the measured Ullrigg data. No conclusion was reached with regards to rate limitations in the choke, but it seems likely that this was not a major influence on the results. This realization of the limitations in the Kaasa model motivates the use of a higher order model for control design, which is the main focus of this thesis.

Chapter 3

Mathematical Modeling

3.1 Hydraulic Model of Well

Developing a model of the well hydraulics was mostly done during the fall project "Advanced Modeling for Managed pressure Drilling." Here, a variable sized model was found based on standard partial differential equations (PDE's) for a hydraulic transmission line. These PDE's are derived from basic mass and momentum balances and can be found for example in [13]. They take the form

$$\frac{\partial p}{\partial t} = -\frac{\beta}{A}\frac{\partial q}{\partial x} \tag{3.1}$$

$$\frac{\partial q}{\partial t} = -\frac{A}{\rho}\frac{\partial p}{\partial x} - \frac{F}{\rho} + gAcos\left(\alpha\left(x\right)\right) \tag{3.2}$$

Where p is pressure, q is volumetric flow, β is bulk modulus, A is cross section area, x is the positive flow direction, ρ is mass density, F is the friction force, g is the gravitational constant and $\alpha\left(x\right)$ is defined as the angle between gravity and the positive flow direction. These equations were discretized using a finite volumes method, and the resulting model is given by the following set of ordinary differential equations (ODE's) for the pressures and flows at different positions in the drill string and well annulus

$$\begin{aligned}
\dot{p}_{1d} &= \frac{\beta_{1d}}{A_{1d}l_{1d}}(q_p - q_{1d}) \\
\dot{p}_{id} &= \frac{\beta_{id}}{A_{id}l_{id}}(q_{id} - q_{(i+1)d}),\ i = 2, 3, ..., N-1 \\
\dot{p}_{Nd} &= \frac{\beta_{Nd}}{A_{Nd}l_{Nd}}(q_{(N-1)d} - q_{bit}) \\
\dot{q}_{id} &= \frac{A_{id}}{l_{id}\rho_{id}}(p_{id} - p_{(i+1)d}) - \frac{F_{id}A_{id}}{\rho_{id}l_{id}} + Ag\frac{\Delta h_{id}}{l_{id}},\ i = 1, 2, ..., N-1 \\
\left(\frac{\rho_{Nd}l_{Nd}}{2A_{Nd}} + \frac{\rho_{1a}l_{1a}}{2A_{1a}}\right)\dot{q}_{bit} &= (p_{Nd} - p_{1a}) - F_{bit} + \frac{g\left(\rho_{Nd}\Delta h_{Nd} - \rho_{1a}\Delta h_{1a}\right)}{2} \\
\dot{p}_{1a} &= \frac{\beta_{1a}}{A_{1a}l_{1a}}(q_{bit} - q_{1a} + q_f)
\end{aligned} \tag{3.3}$$

$$
\begin{aligned}
\dot{p}_{ia} &= \frac{\beta_{ia}}{A_{ia} l_{ia}} (q_{ia} - q_{(i+1)a}),\ i = 2, 3, ..., N-1 \\
\dot{p}_{Na} &= \frac{\beta_{Na}}{A_{Na} l_{Na}} (q_{(N-1)a} - q_c + q_{bpp}) \\
\dot{q}_{ia} &= \frac{A_{ia}}{l_{ia} \rho_{ia}} (p_{ia} - p_{(i+1)a}) - \frac{F_{ia} A_{ia}}{\rho_{ia} l_{ia}} - A_{ia} g \frac{\Delta h_{ia}}{l_{ia}},\ i = 1, 2, ..., N-1
\end{aligned}
$$

Here, the subscripts a, d refer to the annulus and drill string respectively, and the numbers 1 through N refer to the control volume in question. q_{bit} is the flow through the drill bit, and F is the friction force acting on each control volume. Also, l is the length of the control volume and Δh is the height difference over the control volume so that we also account for gravity. See also Figure 3.1. The control inputs to this model are q_p, q_c and q_{bpp} and will be further described later.

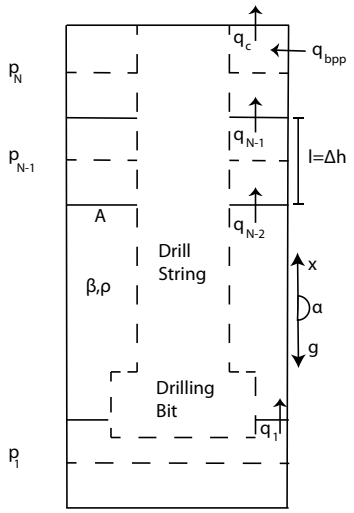

Figure 3.1: Control volumes and geometry for discretized system.

A very large part of the fall project was devoted to modeling the friction force of the drilling fluid, so only a brief summary will be given here. The final choice for the friction model uses standard, Newtonian friction factors, which for laminar flow result in a linear friction force $F = kv$, where v is the average fluid velocity over the cross section, $v = \frac{q}{A}$. This was shown to correspond well to data from full scale tests, and also, for the flow in the annulus, the laminar region was observed to extend beyond the flow rates that we had data for. (See Figure 3.2)

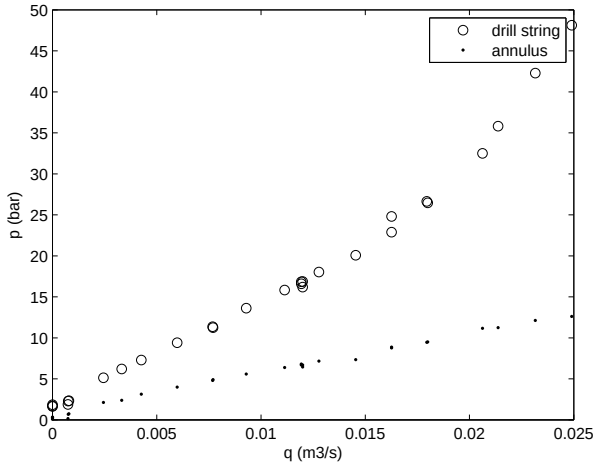

Figure 3.2: Friction losses from observed, full scale testing data as a function of flow rate.

The proportionality constant k is found using the fanning friction factor f. This friction factor is defined through

$$F = \frac{fl\rho v^2}{r_h} \tag{3.4}$$

For laminar flow in an annular geometry, it has been proposed [14] to use a generalized Reynolds number to calculate the friction factor

$$f = \frac{16}{Re^*} \tag{3.5}$$

$$Re^* = \frac{\rho v r_h}{2^{-2} K^*} \tag{3.6}$$

$$K^* = \mu\,(a+b) \tag{3.7}$$

$$r_h = \frac{(d_o - d_i)}{4} \tag{3.8}$$

Here, d_o, d_i are the outer and inner diameters of the annular region respectively, and μ is the dynamic viscosity of the drilling fluid. The constants a, b are related to the geometry of the cross section, and how to calculate them can be found in the appendix. r_h is called the hydraulic radius of the cross section. In total, equations (3.5) through (3.8) calculates the linear friction force (3.4). Notice also that this can be extended to turbulent flow by considering a maximum Reynolds number for laminar flow and then switching to a turbulent friction factor calculated by for instance the Haaland equation.[1]

[1]The interested reader is referred to any work on turbulent pipe friction if the Haaland equation is unknown.

Now, for the specific scenario of a drill string connection, the main mud pump is turned off, the back pressure pump is turned on and there is a one way valve in the drill bit. This means that, effectively, the drill string dynamics are irrelevant, and we can simply consider the annulus as our dynamic system. Also, since there is no externally forced flow through the annulus, the flow rates will be modest and we can justify only considering laminar flow and linear friction.

3.2 Effect of Vertical Drill String Movement

The vertical drill string motion was one of the scenarios considered during the fall project, and several actions were proposed for changing the model in order to capture the pressure fluctuations due to heave motion. As it turns out, there are two effects that are important for the pressure dynamics. The first one is the change in the annulus volume due to the top of the drill string moving in and out of the well. This will lead to changes in the lower most control volume, so we change the differential equation to

$$\dot{p}_{1a} = \frac{\beta_{1a}}{A_{1a}\left(l_{1a} - x_d\right) + x_d\left(A_{1a} + A_{1d}\right)}\left(-q_{1a} - v_d A_d\right) \tag{3.9}$$

Here, x_d is defined as the position of the drill bit relative to the bottom of the well, and v_d is the speed of the drill string, defined positive upwards. Also, $q_{bit} = 0$ because we have no main mud pump flow. See also Figure 3.3.

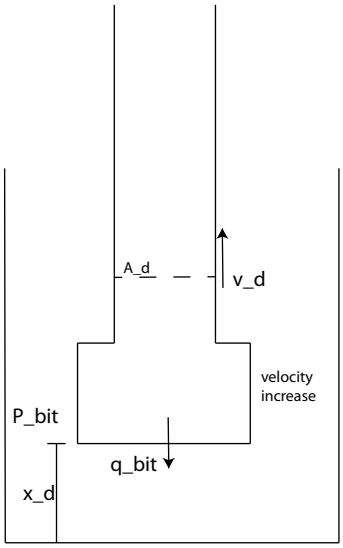

Figure 3.3: Vertical movement of drill string.

The second effect that is important for the pressure dynamics is the fact that the geometry of the drilling bit differs from the circular end of the drill string. Specifically, the drilling bit will have a larger cross section than the rest of the drill string. This causes the generated volume flow around the drill bit to be "squeezed" into a smaller area, increasing the velocity of the fluid and thus increasing the friction losses in this area. See again Figure 3.3. To model this, we could of course calculate the new

velocity of the fluid and then use this to calculate the friction force, but it is more convenient to keep everything in terms of the states of the system, in this case the flow q_{1a}. The net effect of decreasing the cross section area by a factor c is to increase the velocity by the same factor. Thus, this will result in a new friction force that is c times larger than before. When we also incorporate the smaller cross section in the rest of the equation, we get the new equation for q_{1a}

$$\dot{q}_{1a} = \frac{A_{1a}}{l_{1a}\rho_{1a}}(p_{1a} - p_{2a}) - \frac{cF_{1a}A_{1a}}{\rho_{1a}l_{1a}} - A_{1a}g\frac{\Delta h_{1a}}{l_{1a}} \tag{3.10}$$

where the cross section A_{1a} is c times smaller than what it would have been without the drilling bit.

3.3 Final Hydraulic Model

Taking all the above into account, the final hydraulic model of the system for the specific scenario of interest is given as

$$\begin{aligned}
\dot{p}_{1a} &= \frac{\beta_{1a}}{A_{1a}\left(l_{1a} - x_d\right) + x_d\left(A_{1a} + A_{1d}\right)}\left(-q_{1a} - v_d A_{1d}\right) \\
&\vdots \\
\dot{p}_{Na} &= \frac{\beta_{Na}}{A_{Na}l_{Na}}(q_{(N-1)a} - q_c + q_{bpp}) \\
\dot{q}_{1a} &= \frac{A_{1a}}{l_{1a}\rho_{1a}}(p_{1a} - p_{2a}) - \frac{cF_{1a}A_{1a}}{\rho_{1a}l_{1a}} - A_{1a}g\frac{\Delta h_{1a}}{l_{1a}} \\
&\vdots \\
\dot{q}_{(N-1)a} &= \frac{A_{(N-1)a}}{l_{(N-1)a}\rho_{(N-1)a}}(p_{(N-1)a} - p_{Na}) - \frac{F_{(N-1)a}A_{(N-1)a}}{\rho_{(N-1)a}l_{(N-1)a}} - A_{(N-1)a}g\frac{\Delta h_{(N-1)a}}{l_{(N-1)a}}
\end{aligned} \tag{3.11}$$

Here, q_c is the control choke flow and can be controlled through $q_c = K_c g\left(u_c\right)\sqrt{p_c - p_0}$ where u_c is the control signal, $g\left(u_c\right)$ is a nonlinear function giving the choke opening, p_c is the choke pressure, p_0 is the atmospheric pressure downstream the choke and K_c is some constant regarding the area of the choke. Also, the back pressure pump can be controlled, and is modeled by $q_{bpp} = \omega V$ where ω is the frequency and V is the volume it can move per stroke. v_d is taken as a disturbance that we wish to cancel, and it will frequently be assumed to be a harmonic disturbance so that

$$\dot{x}_d = v_d \tag{3.12}$$

$$\dot{v}_d = -\omega_{waves}^2 x_d \tag{3.13}$$

where ω_{waves} is the frequency of the wave disturbance.

3.4 Simulations With Comparison to Ullrigg Data

As a measurement of accuracy, the model was simulated and compared to data from Ullrigg tests, using logged data of the inputs as inputs to the model and logged

measurements of the pressures for comparison. During the Ullrigg tests, several test runs were done with heave emulation by moving the drill string vertically in the well. However, measurements of the down hole pressure were only available for the first test, a pure identification test without the use of a controller. For the rest of the tests, only choke pressure measurements were available.[2] The simulation results with the down hole pressure measurement can be seen in Figure 3.4 and the results for a control system test are presented in in Figure 3.5.

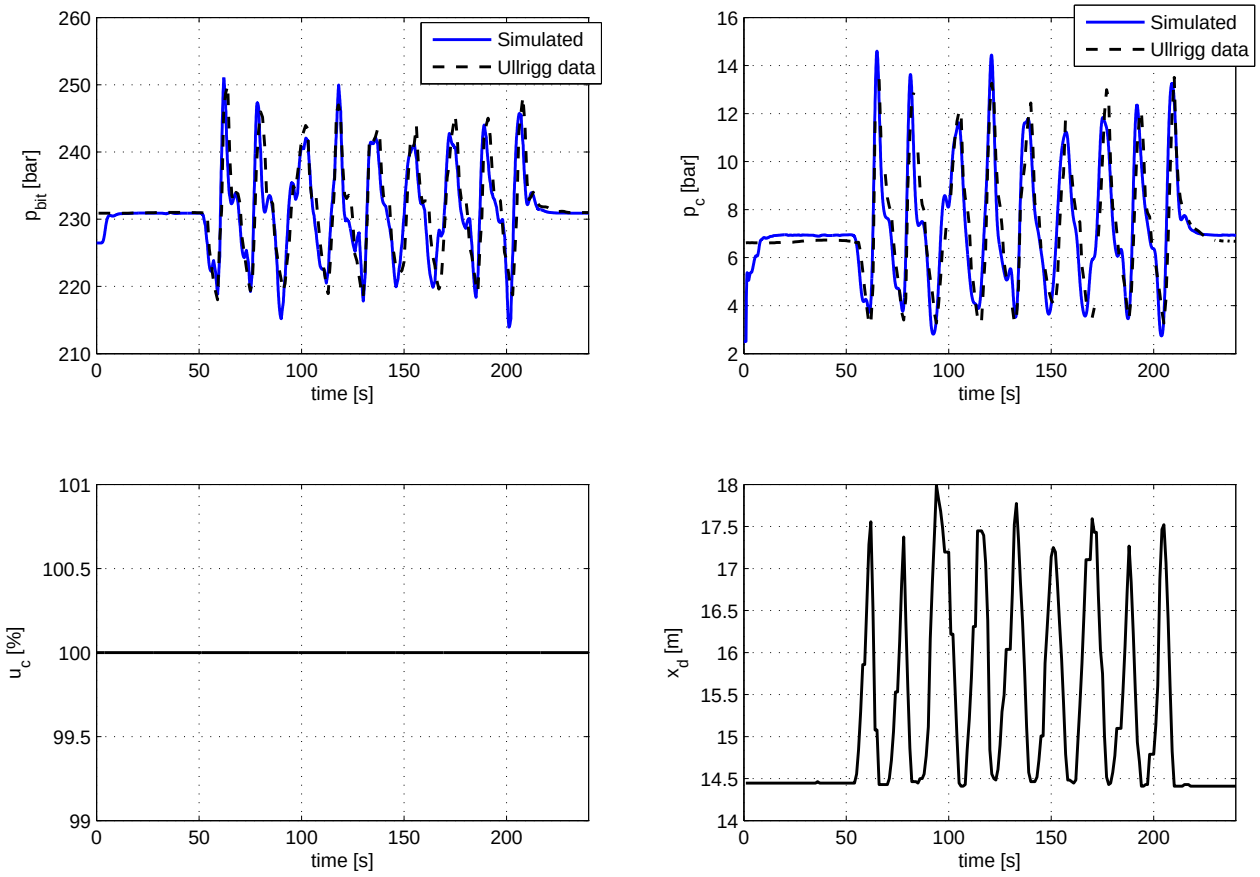

Figure 3.4: Simulation results compared to measured data, Ullrigg identification test. Bottom hole pressure, choke pressure, control signal and drill string movement.

[2]Down hole pressure measurements were actually available, but with a very low sampling rate, rendering them uninteresting for checking the accuracy of the model.

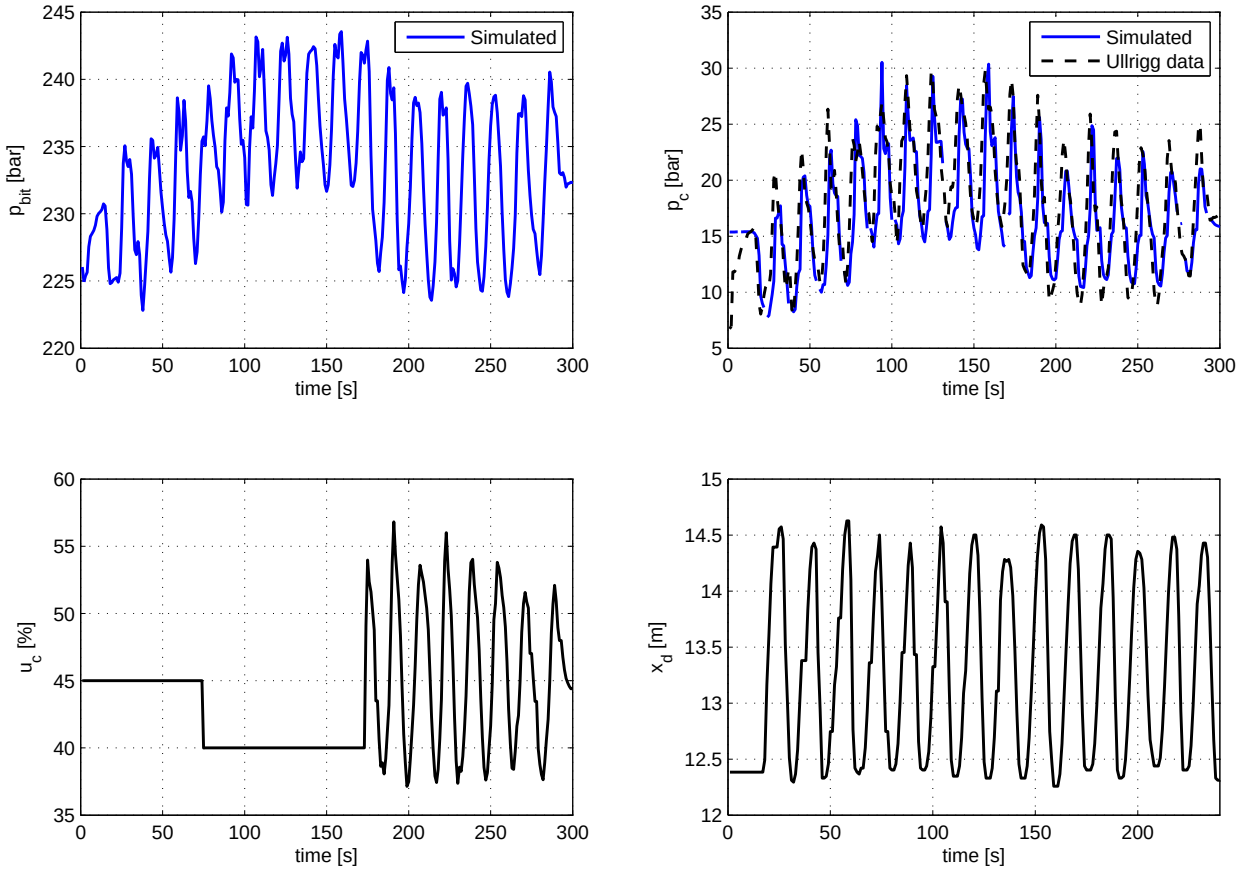

Figure 3.5: Simulation results compared to measured data, Ullrigg control system test. Bottom hole pressure, choke pressure, control signal and drill string movement.

As we can see, the model captures the main pressure dynamics very well. There might be large instantaneous errors in the estimates, but this is mostly due to timing issues and are quickly corrected. The error in the pressure peaks are nowhere larger than a couple of *bar*. Also, to see how the number of control volumes affect the accuracy of the model, the identification scenario was simulated using different numbers of control volumes. The results from this simulation are presented in Figures 3.6 and 3.7.

As we can see, there is really very little difference between the model simulated with different number of control volumes. The model simulated with $N = 5$ control volumes has some slight problems during the fastest pressure changes, and the differences are most of all in the timing. Note however that because of the approximation that the geometry of the drilling bit is valid in the entire lowermost flow volume, the constant c has been differently tuned in the three simulations to match the amplitude of the pressure oscillations. These results show that there is reason to believe that the model presented here might do well when used for controller design, thus we continue to devise control algorithms based on this higher order model.

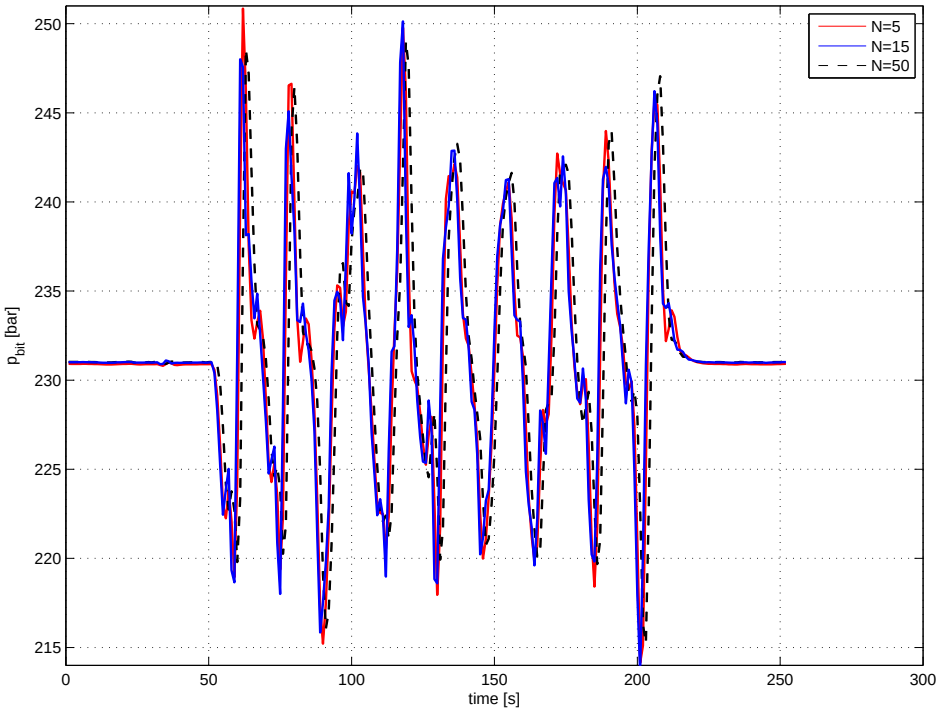

Figure 3.6: Bottom hole pressure as estimated with different number of control volumes.

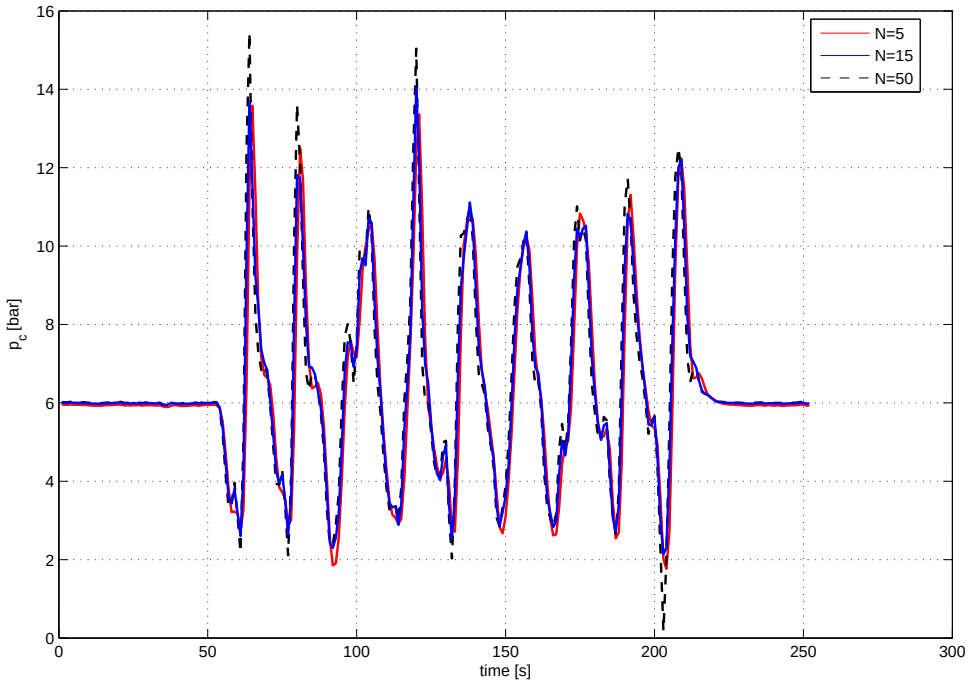

Figure 3.7: Choke pressure as estimated by different number of control volumes.

Chapter 4

Choke Pressure Regulation

As a first approximation to the pressure control problem, it was desirable to devise control algorithms for regulation of the choke pressure. That is, we wanted to find some way of making $\left|p_c - p_c^{ref}\right| \to 0$ as $t \to \infty$ in spite of the disturbance v_d. This is a simpler task than the bottom hole pressure regulation because of the vicinity to the control input, and thus quite standard techniques can be applied.

4.1 Higher Order Model for Controller Design

To illustrate one of the most obvious limitations with the existing controller based on the Kaasa model as described in chapter 2.1, let us first define the relative degree of an output with respect to an input. (This definition is quite standard, and the extension is taken from [15]) We consider a quite general class of SISO nonlinear dynamical system on the form

$$\dot{x} = f(x) + g(x)\,u + \sum_i w_i(x)\,d_i \tag{4.1}$$

$$y = h(x) \tag{4.2}$$

Here, $x \in \mathbb{R}^n$ is the state vector, $u \in \mathbb{R}$ is the control input, $d_i \in \mathbb{R}$ are measurable disturbances and $y \in \mathbb{R}$ is the measured output. For this formulation, we can define the relative degree of y with respect to u as the smallest positive integer r at which

$$L_g L_f^{r-1} h(x) \neq 0 \tag{4.3}$$

In the same way, we can define the relative degree of y with respect to a disturbance d_i as the smallest positive integer γ_i at which

$$L_{w_i} L_f^{\gamma_i - 1} h(x) \neq 0 \tag{4.4}$$

Here, the operator $L_a b(x)$ is the Lie derivative, which in this SISO case reduces to the directional derivative: $L_a b(x) = a(x) \cdot \nabla_x b$, where $b : \mathbb{R}^n \to \mathbb{R}$ and $a : \mathbb{R}^n \to \mathbb{R}^n$. Now, applying this to the Kaasa model (2.1), it is clear that the relative degree of y w.r.t. both the control input u and the measured disturbance v_d are the same; $r = \gamma = 1$. In this case, the theory of feed forward/feedback linearization [15] tells us

that we need to include the measured disturbance in a feed forward manner in our controller. However, it is quite clear intuitively that the relative degree of y w.r.t. the measured disturbance is much higher than that w.r.t. the control input for the case when the regulated output is p_c. The simplest model of the annulus dynamics that still incorporates this difference in relative degree is a two-volume version of the described model (3.11). See also figure 4.1.

$$\begin{aligned} \dot{p_c} &= \frac{\beta}{Al}\left(q + q_{bpp} - K_c g\left(u\right)\sqrt{p_c - p_0}\right) \\ \dot{q} &= \frac{A}{L\rho}\left(p_b - p_c\right) - \frac{A}{L\rho}F\left(q\right) - \frac{gA\Delta h}{L} \\ \dot{p_b} &= \frac{\beta}{Al}\left(-q - v_d A_d\right) \end{aligned} \tag{4.5}$$

For this model, it is clear that $r = 1$ but $\gamma = 3$. Then, the theory tells us that we actually do not need to have a feed forward term to compensate for the disturbance, a feedback linearizing controller is in itself enough to reject it.

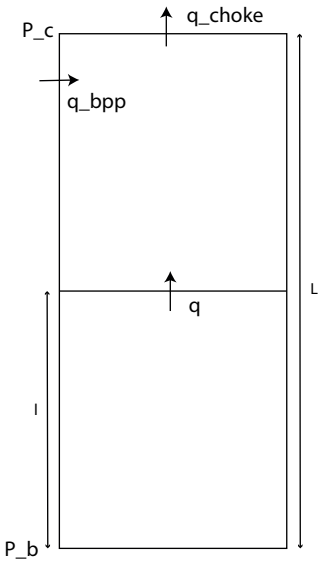

Figure 4.1: Schematic of 2-volume model.

4.2 Improved Controller for Choke Pressure Regulation

Using the two-volume model (4.5) for the controller design, it is a simple task to design a feedback linearizing controller to regulate the pressure output as well as reject the disturbance v_d. We desire the closed loop dynamics

$$\dot{p_c} = k_p\left(p_c^{ref} - p_c\right) \tag{4.6}$$

So, by a simple inspection of (4.5), we can find the required control input as

$$u = g^{-1}\left(\frac{q_c^*}{K_c\sqrt{p_c - p_0}}\right) \tag{4.7}$$

$$q_c^* = q + q_{bpp} - \frac{Al}{\beta}k_p\left(p_c^{ref} - p_c\right) \tag{4.8}$$

Notice of course that q would normally not be available for measurement, so one would also in this case require some form of observer for the unmeasured states. A straight forward choice is to use the same observer as (2.3), only without the drill string movement term. The interesting thing however is that in this case, the order of the hydraulic model used does not matter. This is because of the low relative degree of the output with respect to the control input. It is quite clear that the resulting system is stable, and this can for example be seen by investigating the poles of the closed loop (linear) system from p_c^{ref} to p_c. Also, this controller solves the pressure regulation problem as we have posed it, with exponential tracking of the reference.

Something else that is helpful for pressure regulation is to remember that we also might utilize the back pressure pump to our advantage. It seems that, since the control signal is the choke opening, we might experience saturations of the actuator if we try to tune our controller aggressively. Also, when operating at a certain choke pressure set point, we might experience that we need a quite small or large opening of the choke to reach that set point. This will in turn reduce the available room for actuation in case of large waves threatening to push us away from this set point, resulting in frequent saturation of the actuator and poor disturbance rejection. What is then proposed is to use the back pressure pump in a manner such that the required choke opening to reach the set point (without waves) is 50%. This way, we only need to change the pump flow whenever the choke pressure set point changes, but we will have the maximum available room for actuation in either direction to deal with the wave disturbance. This is achieved by the following pump flow

$$q_{bpp} = \frac{1}{2}K_c\sqrt{p_c^{ref} - p_0} \tag{4.9}$$

This approach has also been adopted for all other controllers in this thesis.

To see the effectiveness of this control strategy on the choke pressure, consider Figure 4.2. Here, we can see the simulation results when implementing the controller (4.7) on a higher order version of the well model and using the measured drill string movement from the Ullrigg test as an input. Notice however that this type of tight control, which has to take quick action when a measured deviance from the set point is noticed, requires a quite aggressive controller and probably a larger dimensioned choke than what was available at Ullrigg tests. For this simulation, it required a maximum choke flow of about 3000 $\frac{l}{min}$ for a pressure set point at 40 bar.

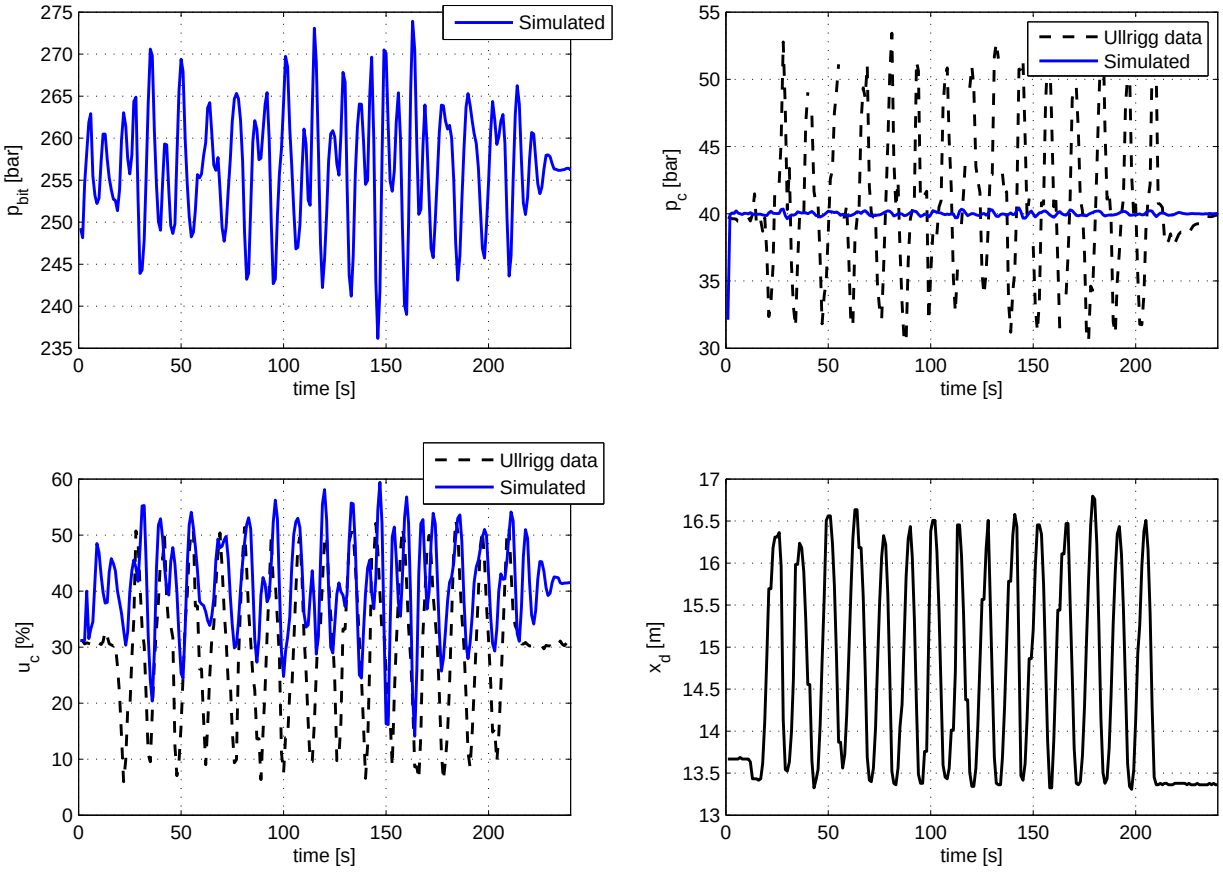

Figure 4.2: Simulation results, improved choke pressure controller. Bottom hole pressure, choke pressure, control signal and drill string movement.

As we can see, the choke pressure is nicely regulated, but notice that this causes great fluctuations of the bottom hole pressure. Seeing that the bottom hole pressure normally is the most vital to control due to the lack of concrete casings in this part of the well[1], the rest of this thesis is devoted to that issue.

[1] During drilling, it is customary to protect the well by installing concrete casings along the sides. This is of course not possible in the bottom hole where one is currently drilling.

Chapter 5

Down Hole Pressure Regulation

In this chapter, we explore the possibility of changing the control objective to regulating the down hole pressure. That is, we wish to device algorithms such that $\left|p_b - p_b^{ref}\right| \leq \epsilon$ as $t \to \infty$. This issue is a much more challenging task than the regulation of the choke pressure, due to the discussion in the last chapter on relative degree, so instead of demanding asymptotic tracking, we might also be satisfied with some small error.

If we now define the regulated variable as p_b, we can check that the relative degree of y w.r.t. the disturbance v_d is $\gamma = 1$, but the relative degree of y w.r.t. the input u in (4.5) is $r = 3$. Of course, we can extend the model of the drill string to an arbitrary number of control volumes N, and thus making $r = 2N - 1$. Actually, since the dynamics of the hydraulic transmission line really is governed by partial differential equations and that the model (3.11) is a discretization, the real system is infinite dimensional and in that respect we would have $r = \infty$. In any case, we have that $r > \gamma$ which means that not only will we need a feed forward from the measured disturbance, but we will also need an arbitrary number of its time derivatives to exactly cancel it.[1] Now, this becomes very difficult in practice unless we make some assumptions on the nature of the disturbance v_d. A natural and not horribly wrong assumption could be that the wave motion, and thus x_d, is a harmonic motion on the form

$$\begin{aligned} x_d &= A cos\left(\omega_{waves} t\right) && (5.1) \\ v_d &= -\omega_{waves} A sin\left(\omega_{waves} t\right) && (5.2) \end{aligned}$$

This would in turn mean that the disturbance is generated by a harmonic oscillator on the form

$$\begin{aligned} \dot{w}_1 &= w_2 \\ \dot{w}_2 &= -\omega_{waves}^2 w_1 && (5.3) \\ v_d &= w_2 \end{aligned}$$

[1] The number of time derivatives is equal to the relative degree, or equivalently, the number of states.

To be more sophisticated in our disturbance model, we could also make it the sum of several harmonic signals. This would make it closer to the real waves on the open sea, but it might be natural to assume that there is one main component with the largest amplitude that we wish to reject. The most general disturbance model that will be investigated is an arbitrary periodic signal with known period.

5.1 Some Intuition and an Adaptive Approach

We wish to start off by thinking intuitively on the problem to see what a controller might be expected to do. By inspecting the differential equation for p_b (3.9), it is clear that if we can design a controller that generates a flow down at the bit $q = -v_d A_d$, this flow will make $\dot{p_b} = 0$, and the problem would be solved. Then, thinking about the pressure transportation down the well annulus, a change in the pressure at the choke will appear some time later down in the bottom hole. So, assuming the harmonic disturbance (5.3), one would think that it should be possible to apply a control signal that would make the choke pressure p_c oscillate with the right frequency, amplitude and phase shift as to generate the correct q. Now, the fact that there is friction involved means that it is difficult to say, without the use of a detailed model, what the amplitude and phase shift of these oscillations should be. Thus, we turn to the model (4.5) to try to derive a controller. As stated, we wish to have

$$
\begin{aligned}
q &= -v_d A_d && (5.4)\\
&\Downarrow \\
\dot{q} &= \omega_{waves}^2 x_d A_d && (5.5)\\
&\Downarrow \\
\omega_{waves}^2 x_d A_d &= \frac{A}{L\rho}\left(p_b - p_c^{desired}\right) - \frac{A}{L\rho} F q - \frac{gA\Delta h}{L} && (5.6)\\
&\Downarrow \\
p_c^{desired} &= p_b - Fq - \rho g \Delta h - \frac{\omega_{waves}^2 x_d A_d L \rho}{A} && (5.7)
\end{aligned}
$$

Now, assuming that p_b is kept constant, as per our wish, and substituting the desired value for q, we get

$$
\begin{aligned}
\dot{p_c}^{desired} &= -F\omega_{waves}^2 x_d A_d - \frac{\omega_{waves}^2 v_d A_d L \rho}{A} && (5.8)\\
&\Downarrow \\
-F\omega_{waves}^2 x_d A_d - \frac{\omega_{waves}^2 v_d A_d L \rho}{A} &= \frac{\beta}{Al}\left(-v_d A_d + q_{bpp} - K_c g\left(u\right)\sqrt{p_c - p_0}\right) && (5.9)\\
&\Downarrow \\
u &= g^{-1}\left(\frac{-v_d A_d + q_{bpp} + \frac{F\omega_{waves}^2 x_d A_d A l}{\beta} + \frac{\omega_{waves}^2 v_d A_d L l \rho}{\beta}}{K_c\sqrt{p_c - p_0}}\right) && (5.10)
\end{aligned}
$$

The above derivation shows that the desired choke pressure is essentially the sum of two sinusoids, and if we use a higher order model, it would have shown that we need the sum of a larger number of sinusoids. The interesting thing is however that these sine functions all have the same period, namely the period of the wave disturbance. The Harmonic Addition Theorem (see the appendix, A.5) then tells us that it is always possible to write the sum of an arbitrary number of sinusoidal function with the same frequency as a single, phase shifted sinusoid

$$\sum_i A_i cos\left(\omega t + \delta_i\right) = Acos\left(\omega t + \delta\right) \tag{5.11}$$

Here, the amplitude A and phase shift δ are both functions of all the amplitudes A_i and phase shifts δ_i. Thus we have confirmed our suspicion that we can control the bottom hole pressure by applying the correct sinusoid to the choke pressure, and we have also found the control signal that would produce this sinusoid. However, this calculation is based on a pretty low order model of the system, and seeing how the system is really infinite dimensional, it could potentially require a lot of work to calculate a sufficiently accurate control signal. Instead, we might try to go about this in a more model independent way: We have already shown that the desired choke pressure should be

$$p_c^{desired} = p_{nom} + Csin\left(\omega_{waves} t + \phi\right) \tag{5.12}$$

where $p_{nom} = p_b^{ref} - \rho g \Delta h$, and the amplitude C and phase ϕ are unknowns to be estimated. In this case, we can derive the control law by

$$\begin{aligned}
\dot{p}_c^{desired} &= \omega_{waves} C cos\left(\omega_{waves} t + \phi\right) && (5.13)\\
&\Downarrow && (5.14)\\
\omega_{waves} C cos\left(\omega_{waves} t + \phi\right) &= \frac{\beta}{Al}\left(q + q_{bpp} - K_c g\left(u\right)\sqrt{p_c - p_0}\right) && (5.15)\\
&\Downarrow && (5.16)\\
u &= g^{-1}\left(\frac{q + q_{bpp} - \frac{Al\omega_{waves} C cos(\omega_{waves} t + \phi)}{\beta}}{K_c\sqrt{p_c - p_0}}\right) && (5.17)
\end{aligned}$$

Again, one would of course have to estimate the flow q. A bigger issue is how to estimate the two unknown parameters C and ϕ, and one would probably search for some kind of adaptive law to update these parameters. If we write the bit pressure as

$$p_b = p^{ref} + Bsin(\omega_{waves} t + \psi) \tag{5.18}$$

we would like to find adaptive laws

$$\begin{aligned}
\dot{C} &= f_1\left(B, \psi\right) && (5.19)\\
\dot{\phi} &= f_2\left(B, \psi\right) && (5.20)
\end{aligned}$$

so that we would have a stable equilibrium

$$f_1\left(0, 0\right) = 0 \tag{5.21}$$

$$f_2(0,0) = 0 \tag{5.22}$$

meaning that $p_b = p^{ref}$. However, measuring B and ψ is quite difficult and time consuming, and it is not very clear how to design the adaptive laws. What makes this very difficult is that both B and ψ are functions of both C and ϕ in an implicit manner (which can be seen from several times applying the harmonic addition theorem). Thus, the literature was searched for more established control approaches for disturbance rejection.

5.2 Output Regulation Theory

One interesting approach for tracking/disturbance rejection for nonlinear systems is the uniform output regulation controller, and the theory in this section is completely taken from the book [16]. We consider a system on the form

$$\dot{x} = f(x,w,u) \tag{5.23}$$
$$e = h_r(x,w) \tag{5.24}$$
$$y = h_m(x,w) \tag{5.25}$$

Here, $x \in \mathbb{R}^n$ is the state vector, $u \in \mathbb{R}^k$ is the control input, $e \in \mathbb{R}^{l_r}$ is the regulated output and $y \in \mathbb{R}^{l_m}$ is the measured output. The external input $w \in \mathbb{R}^m$ is generated by a so called exosystem on the form

$$\dot{w} = Sw \tag{5.26}$$

It is important to notice that this exosystem could include a harmonic disturbance on the form (5.3) as well as a constant reference signal for the regulated output. Now, the theory tells us that a controller solving the output regulation problem will, for certain boundedness assumptions on w, make the system (5.23) globally uniformly convergent, and make the regulated output $e(t)$ tend to zero. The convergent property is defined in the following way:

Definition 1. [Convergent Systems]
A system $\dot{z} = F(z,t)$, where $z \in \mathbb{R}^d$, $t \in \mathbb{R}$ and F is locally Lipschitz in z and piecewise continuous in t is said to be:

- Convergent in a set $\mathcal{Z} \subset \mathbb{R}^d$ if there exists a solution $\bar{z}(t)$ satisfying the following conditions:
  (i) $\bar{z}(t)$ is defined and bounded for all $t \in \mathbb{R}$
  (ii) $\bar{z}(t)$ is asymptotically stable in $\mathcal{Z}$.
- Uniformly convergent in $\mathcal{Z}$ if it is convergent in $\mathcal{Z}$ and $\bar{z}(t)$ is uniformly asymptotically stable in $\mathcal{Z}$.
- If it is uniformly convergent in $\mathcal{Z} = \mathbb{R}^d$, then it is said to be globally uniformly convergent.

The definitions of stability are the more or less standard definitions of Lyapunov stability from nonlinear systems theory. These can be found in any text book on nonlinear systems, but are included in the appendix for completeness. In other words, a controller based on the uniform output regulation theory would guarantee both the stability of the closed loop system as well as the asymptotic rejection of the disturbance.

The theory tells us that if the output regulation problem is solvable, then there exist continuous mappings $\pi(w)$ and $c(w)$ that satisfy the regulator equations

$$\dot{\pi} = f(\pi(w(t)), w(t), c(w(t))) \tag{5.27}$$
$$0 = h_r(\pi(w(t)), w(t)) \tag{5.28}$$

Then, having solved these equations, the uniform output regulation problem is solved by the controller

$$u = c(w) + K(x - \pi(w)) \tag{5.29}$$

Here, K is a matrix that makes the matrix function $A(\mathcal{X}) + B(\mathcal{X})K$ quadratically stable over $\mathcal{X} \in \mathbb{R}^{n+m+k}$. The matrices are defined by

$$A(\mathcal{X}) := \frac{\partial f}{\partial x}(x, w, u) \tag{5.30}$$
$$B(\mathcal{X}) := \frac{\partial f}{\partial u}(x, w, u) \tag{5.31}$$

The definition of quadratic stability can also be found in the appendix, Chapter A.3. For a proof that this controller actually solves the output regulation problem, see [16].

The obvious and immediate attractiveness about this theory is that it guarantees that $e(t)$ will tend to zero, which is a quite strong result. However, a significant disadvantage is that this requires perfect knowledge of both the system model and the disturbance model. Neither of these will in general be perfectly known, so there is a question about the performance and robustness of the controller under non-ideal circumstances.

5.3 Output Regulation Controller for Low Order Model

Using the two-volume model for the annulus dynamics (4.5), one can formulate the regulator equations and solve them to find the controller that solves the output regulation problem. The regulator equations take the form

$$\dot{\pi_1} = \frac{\beta}{Al}\left(\pi_2 + q_{bpp} - K_c g(c)\sqrt{\pi_1 - p_0}\right) \tag{5.32}$$
$$\dot{\pi_2} = \frac{A}{L\rho}(\pi_3 - \pi_1) - \frac{A}{L\rho}F\pi_2 - \frac{gA\Delta h}{L} \tag{5.33}$$

$$\begin{aligned}
\dot{\pi_3} &= \frac{\beta}{Al}\left(-\pi_2 - w_2 A_d\right) && (5.34)\\
0 &= w_3 - \pi_3 && (5.35)\\
\dot{w_1} &= w_2 && (5.36)\\
\dot{w_2} &= -\omega_{waves}^2 w_1 && (5.37)\\
\dot{w_3} &= 0 && (5.38)
\end{aligned}$$

Here, the regulated output has been defined as $e = p_b^{ref} - p_b = w_3 - p_b$. Now, solving this is a matter of simple back substituting starting from $w_3 = \pi_3$. The derivations can be found in the appendix, Chapter A.2, but the results are given by

$$\begin{aligned}
\pi_3 &= w_3 && (5.39)\\
\pi_2 &= -w_2 A_d && (5.40)\\
\pi_1 &= w_3 - \frac{L\rho\omega_{waves}^2 w_1 A_d}{A} - F\pi_2 - \rho g \Delta h && (5.41)\\
c &= g^{-1}\left(\frac{-w_2 A_d + q_{bpp} + \frac{Ll\rho\omega_{waves}^2 w_2 A_d}{\beta} + \frac{F\omega_{waves}^2 w_1 A_d Al}{\beta}}{K_c\sqrt{\pi_1 - p_0}}\right) && (5.42)
\end{aligned}$$

Then, as described earlier, the controller takes on the form

$$u = c + K\left(x - \pi\right) \tag{5.43}$$

for some matrix $K = \begin{bmatrix} k_1 & k_2 & k_3 \end{bmatrix}$ which satisfies the quadratic stability property. Also, $\pi = \begin{bmatrix} \pi_1 & \pi_2 & \pi_3 \end{bmatrix}^T$.

The first interesting aspect to notice here is that the first part of the controller, c, corresponds exactly to the intuitive derivation (5.10). This means that the output regulator first applies what we can think of as an "open loop" attempt to produce the exact signal that will counteract the disturbance. The second part, $K\left(x - \pi\right)$, is something like a proportional controller that tries to penalize deviation from the "dynamic reference" π. The justification for calling this a reference comes from inspecting the previous derivation. We can first of all see that $\pi_3 = w_3 = p_b^{ref}$, but also π_2, which corresponds to q, takes on the desired value that would exactly cancel the heave-generated flow. Now, this is of course a step up from what we derived in (5.10) because of the second part, but one might still be worried that this controller would not perform very well on the real system, as the model used here is still of very low order. Thus, we inspect the output regulation controller for a higher order model as well.

5.4 Output Regulation Controller for Higher Order Model

As described earlier, the main problem of the existing controller used in full scale tests is that it does not make any distinction between the pressure dynamics at the bit and the pressure dynamics at the choke. The two-volume model used in the previous section does, but the fact that it is of such low order means that it will

inevitably wrongly estimate the time distribution for a pressure wave traveling from the bit to the choke and vice versa. Now, this can be remedied by using a higher order model of the annulus dynamics and applying the same theory as earlier. Of course, this will greatly complicate the regulator equation and increase the dimensions, but the structure of the equations will nevertheless make it a question of mechanical back substituting from the output error equation. In this work, this was done for a total of five control volumes describing the annulus pressure dynamics in the form of (3.11). The solution of the regulator equations can once again be found in the appendix, Chapter A.2. The final controller is of the exact same form, only this time $K \in \mathbb{R}^{1\times 2N-1}$ where N is the number of control volumes. Of course, this will also greatly increase the dimension of the state vector x, and it is natural to assume that most of these states will not be available for measurement. Thus, there will most likely be a need for some observer to be included in this control strategy.

5.5 Output Feedback Controller for Output Regulation

For the most general case, we can assume that neither the full state x nor the full exosystem w are measured, but that the measurement y consists of some combination of states and external signals. In this case, we can replace the measured x and w by their estimated values $\hat{x}$ and $\hat{w}$ returned from some observer. The entire control system would then be described by

$$\begin{aligned} u &= c(\hat{w}) + K(\hat{x} - \pi(\hat{w})) && (5.44)\\ \dot{\hat{x}} &= f(\hat{x}, \hat{w}, u) - L_x(\hat{y} - y) && (5.45)\\ \dot{\hat{w}} &= S\hat{w} - L(\hat{y} - y) && (5.46)\\ \hat{y} &= h_m(\hat{x}, \hat{w}) && (5.47) \end{aligned}$$

This is of course contingent on some detectability condition on the system, and in this case we must also ensure that the matrix equation

$$\begin{bmatrix} A(\mathcal{X}) & B(\mathcal{X}) \\ 0 & S \end{bmatrix} + L \begin{bmatrix} C(\mathcal{X}) & H(\mathcal{X}) \end{bmatrix} \tag{5.48}$$

is quadratically stable over $\mathcal{X} \in \mathbb{R}^{m+n+k}$. Here, the additional matrices are defined by

$$\begin{aligned} C(\mathcal{X}) &= \frac{\partial h_m}{\partial x}(x, w) && (5.49)\\ H(\mathcal{X}) &= \frac{\partial h_m}{\partial w}(x, w) && (5.50)\\ L &= \begin{bmatrix} L_x^T & L_w^T \end{bmatrix}^T && (5.51) \end{aligned}$$

5.6 Internal Model Principle

A very powerful and popular way of designing linear control systems for reference tracking or disturbance rejection is through the internal model principle, which states

that we simply need to include a model of the reference or disturbance in our controller. We will first go through the basics of this principle and then show how this can be used in our case. The theory on the internal model principle that is given here is loosely based on that from [17].

First of all, let us define the external signal that we wish to reject or track. In our case, this is a disturbance, and to make it general, let us assume that the disturbance d_g can be described by the following differential equation

$$\frac{d^q d_g(t)}{dt^q} + \sum_{i=0}^{q-1} \kappa_i \frac{d^i d_g(t)}{dt^i} = 0 \tag{5.52}$$

Then, we can take the Laplace transform of the signal as

$$D_g(s) = \frac{N_d(s)\, x_d(0)}{\Gamma_d(s)} \tag{5.53}$$

where $\Gamma_d(s)$ is called the disturbance generating polynomial and is defined by

$$\Gamma_d(s) = s^q + \sum_{i=0}^{q-1} \kappa_i s^i \tag{5.54}$$

To illustrate, if we let the disturbance signal be the harmonic disturbance described earlier, we can set $d_g(t) = -\omega_{waves} A sin(\omega_{waves} t + \phi)$. This will in turn lead us to find $\Gamma_d(s) = s^2 + \omega_{waves}^2$. As we shall see, this is good news, because the disturbance generating polynomial is all we need to know about the disturbance, and thus only the frequency needs to be known. The amplitude and phase can be contributed to initial conditions, so we do not need to concern ourselves with these unknowns.

Now, to continue the quite general discussion, let us assume that the disturbance can enter the system at any location, and let us call the plant transfer function $G(s)$, which can be factored into $G(s) = G_1(s) G_2(s)$, according to the factors before and after the disturbance enters the system. See also Figure 5.1 for clarification. Looking at this figure, we see that the effect on the output from the disturbance can be written as

$$Y(s) = S(s) G_2(s) D_g(s) \tag{5.55}$$

where the sensitivity function is written

$$S(s) = \frac{1}{1 + G_1(s) G_2(s) C(s)} \tag{5.56}$$

Now, rewriting the controller as $C(s) = \frac{N_c(s)}{D_c(s)}$, we can express the transfer function as

$$Y(s) = \frac{D_c(s)}{D_c(s) + G_1(s) G_2(s) N_c(s)} G_2(s) D_g(s) \tag{5.57}$$

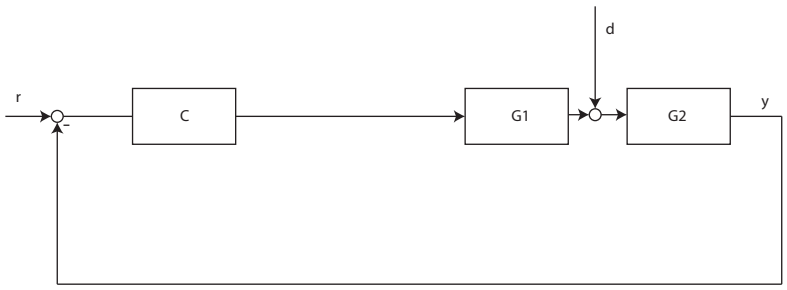

Figure 5.1: Block diagram of disturbance, system and controller.

At this point it is clear that if the denominator of the controller, $D_c(s)$, contains the factors of the disturbance generating polynomial, $\Gamma_d(s)$, the influence of the disturbance will vanish asymptotically.[2] Thus, if we know a sufficiently accurate model of the disturbance, it is enough to include this disturbance generating polynomial in our controller, assuming we have closed loop stability.

5.7 Internal Model Principle Controller for Down Hole Pressure

The internal model principle is, as stated, a very powerful and popular tool for disturbance rejection, but the analysis given earlier is only applicable to linear systems. Our well system is nonlinear, but when we assume linear friction, like argued earlier, the nonlinearity is just around the choke input. Looking to the literature, there is a lot of theory on feedback linearization, but in our case, we can actually get away with something really simple and still have a true linear input-output map even without knowing very much about the rest of the system. Let the system be given by the model (3.11), and let us state the first step of this controller design to be

$$u = g^{-1}\left(\frac{q*}{K_c\sqrt{p_c - p_0}}\right) \tag{5.58}$$

$$q* = q_{bpp} - \bar{u} \tag{5.59}$$

Then, we will have a true linear input-output map from $\bar{u}$ to $y = p_b$, which can be described by the transfer function $G_0(s)$. This will then enable us to use the full spectrum of powerful linear SISO control design tools including the internal model principle. However, before we do that, we might want to add an additional step to the control design procedure. The system described by $G_0(s)$ is not very well behaved when it comes to the placement of the eigenvalues. Specifically, for any order approximation, it will have a zero eigenvalue, and the rest of the eigenvalues will be complex with relatively small, negative real values. Thus, to make the system more well behaved and robust, we might want to do some additional loop shaping in an intermediate step. Now, it can easily be verified that the system is controllable from $\bar{u}$, so what is proposed is to use a simple pole placing technique and find a

[2]Notice that, for a constant reference or disturbance, $D_g(s) = \frac{1}{s}$. In other words, integral action is the simplest form of the internal model principle.

constant state feedback on the form

$$\bar{u} = v + K(r - x) \tag{5.60}$$

where v is the input from the next step, K is the constant feedback matrix found by pole placement, r is the (constant, $2N-1$-dimensional) reference signal and x is the state vector. This will render the transfer function from v to y, $G(s)$, as well behaved as we like, and will simplify the design of the last step. One should however notice already at this stage that a full state feedback is of course not available, so we will probably need an observer. Also, the input u saturates between 0 and 1, so this will also affect the possibility to choose the poles at any desired location.

Proceeding with the controller design, it is now sufficient to find a controller $C(s)$ that maintains the closed loop stability and at the same time includes the disturbance generating polynomial in the denominator. There are probably several different ways of ensuring this, but a simple and straight forward way is the following: Consider a disturbance $d_g(t)$ on the form

$$d_g(t) = \sum_{j \in \mathcal{J}} \mathsf{d}_j e^{i\omega_j t} \tag{5.61}$$

where $\mathcal{J}$ is a finite set of integers and $\omega_j \in \mathbb{R}$. That is, the disturbance is a superposition of a constant and a finite number of sinusoids. Then the internal model controller can be written as

$$C(s) = Q_0 + \frac{Q_1}{s} + \sum_{j \in \mathcal{J}} \frac{Q_j s}{s^2 + \omega_j^2} \tag{5.62}$$

where $Q_j, j \in \mathcal{J} \cup \{0, 1\}$ are appropriate constants. Notice that the first term is a proportional controller and the second term adds integral action to account for constant disturbances or model errors. The final sum contains the generating polynomial for all the finite number of sinusoids present in the disturbance. On the issue of stability, we now obviously have a stable open loop consisting of the controller $C(s)$ in series with the plant $G(s)$ provided the constant state feedback places the poles of $G(s)$ in the left half plane. Thus, one can resort to classical frequency domain techniques for unity feedback systems to tune the constants Q_j for closed loop stability.

One more reason for being interested in this type of controller is the results from [18]. They show that a small gain controller on the form (5.62) guarantees stability for all exponentially stable and well-posed linear systems, also including infinite dimensional systems. Although we have only used this controller on a finite dimensional approximation of the real system, the system described by the infinite dimensional partial differential equations could probably be described as a well-posed system and this controller would guarantee stability.

The entire control scheme can be summarized by the following block diagram, Figure 5.2.

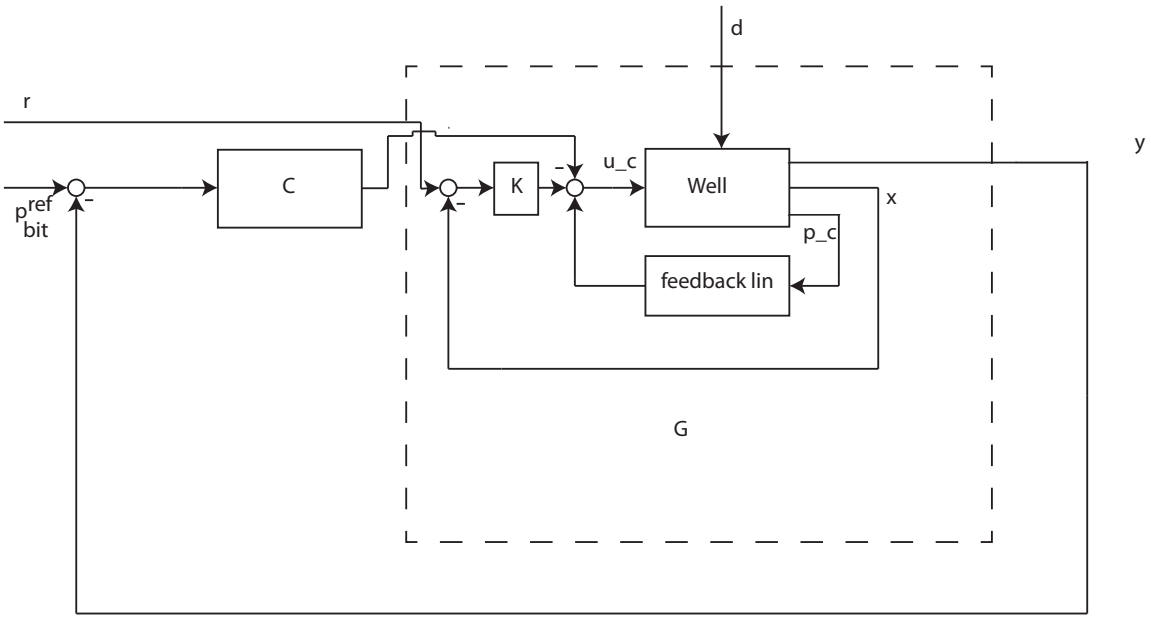

Figure 5.2: Block diagram of entire IMC structure.

5.8 Repetitive Controller for Down Hole Pressure

A version of the internal model principle that has received some attention is the so called repetitive controller [19]. The idea behind this approach is that if we can find a generator for a general periodic signal, the internal model principle tells us that if this generator can be included in the feedback loop at the same time as the unity feedback loop is stabilized, we will be able to reject any periodic disturbance asymptotically. Such a periodic signal generator can actually quite simply be found by the positive unity feedback on a delay element of the appropriate period time. Including this in the feedback loop, like in Figure 5.3, the internal model principle then tells us that we should be able to reject any periodic disturbance with the appropriate period.

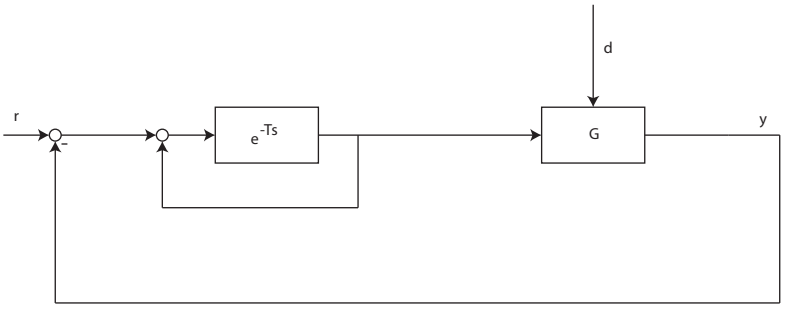

Figure 5.3: Block diagram of pure repetitive controller.

Of course, this probably sounds too good to be true, and is also just that. It can be shown by the small gain theorem [19] that a sufficient condition for the stability of

the feedback system in Figure 5.3 is

$$\|1 - G\|_\infty < 1 \tag{5.63}$$

where $\|*\|_\infty$ denotes the standard H^∞ norm. Furthermore, this will only be satisfied by a direct transmission in G, i.e. G must have relative degree zero. In other words, the pure repetitive controller is often unstable for systems of practical interest.[3] However, the situation is perhaps not as dark as it seems: The repetitive controller as it is stated takes on an almost impossible task: to track or reject any periodic signal. This would also include for instance a square signal consisting of infinitely many frequency components, and especially components in a very high frequency range. Any physical disturbance signal would be bounded by some upper frequency bound, and so we would be happy to disregard anything above this bound. Thus, a simple way of trading off stability properties against unnecessarily powerful disturbance rejection is to include a low-pass filter $f(s)$ in the delay element, with $\|f\|_\infty = 1$ and cut-off frequency above the required bound. Another simple way of helping the stability properties of the closed loop system is to include some other controller $C(s)$ in series with the repetitive generator, like shown in Figure 5.4. The new sufficient condition for stability is then that

$$\|f(1 - CG)\|_\infty < 1 \tag{5.64}$$

which is much easier to satisfy, and is actually exactly the same as the model matching problem in H^∞ control. Thus, several different methods for robustly designing the filter and controller have been proposed in the literature.

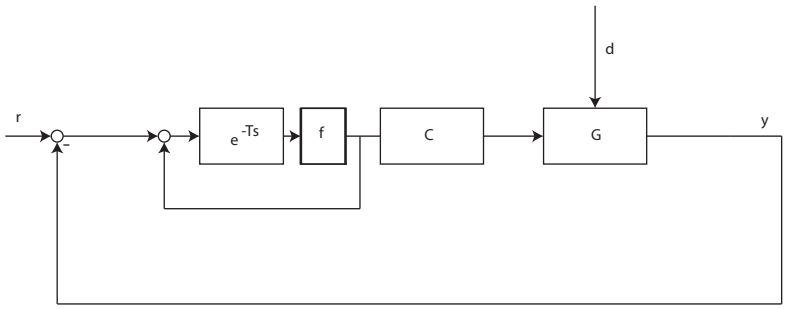

Figure 5.4: Block diagram of altered repetitive control.

Now, applying this to our system, we would take the two first steps to linearize and loop shape exactly like explained earlier. Then, the last step would be to design the filter f and controller C so as to get good disturbance rejection while maintaining the closed loop stability of the overall system. A simple and natural choice for the filter is a first order low-pass filter with cut-off frequency $\omega_f \gg \omega_d$ where ω_d is the largest frequency component of the disturbance. That is, the filter

$$f(s) = \frac{\omega_f}{s + \omega_f} \tag{5.65}$$

[3]The condition is sufficient but not necessary. However, it is probably close to necessary.

For the controller C, the choices are probably many, but a straight forward choice would be to invert the plant model G (it has no zeros) and filter this by an appropriate low-pass filter so that we for low frequencies have a good approximation to the inverted model, but still have a proper transfer function

$$C(s) = \frac{1}{G(s)(s+\omega_c)^r} \tag{5.66}$$

where r is the relative degree of G.

A small, but helpful trick, taken from [20], that actually is quite important for the performance of this controller is related to the choice of the time delay T. The obvious thing is to set T equal to the period of the disturbance. This works, but is however not the best choice because of the added low pass filter f. It is clear that this low-pass filter will add a small, additional phase delay to the delayed signal, and we can look at the Taylor expansion of the term $f(s)e^{-Ts} = f_1(s)e^{-T_1 s}$, where T_1 is the period of the disturbance and $f_1(s)$ should be as close as possible to 1 for all frequencies in the interesting range. Now, we have that the Taylor expansion of $f_1(s)$ is equal to $f_1(s) = 1 + \left(T_1 - T - \frac{1}{\omega_f}\right)s + O\left(|s|^2\right)$. Thus, the best choice for the time delay is actually $T = T_1 - \frac{1}{\omega_f}$. For instance, if the period of the disturbance is $T_1 = 12\ s$ and we use a cut-off frequency of $\omega_f = 5\ \frac{rad}{s}$, we would use a delay of $T = 11.8\ s$.

5.9 Relaxing The Assumptions

So far, several different ways of efficiently rejecting a periodic disturbance have been described. Still, all of them have weaknesses that make them more or less unsuitable for practical use: The output regulations controller is dependent on a perfect model of both the system and the disturbance, the internal model controller and the repetitive controller were described using a state feedback that does not exist, and the repetitive controller described would also need a good model of the system for the inverted plant transfer function. Thus, in order to close in on a practical solution to the problem, relaxation of some of the necessary knowledge for the disturbance rejecting controller is needed. Of course, there will always be a trade-off between knowledge and performance. As we will see, the output regulation controller will achieve perfect rejection, but it also needs perfect information. The controller that actually offers the most for least seems to be the internal model principle controller, which only needs to know the frequency of the disturbance and a stable closed loop in order to asymptotically reject the disturbance. (Although it may take longer than the output regulation controller.) Also, the repetitive controller can be seen as a variant of (5.62) if we let the disturbance model grow infinitely in the manner of a Fourier series, so they are really not very different. Now, the internal model controller was presented in a way that requires us to know the choke model and use a state feedback, both criteria that are actually not needed for the stability of the closed loop system. It can be shown [21] that even on a passive nonlinear system, the output feedback controller (5.62) will make the closed loop stable, so there might not be a need for the feedback linearizing control (5.58). Note however that the nonlinear dynamics might

introduce other harmonics that are not compensated for, so we might not achieve asymptotic rejection. The entire controller would then be on the form

$$u = g^{-1}(-v) \tag{5.67}$$

where v is the output signal from the IMC. The reason for the negative value of v is the fact that the choke flow has a negative influence on the time derivative of p_c. (Compare for instance to (5.58) and (4.5).) This polarity, together with the dissipative nature of the friction force, is necessary for the passivity of the system from v to p_b. A proof of this passivity is included in the appendix, Chapter A.1. Also, even when considering the linear input-output map of the feedback linearized system, the only conditions for asymptotic rejection of the disturbance is that the generating polynomial is a part of the controller and that the closed loop system is stable. Of course, a full state feedback would allow us to make the system very well behaved, but it should be the case that we can make due with a more classical error feedback PID controller in parallel with the internal model in order to have a stable closed loop system. In fact, it is true that for any order approximation of the well pressure dynamics, the closed loop system using (5.62) and appropriately sized coefficients might be unstable, especially without the additional state feedback. However, this controller can actually be seen as a PI controller in parallel with the required internal model, so if we just elevate the phase response with a partial derivative action on the form $\frac{\tau s}{\tau s+1}$, we might be able to achieve a well behaved closed loop response.

Having all of these different approaches to the down hole pressure regulation at our disposal, we are confident that we will be able to achieve the desired pressure regulation. Thus, we continue by implementing them and assessing their performance in simulations.

Chapter 6

A Simulation Study and Comparison of the Proposed Controllers

To compare the performance of the different controllers under different assumptions, it was decided to do a simulation study imposing different conditions, i.e. errors in system and disturbance models. All the controllers described earlier were tested on a model of the system with different orders and a more realistic version of the wave disturbance, and the results are presented in this chapter. We begin the simulation study by showing some low-order results for the repetitive controller, as more of a "proof of concept", because the higher order results are very poor. Then, we will go through combinations of a 5-volume version of the well model, a 15-volume version, a 1st order version of the disturbance and a 3rd order version of the disturbance.[1] But first, let us look closer at how the higher order wave disturbance is modeled.

6.1 A More Realistic Wave Model

There has actually been done a lot of work on characterizing the wave patterns at sea, as this is quite important for a lot of applications in the maritime and offshore businesses, e.g. for dimensioning of ships and other offshore vessels or for designing dynamic positioning systems. In the late 1960's, an extensive measurement program was carried out in the North Sea, known as the Joint North Sea Wave Project (JONSWAP), which resulted in an empirical characterization of the energy spectrum of the observed waves. A typical form of this spectrum can be seen in Figure 6.1. Depending on the parameters, the spectrum is quite sharp, and there seems to be a quite narrow frequency range through which most of the energy is delivered. This could be an indication that a single harmonic disturbance is sufficient, but we still want to make things a bit more realistic. Now, this is of course the spectrum of the waves themselves, and it is natural to assume that a floating rig will act as a low-pass

[1] The reason for choosing the 5 and 15 volume versions is the following: On one hand, a 5-volume model will lead to a 9th order set of ODE's, which is about the largest order that is practical for controller design of the controllers used here. On the other hand, the 5-volume model is maybe not a sufficiently accurate model of the real system, but as it was shown earlier, increasing the number of control volumes beyond 15 makes little difference.

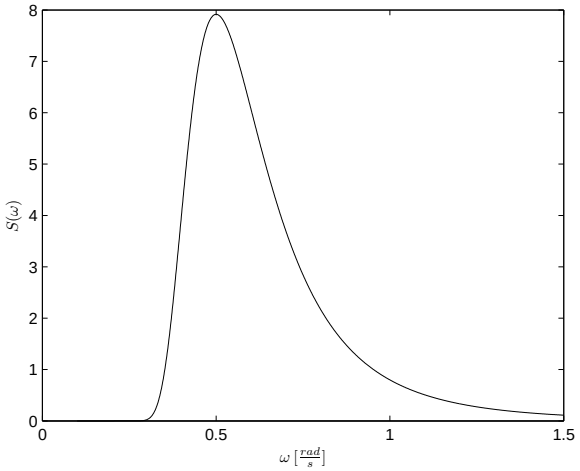

Figure 6.1: JONSWAP wave energy spectrum.

filter seen from the vertical position of the water to the vertical position of the rig. Thus, it seems fair to assume that not only can we disregard high frequency waves, but we might also be justified in assuming that the amplitude of the rig movement is somewhat smaller than the amplitude of the waves. Also, there is an international standard for the so-called sea state, which is replicated in Table 6.1. Here we can see that, even in the north sea where the conditions are worse than average, about 90% of the time, the observed wave height is less than $4.0m$.

Code	Description	Wave height	% world wide	% north atlantic	% northern north Atlantic
0	Glassy	$0m$	-	-	-
1	Calm	$0 - 0.1m$	11.2486	8.3103	6.0616
2	Smooth	$0.1 - 0.5m$	-	-	-
3	Slight	$0.5 - 1.25m$	31.6851	28.1996	21.5683
4	Moderate	$1.25 - 2.5m$	40.1944	42.0273	40.9915
5	Rough	$2.5 - 4.0m$	12.8005	15.4435	21.2383
6	Very rough	$4.0 - 6.0m$	3.0253	4.2938	7.0101
7	High	$6.0 - 9.0m$	0.9263	1.4968	2.6931
8	Very high	$9.0 - 14.0m$	0.1190	0.2263	0.4346
9	Phenomenal	$> 14.0m$	0.0009	0.0016	0.0035

Table 6.1: Sea state descriptions.

Tying these things together, it can be shown that a way to generate wave-induced responses in the time domain is to discretize the spectrum and write the wave elevation $\xi(t)$ as a function of N harmonic components [22]

$$\xi(t) = \sum_{i=1}^{N} A_k cos(\omega_k t + \epsilon_k) = \sum_{i=1}^{N} \sqrt{2S(\omega_k)\Delta\omega} cos(\omega_k t + \epsilon_k) \tag{6.1}$$

Here, $S(\omega_k)$ is the value of the wave spectrum evaluated at frequency ω_k, $\Delta\omega$ is the discretization step and ϵ_k is a random phase shift. Further, to reduce the number of

frequencies needed, it is a good idea to choose the frequencies randomly within their intervals. Finally, seeing how the frequency interval of interest is quite narrow, we propose the following: Divide the total spectrum from $\omega = 0.35\frac{rad}{s}$ to $\omega = 0.55\frac{rad}{s}$ in $N = 3$ equal intervals and choose one frequency randomly from each interval. Then, fit the amplitudes A_k such that the total amplitude is within reasonable values for the sea state, keeping in mind that the highest energy should be in the middle of the interval. The phase delays ϵ_k are also chosen randomly on the interval $[0, 2\pi)$.

6.2 Low Order Simulation with Repetitive Controller

To start off the simulation study, some simulations were done using the 2-volume version of the well model (4.5) and the repetitive controller described in chapter 5.8. In this simulation, the exact linear input-output map from v to p_b was inverted and low-pass filtered and used as a series compensator $C(s)$, as described in the same chapter. The results are shown here, mostly as a "proof of concept," seeing that it turned out to be extremely difficult to tune and stabilize the controller for higher orders of the well model. The disturbance used was a single sinusoid with a period of 12 s, similar to that used in Ullrigg experiments [11]. The plots of the different pressure responses, choke opening and disturbance signal can be seen in Figure 6.2. As we can see, the repetitive controller quite successfully rejects the disturbance, and after a short, transient period, the oscillations around the desired pressure is in the order of $10^{-2} bar$. However, as we shall see later, the situation drastically deteriorates for higher orders of the well model.

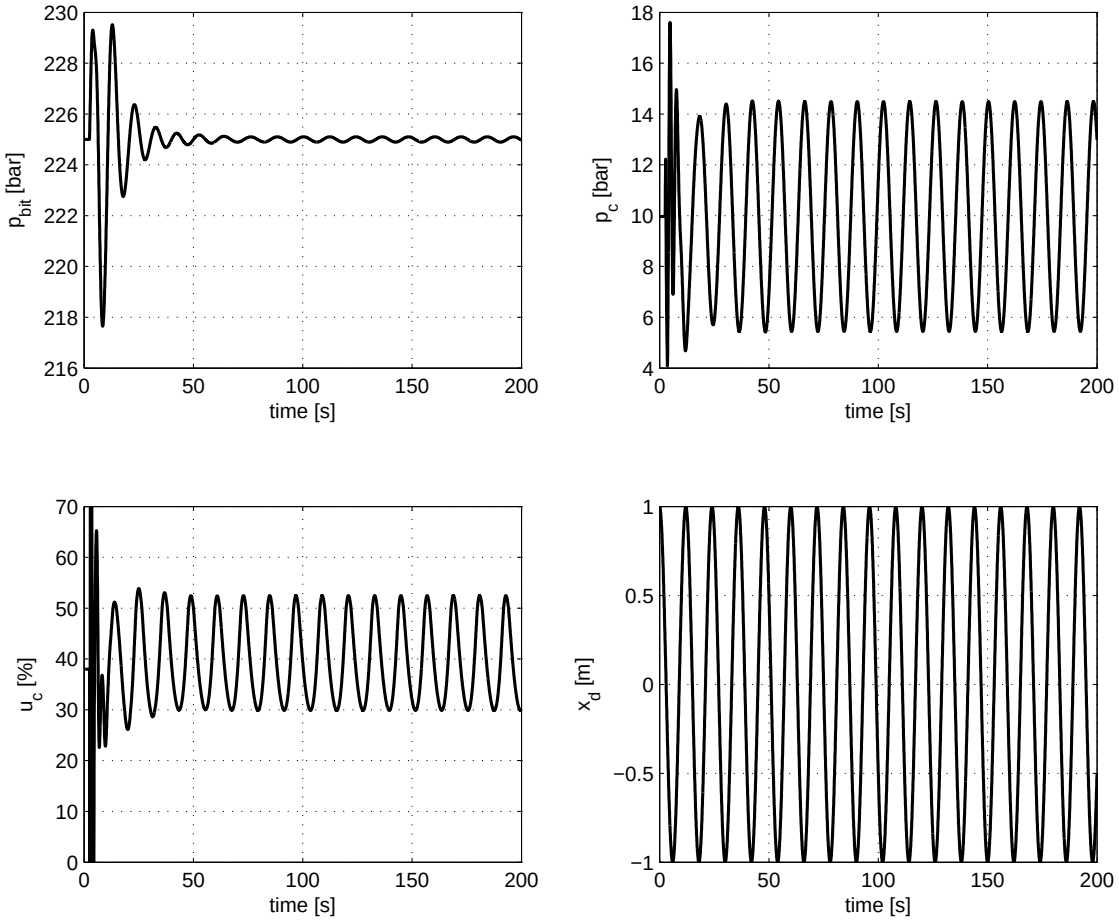

Figure 6.2: Simulation results, 2-volume model and repetitive controller. Bottom hole pressure, choke pressure, control signal and drill string movement. The bottom hole pressure set point is 225 bar.

6.3 5-volume Known Model and 1st Order Disturbance

In this section, we will compare the performance of the different controllers under the conditions that we know the perfect 5-volume model and that we know the frequency of the single harmonic disturbance. This could be seen as some kind of nominal situation where the conditions are perfect and we know all the information we need. For this scenario, we will present simulation results for the following controllers:

- Output regulation controller, described in chapter 5.4.
- Internal model controller with feedback linearization and state feedback, as described in chapter 5.7.
- Internal model controller without feedback linearization and state feedback, as described in chapter 5.9.

- Repetitive controller, described in chapter 5.8.

The harmonic disturbance still has the same period of 12 s. The results can be seen in Figures 6.3 through 6.6, and as a comparison, the responses for a "do nothing" strategy of keeping the choke constantly half-open is shown in Figure 6.7.

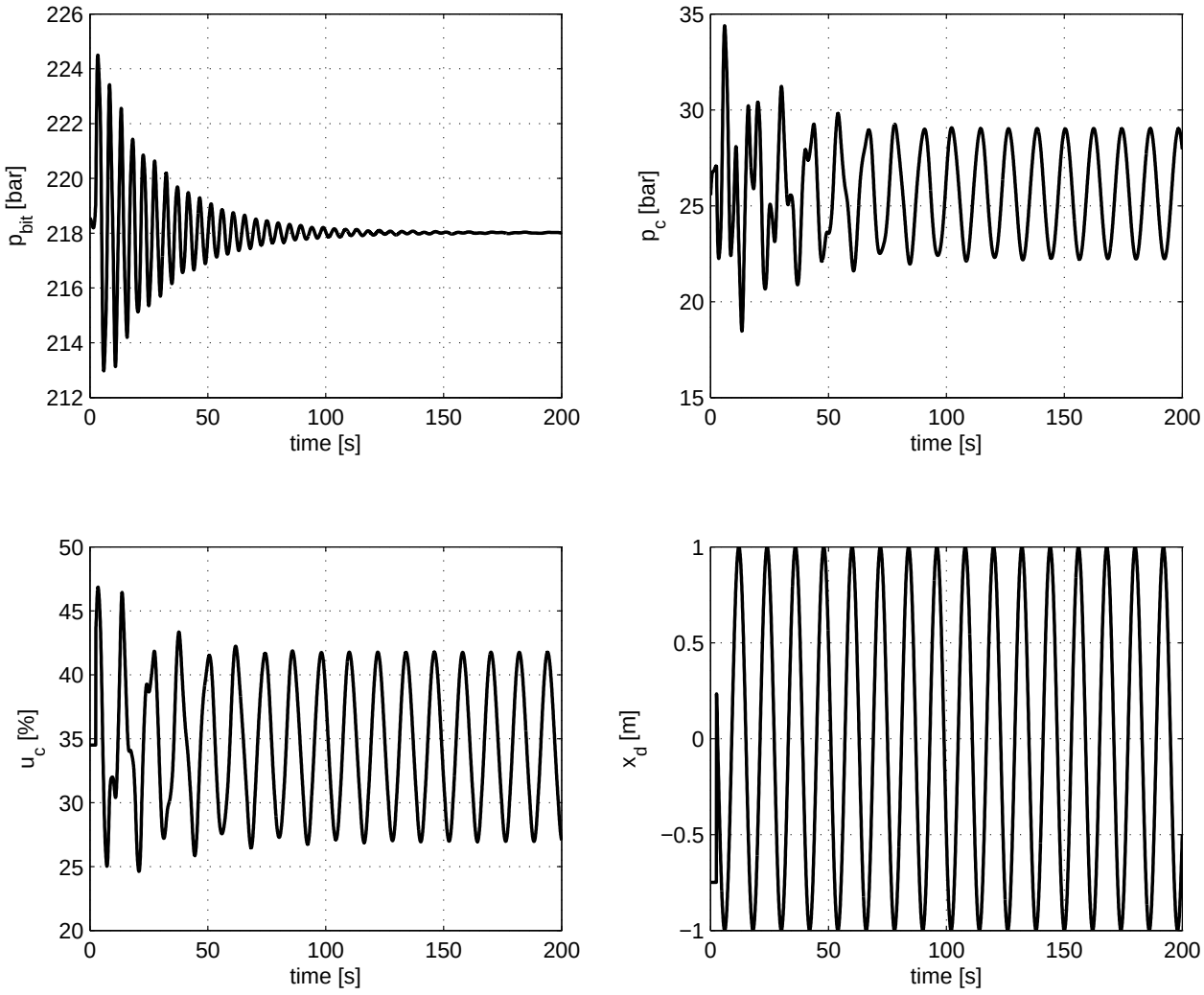

Figure 6.3: Simulation results for output regulation controller, known model and disturbance. Bottom hole pressure, choke pressure, control signal and drill string movement. The bottom hole pressure set point is 218 bar.

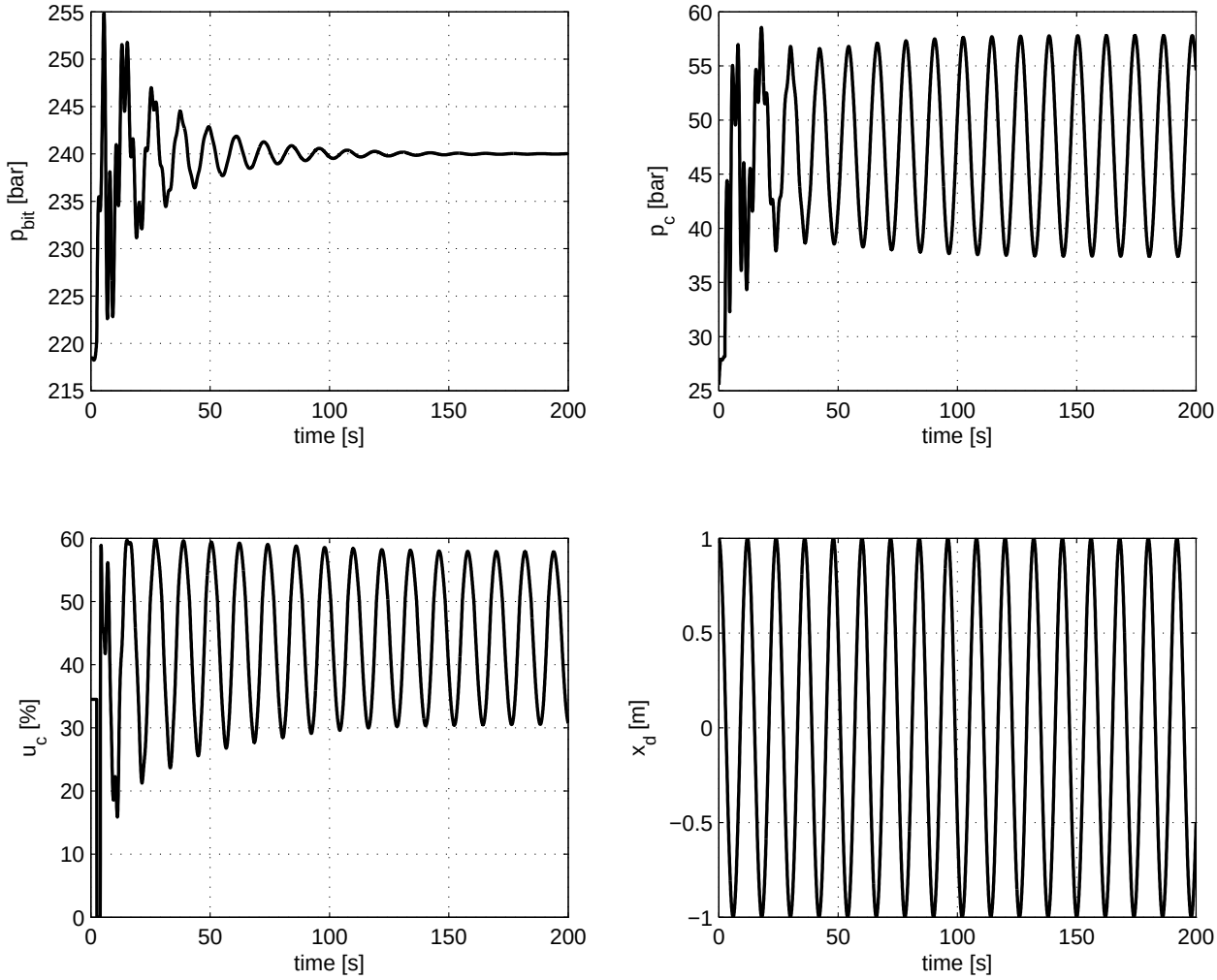

Figure 6.4: Simulation results, IMC with feedback linearization and state feedback, known model and disturbance. Bottom hole pressure, choke pressure, control signal and drill string movement. The bottom hole pressure set point is 240 bar.

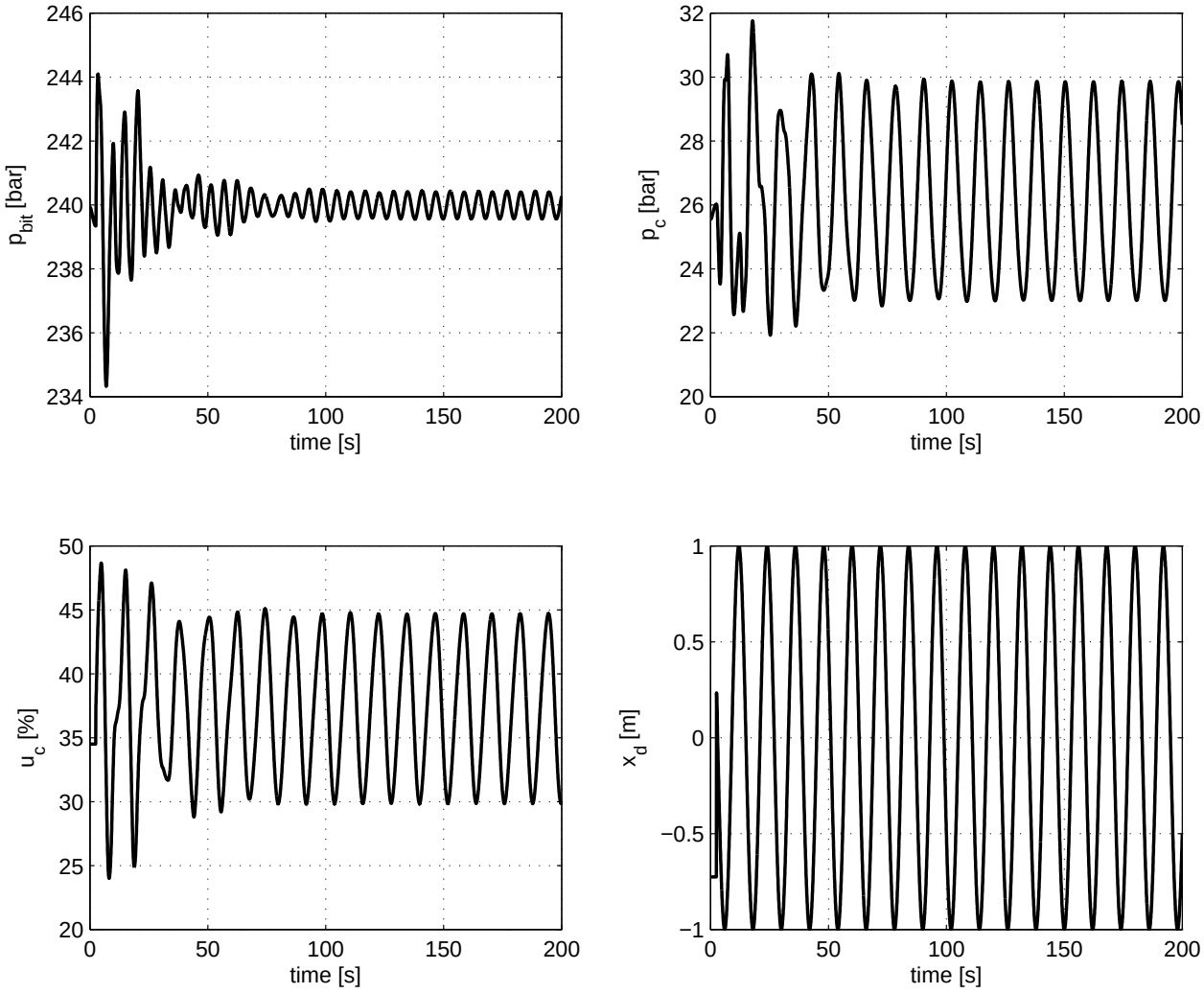

Figure 6.5: Simulation results, IMC without feedback linearization, known model and disturbance. Bottom hole pressure, choke pressure, control signal and drill string movement. The bottom hole pressure set point is 240 bar.

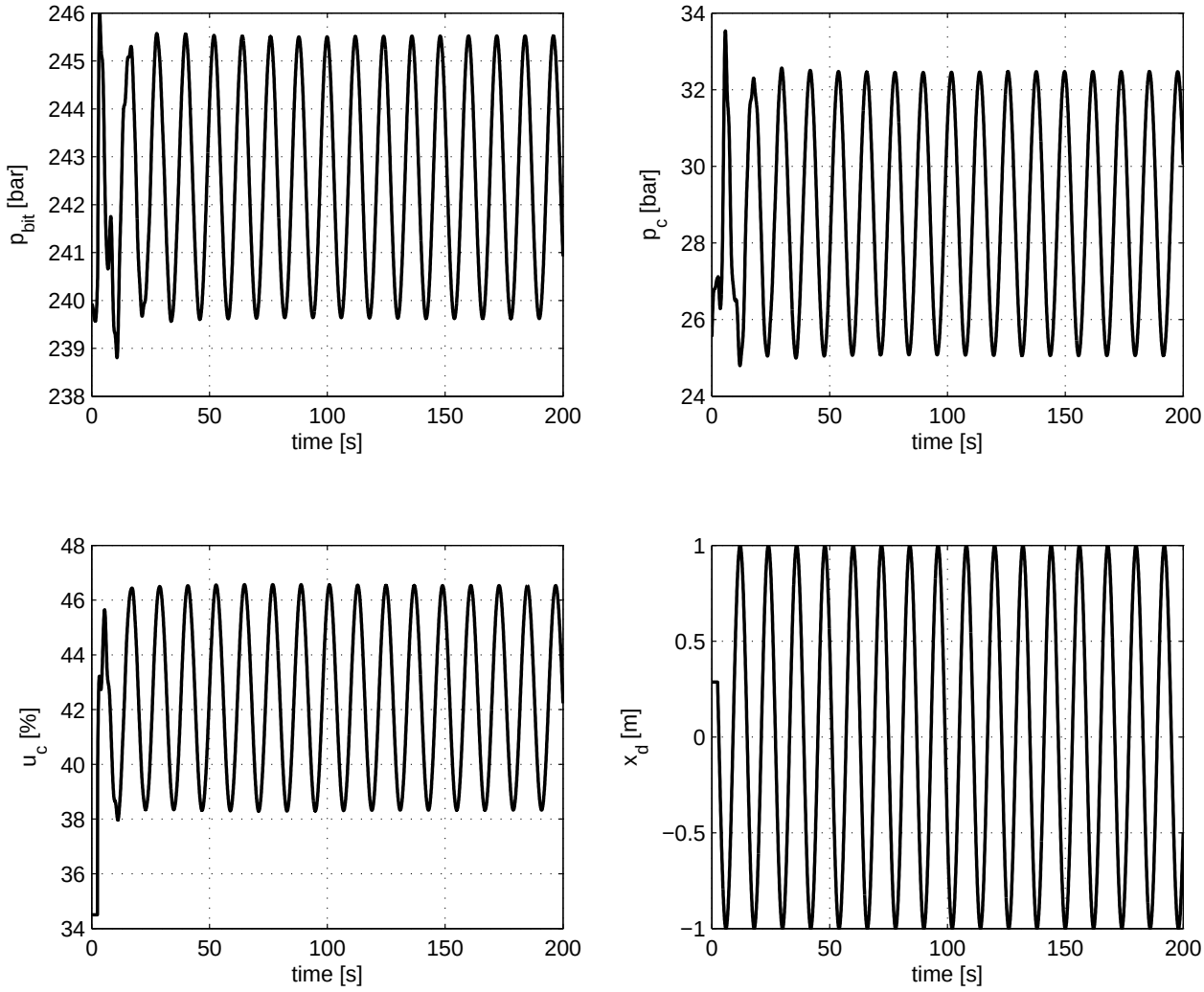

Figure 6.6: Simulation results, repetitive controller, known model and disturbance. Bottom hole pressure, choke pressure, control signal and drill string movement. The bottom hole pressure set point is 240 bar.

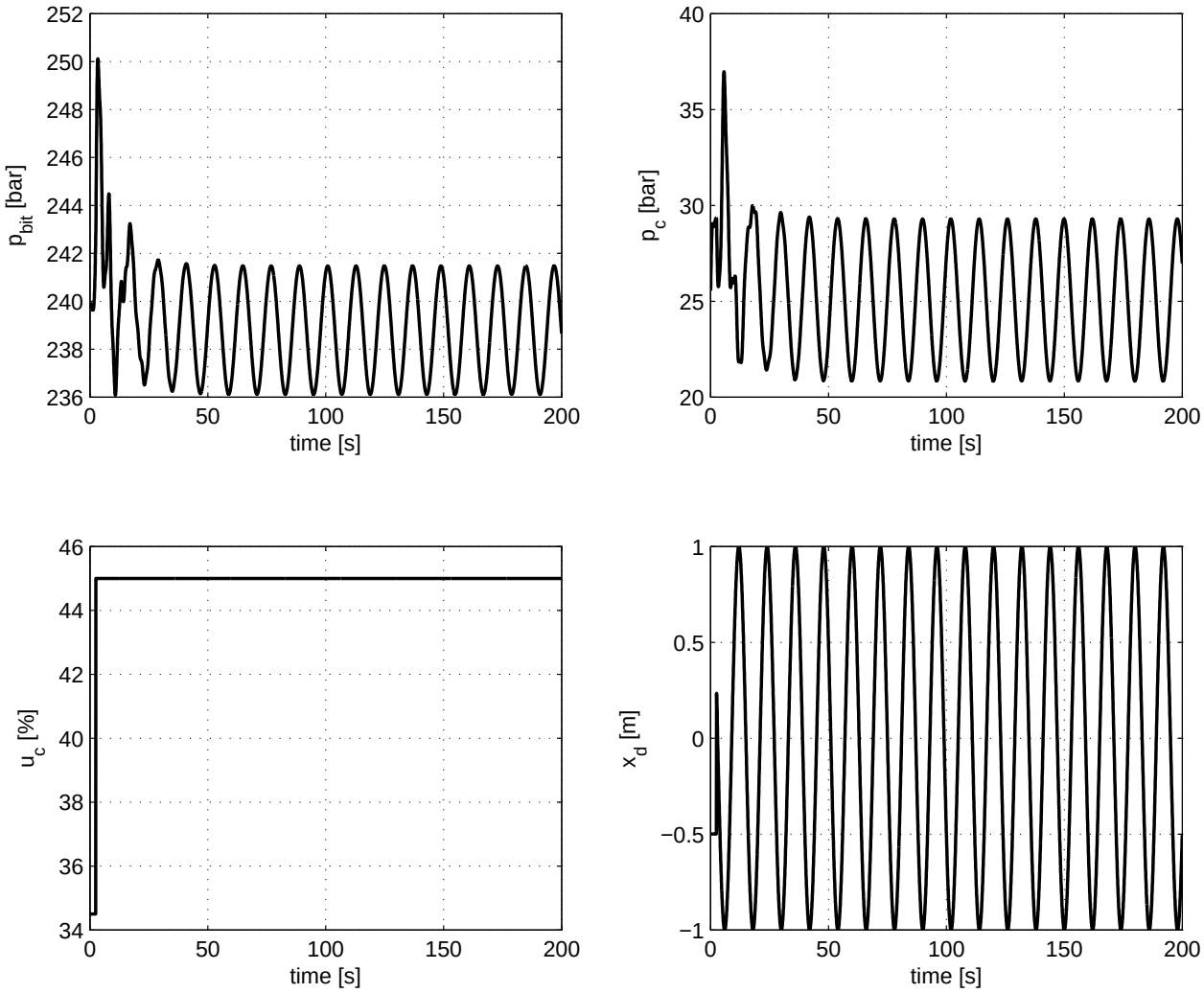

Figure 6.7: Simulation results, "do nothing". Bottom hole pressure, choke pressure, control signal and drill string movement.

As we can see, several of the controllers perform reasonably well under these conditions. Both the output regulation controller and the IMC with feedback linearization achieve asymptotic rejection of the disturbance. They also have about the same settling time, but the IMC has a much higher amplitude of the transient error. However, the output regulation controller causes oscillations at a higher frequency in the transient response, although these differences are probably to some extent a result of the different tuning of the controllers. The IMC without feedback linearization quite quickly regulates the pressure within a reasonable bound, but because of the nonlinearity, asymptotic rejection is not achieved. Sadly, the repetitive controller is a complete failure even with this perfect information. The large errors are mostly because of the fact that to get stability of the closed loop, it was necessary to tune

the gain of the controller such that its impact is almost invisible. The real control action can be mostly credited to a proportional controller in parallel. Anyway, this goes to show that the repetitive controller introduces real stability issues, and will be disregarded for the following simulations. In fact, for the way it was tuned in this example, it is almost no better than the "do nothing" strategy.

Quantitative performance measures have also been formulated, but we will delay the explanation and presentation of these to the end of the chapter, in order to make comparisons for all controllers under all conditions.

6.4 15-volume Model and 1st Order Disturbance

In this section, we will compare the performance of the different controllers under the assumption that the real well is governed by a higher order model than what we design the controller with. The controllers (for those that need a system model) will be designed using the 5-volume model from the last section, and the disturbance is once again assumed to be the known 1st order harmonic. This could be seen as an attempt to characterize the performance of the controllers under uncertain conditions on the system model, specifically to address the issue that the real system is really of infinite order, while we design the controller based on a lower order approximation. However, for those controllers where it is needed, a 5-volume model observer was designed using the measured choke and bit pressures as input, in such a manner that the parameters of the observer "adds up" to the parameters of the real system even though their orders are different.[2] For this scenario, we will present simulation results for the following controllers:

- Output regulation controller with observer.
- Internal model controller with feedback linearization and state feedback from observer.
- Internal model controller with feedback linearization but only feedback from measured p_c and p_{bit}.
- Internal model controller without feedback linearization.

The results for the different controllers can be seen in Figures 6.8 to 6.11.

[2] That is, the steady state pressures would be equal for the observer and the "real" system.

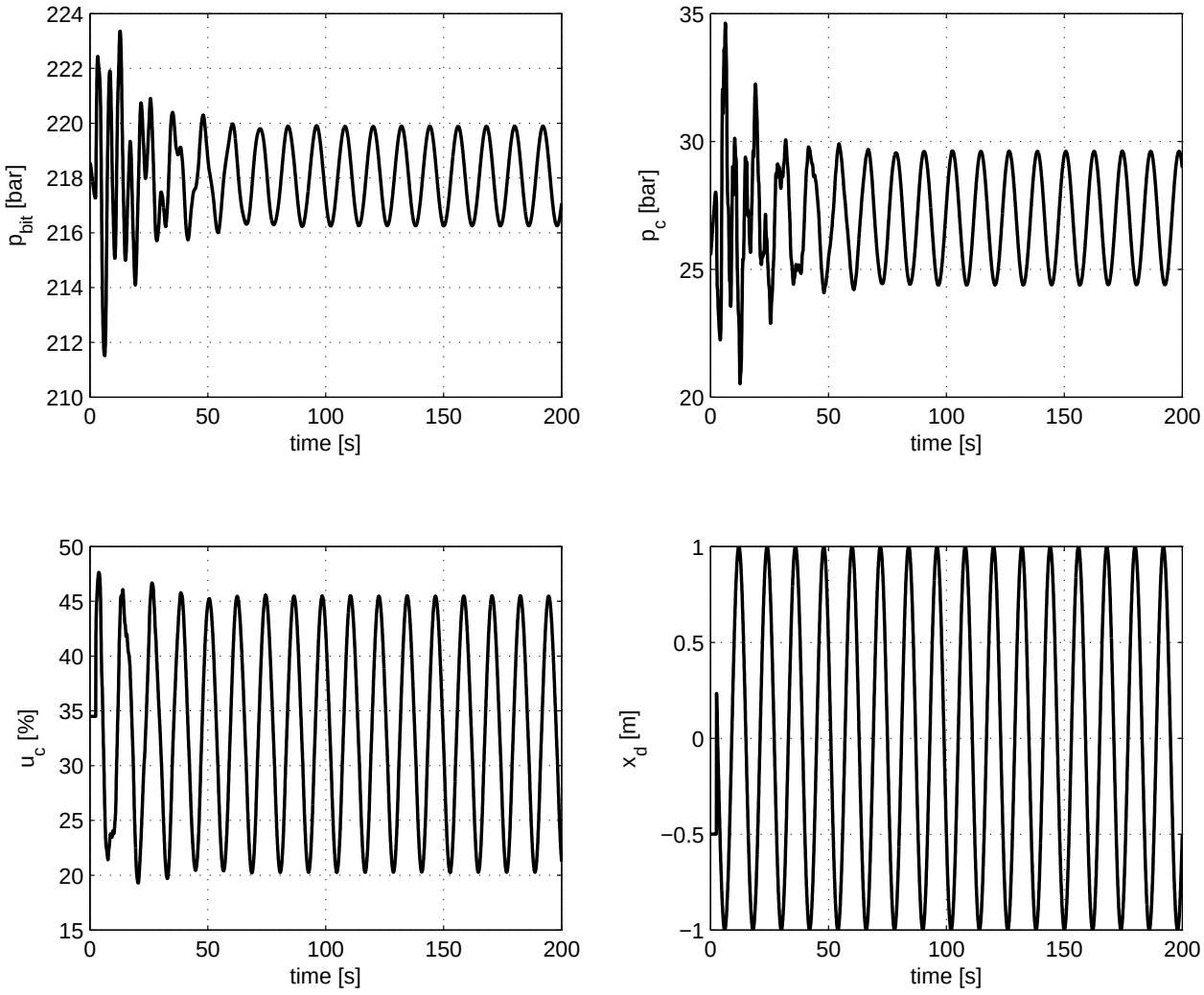

Figure 6.8: Simulation results, output regulation controller using observer. Bottom hole pressure, choke pressure, control signal and drill string movement. The bottom hole pressure set point is 218 bar.

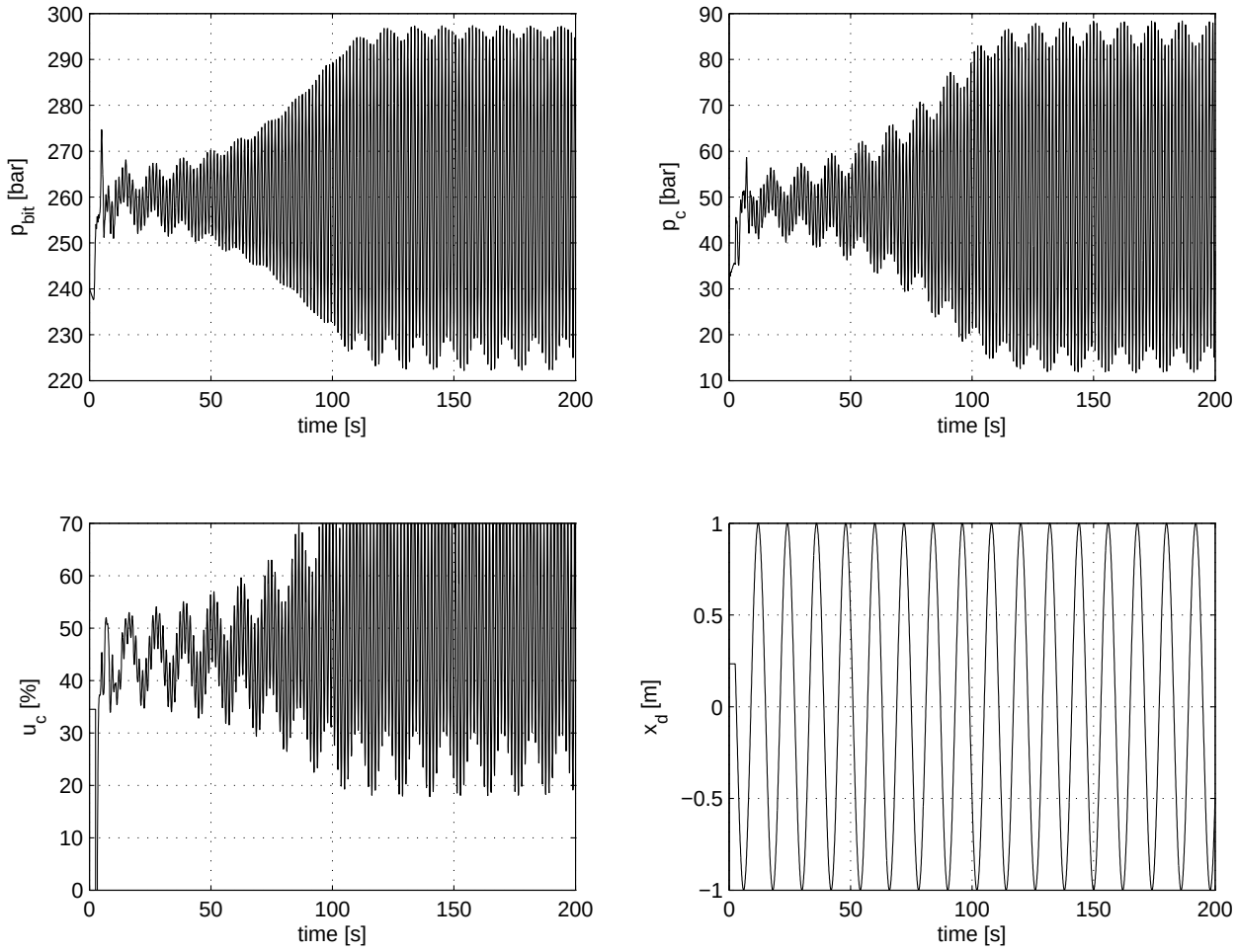

Figure 6.9: Simulation results, IMC with observer. Bottom hole pressure, choke pressure, control signal and drill string movement. The bottom hole pressure set point is 240 bar.

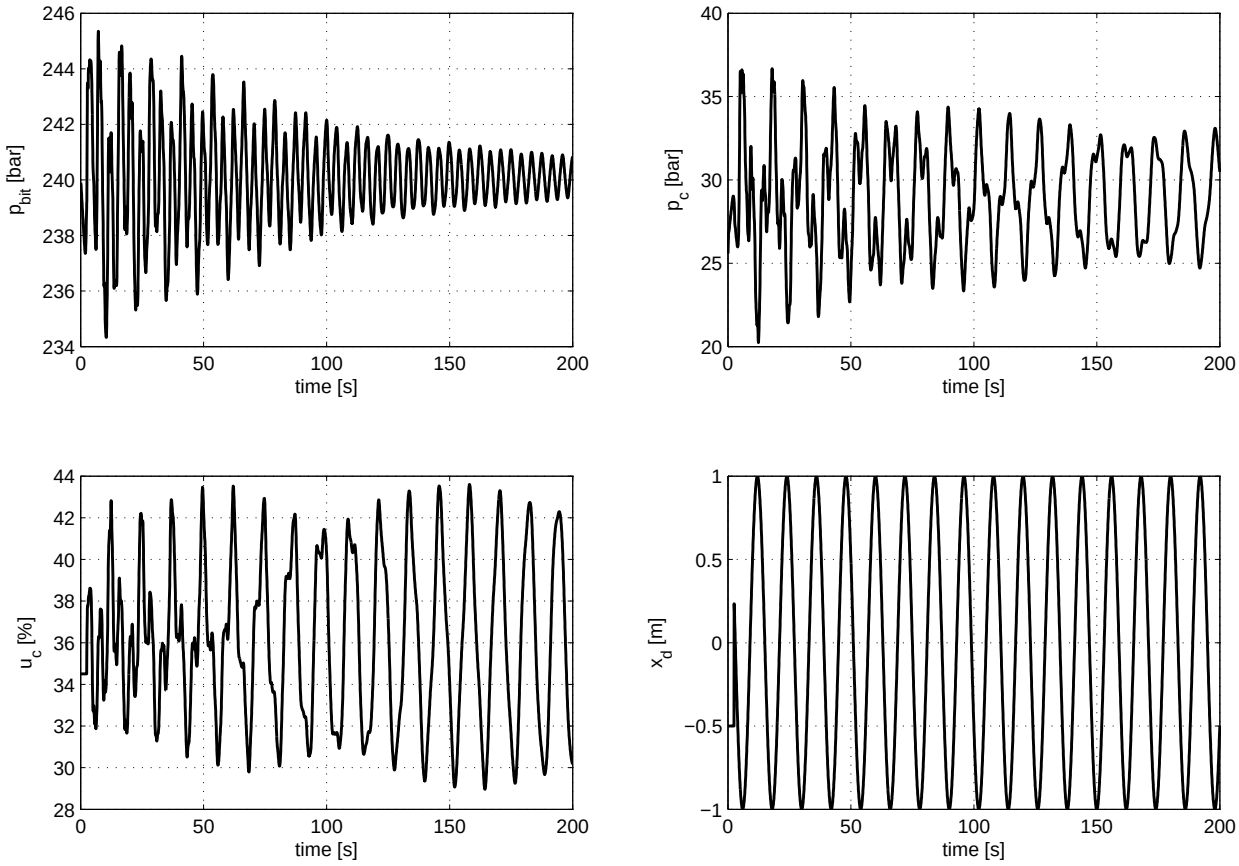

Figure 6.10: Simulation results, IMC with feedback from measurements. Bottom hole pressure, choke pressure, control signal and drill string movement. The bottom hole pressure set point is 240 bar.

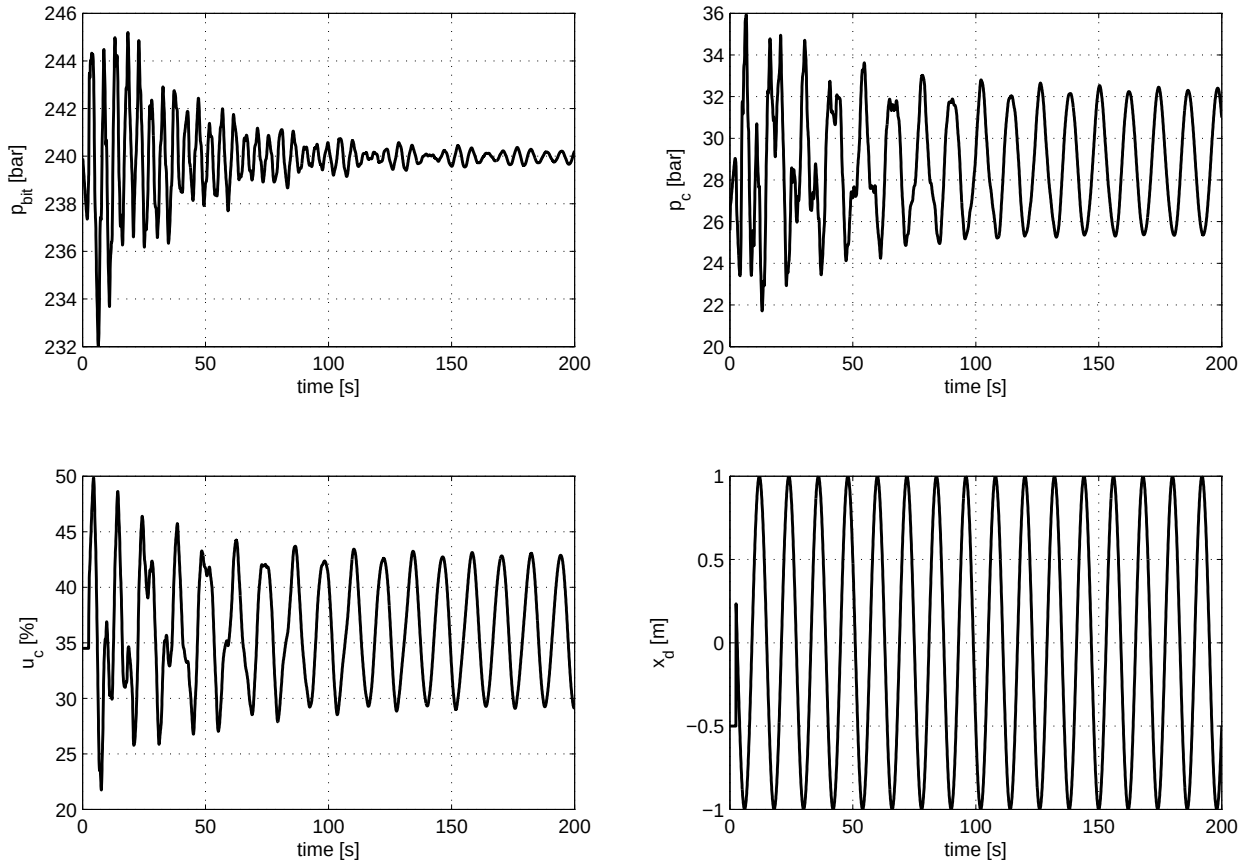

Figure 6.11: Simulation results, IMC without feedback linearization. Bottom hole pressure, choke pressure, control signal and drill string movement. The bottom hole pressure set point is 240 bar.

From these results, we can see that the output regulation controller unfortunately deteriorates and we do no longer achieve the asymptotic tracking. However, it does quite quickly manage to confine the fluctuations to a reasonable bound. The worst performance is definitely seen from the IMC with observer where we can see that the difference in the modeled and the "real" dynamics effectively makes the controller useless. However, by not using the full state for feedback, but only p_c and p_{bit}, it is possible to salvage something and be within roughly the same bounds as the output regulation controller, although after a worse transient response. At this point, one might come to appreciate the IMC without feedback linearization, which is by far the best performer in spite of the induced harmonics. This is due to its complete independence of the system model/order.

6.5 15-volume Model and 3rd Order, Unknown Disturbance

For the final scenario, we will compare the performance of the different controllers in the most realistic conditions. Here, the model will be the same as in the previous

section and with the same kind of observer where it is needed. However, for the wave disturbance, we will use the randomly generated signal described in chapter 6.1. To compensate for this, the controllers will also be extended to compensate for three distinct frequencies, but contrary to earlier, we will not know the exact frequencies of the disturbance. The frequencies used in the controllers will also be generated randomly within the interval of interest. In an actual implementation one might want to do a fast Fourier transform of the vertical position measurement of the drilling rig in order to find the most suitable frequencies for the controllers. However, the simulations presented here will in any way illustrate the performance when the frequencies are not exactly known and the waves contain more than one isolated frequency. For this scenario, we will present simulation results for the following controllers:

- Output regulation controller with observer.
- Internal model controller with feedback linearization but only feedback from p_c and p_{bit}.
- Internal model controller without feedback linearization.

The results from the different controllers can be found in Figures 6.12 to 6.14. As a comparison, a "do nothing" simulation was also performed with this disturbance, as seen in Figure 6.15.

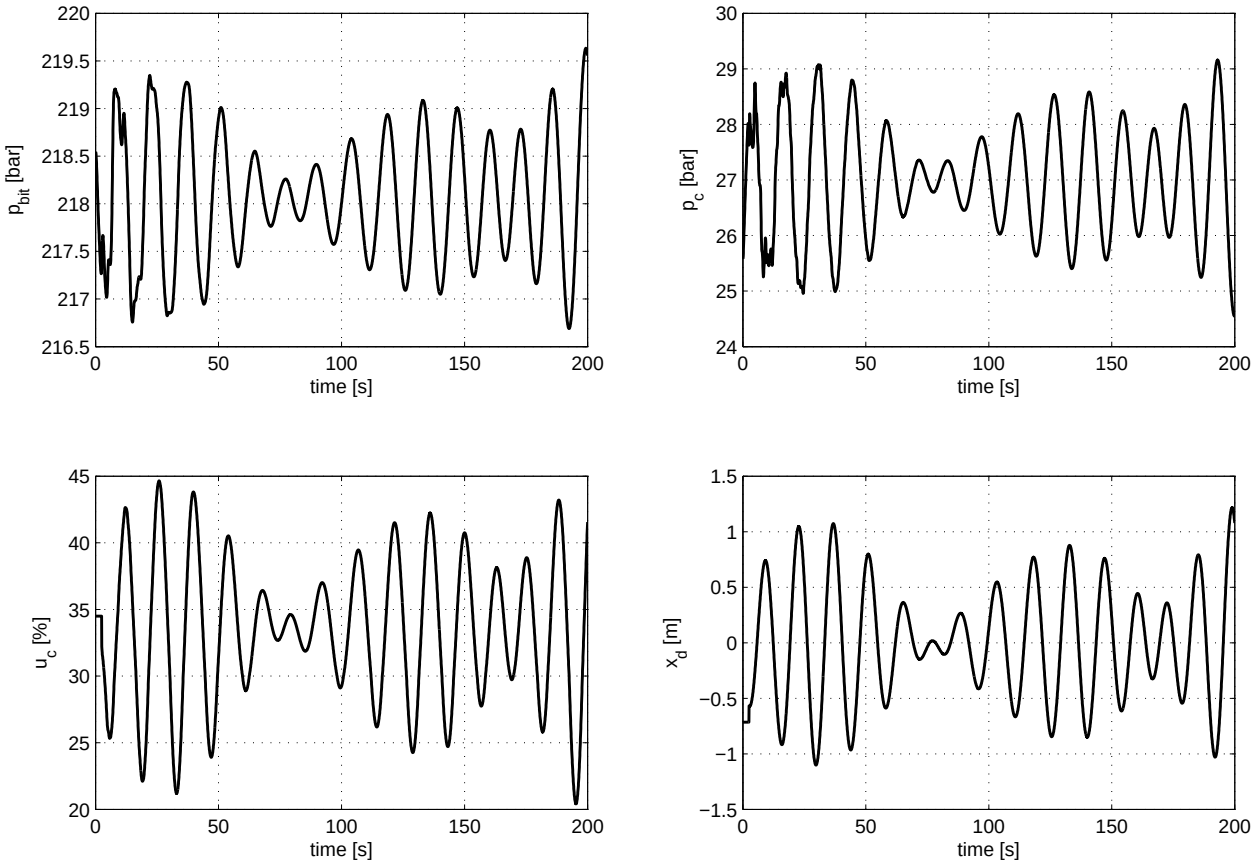

Figure 6.12: Simulation results, output regulation controller with observer and 3rd order harmonic disturbance. Bottom hole pressure, choke pressure, control signal and drill string movement. The bottom hole pressure set point is 218 bar.

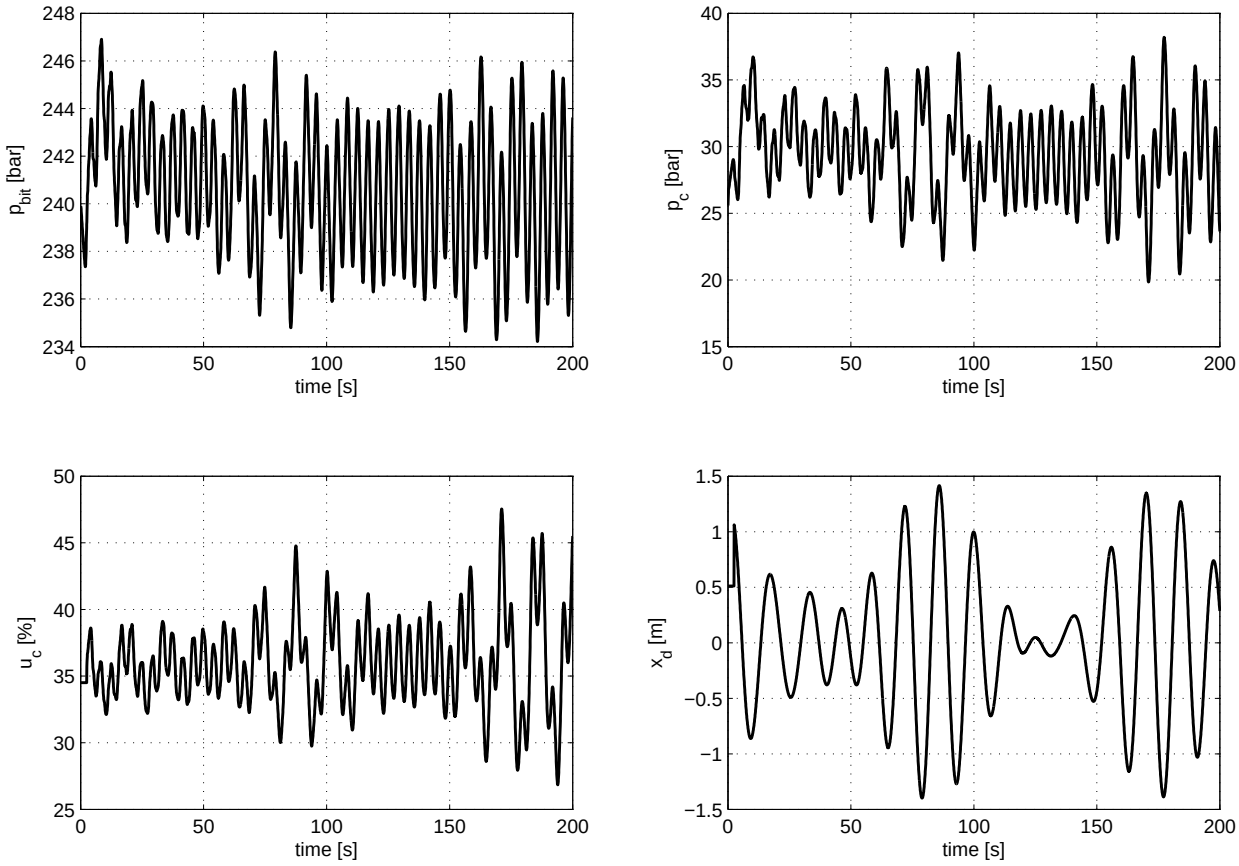

Figure 6.13: Simulation results, IMC with feedback linearization and 3rd order harmonic disturbance. Bottom hole pressure, choke pressure, control signal and drill string movement. The bottom hole pressure set point is 240 bar.

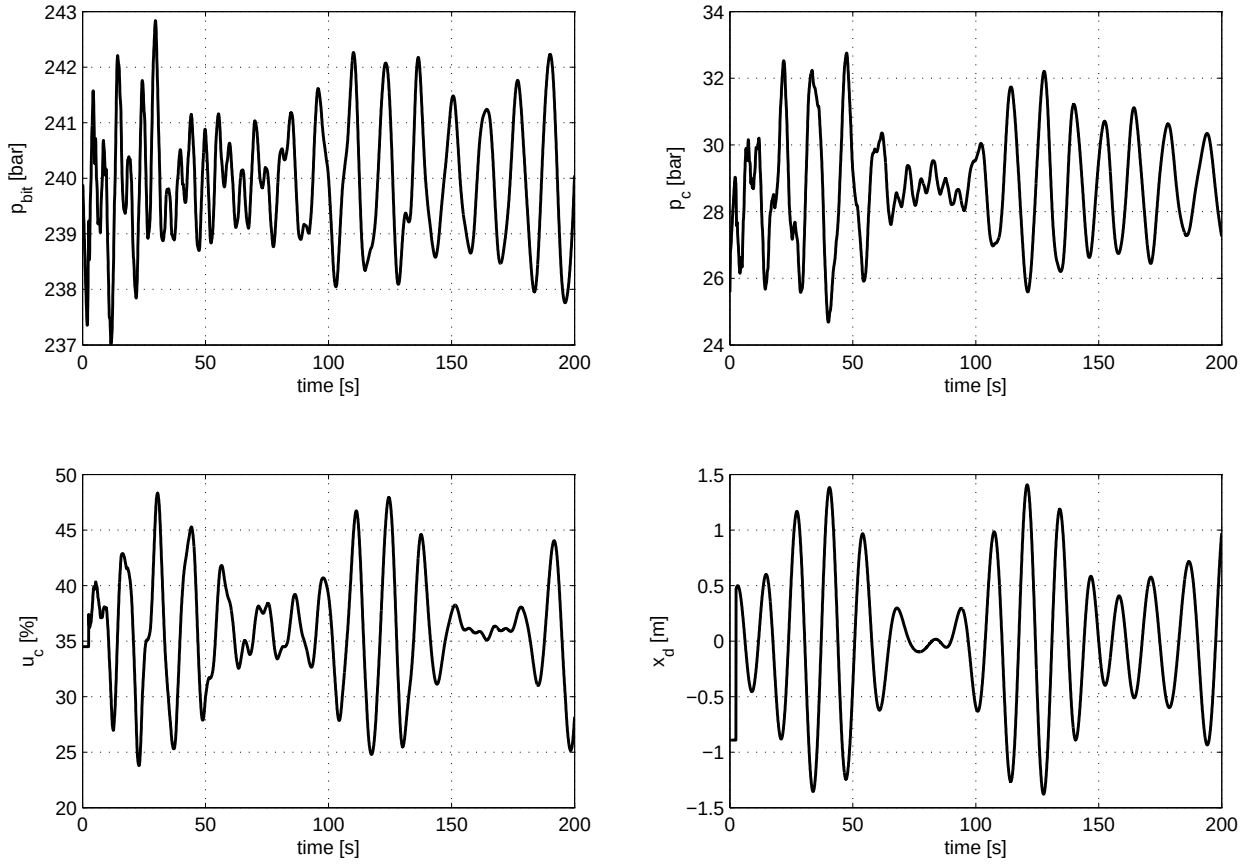

Figure 6.14: Simulation results, IMC without feedback linearization. Bottom hole pressure, choke pressure, control signal and drill string movement. The bottom hole pressure set point is 240 bar.

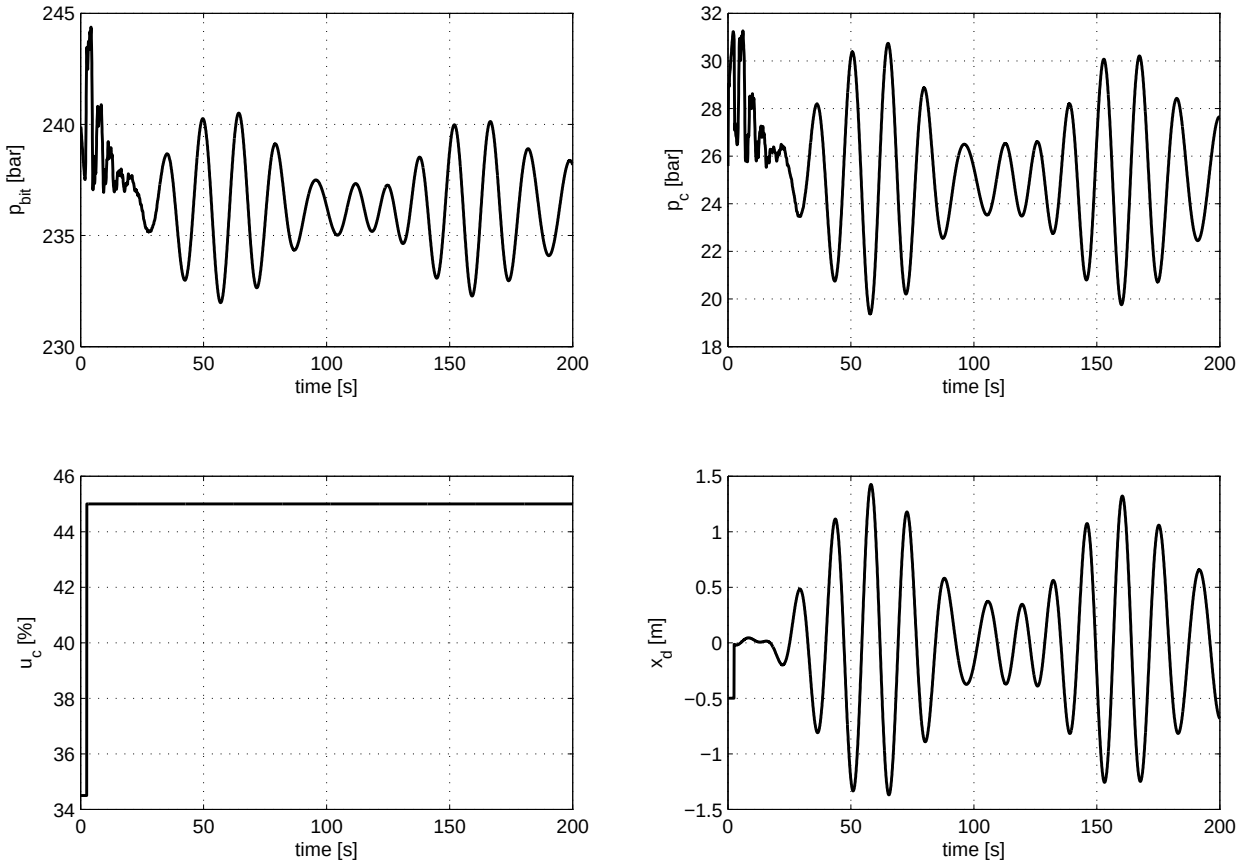

Figure 6.15: Simulation results, "do nothing" strategy. Bottom hole pressure, choke pressure, control signal and drill string movement. The bottom hole pressure set point is 218 *bar*.

The most striking thing to notice with these simulations is that, to a large extent, the higher order controllers eliminate the large, initial transient errors, and keep the pressure within a reasonable bound for the entire duration of the simulation. This could probably be attributed to the fact that they add compensation to a larger frequency range than earlier. Also, the output regulation controller performs no worse than in the last case, but the IMC both with and without feedback linearization deteriorates. Worst is the performance of the IMC with feedback linearization, and this is probably to some extent due to the added series compensation introduced for stabilization, like explained in chapter 5.9.

6.6 Quantitative Performance Measures

To be able to quantitatively measure the performance of the controllers in the previous simulations, some performance measures were defined. On one hand, we would be interested in the maximum error made by the controllers, so we measured the peak deviation from the set point over the duration of the simulation. However,

since there is also a certain randomness in the wave influence, the error measure was defined relative to the peak displacement of the drill string, that is

$$e_{peak} = \frac{\max_t \left| p_b - p_b^{ref} \right|}{\max_t |x_d|} \tag{6.2}$$

On the other hand, some of the controllers will have a large transient error but then achieve asymptotic tracking after a while, so one would also be interested in the average error made over the entire interval. A nice measure of average values for harmonic signals is the root mean square (RMS) value, which avoids the problem of the average error tending to zero. Also in this case, we wanted to include the randomness of the waves, so we defined the error as

$$e_{RMS} = \frac{\sqrt{\frac{1}{T-t_0}\int_{t_0}^{T}\left(p_b - p_b^{ref}\right)^2 dt}}{\sqrt{\frac{1}{T-t_0}\int_{t_0}^{T} x_d^2 dt}} \tag{6.3}$$

These two errors were then measured during the simulations, and the numerical results can be seen in Table 6.2.

Controller/Case	e_{peak}	e_{RMS}
Model order 5, single harmonic disturbance:		
Output Regulation Controller	$4.23\frac{bar}{m}$	$1.21\frac{bar}{m}$
IMC w. feedback linearization	$5.55\frac{bar}{m}$	$1.80\frac{bar}{m}$
IMC w.o. feedback linearization	$5.60\frac{bar}{m}$	$1.24\frac{bar}{m}$
Repetitive Controller	$3.63\frac{bar}{m}$	$2.88\frac{bar}{m}$
Do Nothing	$10.87\frac{bar}{m}$	$3.05\frac{bar}{m}$
Model order 15, single harmonic disturbance:		
Output Regulation Controller	$7.34\frac{bar}{m}$	$2.29\frac{bar}{m}$
IMC w. feedback linearization, observer	-	-
IMC w. feedback linearization, no observer	$5.71\frac{bar}{m}$	$2.37\frac{bar}{m}$
IMC w.o. feedback linearization	$7.89\frac{bar}{m}$	$1.98\frac{bar}{m}$
Model order 15, 3rd order unknown disturbance:		
Output Regulation Controller	$1.82\frac{bar}{m}$	$1.50\frac{bar}{m}$
IMC w. feedback linearization, no observer	$4.58\frac{bar}{m}$	$4.40\frac{bar}{m}$
IMC w.o. feedback linearization	$2.05\frac{bar}{m}$	$1.80\frac{bar}{m}$

Table 6.2: Measured errors during simulations.

6.7 Summary and Recommendation

A summary of this chapter can quite nicely be seen as a summary of Table 6.2. It is quite clear that the repetitive controller is very difficult to tune and stabilize, so it seems to be a bad choice for a practical implementation in spite of its intuitive simplicity and good disturbance rejection properties. The IMC with feedback linearization and observer for unmeasured states is a complete failure and it seems that

also this controller is a bad choice in practice. If one were to drop the observer in the IMC structure, the closed loop system is stable, but the performance is quite poor in all cases. The two top performers are in all cases the IMC without feedback linearization and the output regulation controller, and it seems that the choice should be between them. The reason that these nonlinear control approaches give the best performance may not be so much due to the IMC structure, but rather a reflection of the fact that the linearized hydraulic well model is not very well behaved. This results in the need for additional series compensators that are not needed when dealing directly with the nonlinear system.

In the performance in the most realistic scenario, the output regulation controller is the winner, but it should be kept in mind that these numerical values are from one certain tuning of the controller parameters, and it is fully possible that another tuning would give slightly different results.[3] Also, the output regulation controller relies more heavily on the system parameters, so the controller that gives best performance based on least information seems to be IMC without feedback linearization. If it is the case that there is a large uncertainty in the system parameters, then it seems that this is the best choice. As a general remark, one of the most valuable lessons learned from this simulation study is that, even if one can sufficiently model the disturbance as a single harmonic, it seems to be a good idea to extend the controllers with a larger number of frequencies just to reduce transient errors.

Finally, having concluded the simulation study, one might feel that there is one vital piece missing, namely the fact that in a real, practical situation, assuming more or less standard instrumentation of the drilling set up, the down hole pressure measurement would not be available. However, this introduces an issue of a more philosophical nature: How does one regulate an output that does not exist? These simulations were done under the assumption that this measurement is available, or that it at least can be estimated accurately enough, possibly with a different type of estimator. [4] Anyway, it seems likely that it is always possible to achieve perfect regulation of any estimated pressure, as this is inevitably calculated by a known model, so in the opinion of the author, the study shown here is well suited for evaluation of the actual performance of the proposed controllers.

[3] However, given the saturation of the choke opening, the space of possible tunings is quite limited.

[4] There is currently a lot of activity on exactly the issue of bottom hole pressure estimation, and this is the subject of more than one master thesis from recent years.

Chapter 7

Testing the Performance on a High Fidelity Drilling Simulator

IRISDrill for MATLAB is a high fidelity simulator for the well hydraulics that is developed by IRIS, and it was chosen as a next step in assessing the performance of the controllers, lacking the possibility of doing costly real life experiments. This simulator is very complex and accurate, and it goes beyond this thesis to describe all of its functionality, but it can be set up to include all the different inputs and outputs necessary to simulate the scenario described in this thesis:

- The speed and position of the drill string, v_d and x_d.
- The back pressure pump flow, q_{bpp}.
- The choke opening, u_c.
- Pressure outputs at choke and bottom hole, p_c and p_{bit}.

It is also possible to measure flow and pressure at many other positions in the hydraulic system, as well as to use a large number of different inputs, but these are the ones that correspond to the heave motion during pipe connection scenario. The simulator itself comes as a set of dynamically linked libraries that require a license from IRIS. To use these dll's, there exists a MATLAB interface that makes it possible to create IRISDrill objects that control the simulations. Then, one can write MATLAB scripts and functions that run simulations, set the different inputs and read the different outputs, much like in any other MATLAB program.

7.1 Choke Pressure Regulation

To assess the performance of the choke pressure regulation, the controller (4.7) was implemented and used in a simulation with heave influence. An observer based on the model (3.11) was used to estimate the flow into the "choke pressure control volume," which is used in the feedback linearization. The proportionality constant used in the controller was $k_p = 10$. The simulation results can be seen in Figure 7.1.

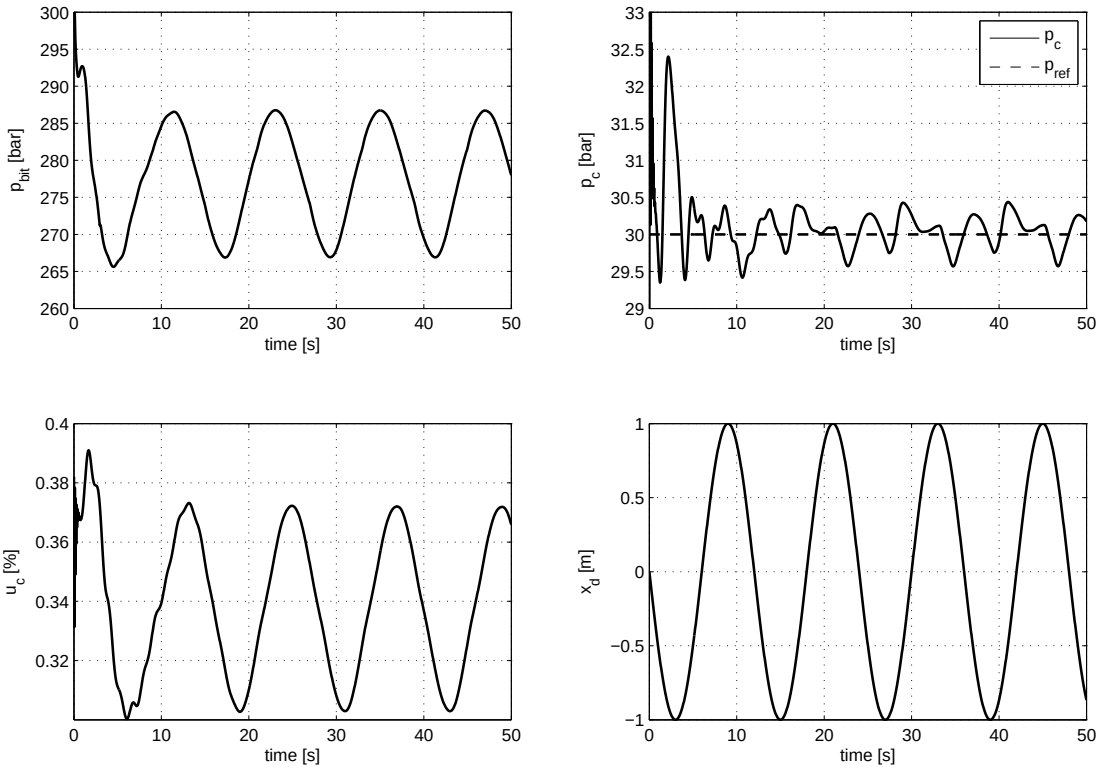

Figure 7.1: Simulation results from choke pressure regulation on IRISDrill for MATLAB. Bottom hole pressure, choke pressure, control signal and drill string movement.

We can see that the controller performs fairly well, and after a short transient period, the pressure fluctuations at the choke are reduced to an amplitude of about $0.4\,bar$. The performance of this regulation is heavily based on the ability to estimate the flow in the top of the well annulus as well as knowing the choke characteristics. At the time of these simulations, there was an error in the simulator in the choke flow measurement, so this measurement could not be used in the estimation. It is likely that using this measurement to adapt to the choke characteristics could further improve the pressure regulation.

7.2 Downhole Pressure Regulation by Internal Model Controller

The first attempt at the downhole pressure regulation was done by using the internal model controller described in Chapter 5.9. This is by far the easiest controller to implement, but it suffers from lack of rejection guarantees. The parameters used in the controller were

$$Q_2 = 0.7 * 10^{-8} \tag{7.1}$$

$$Q_0 = Q_1 = 0.2 * 10^{-7} \tag{7.2}$$

The simulation results can be seen in Figure 7.2, and as a reference, the results of a "do nothing" strategy can be seen in Figure 7.3.

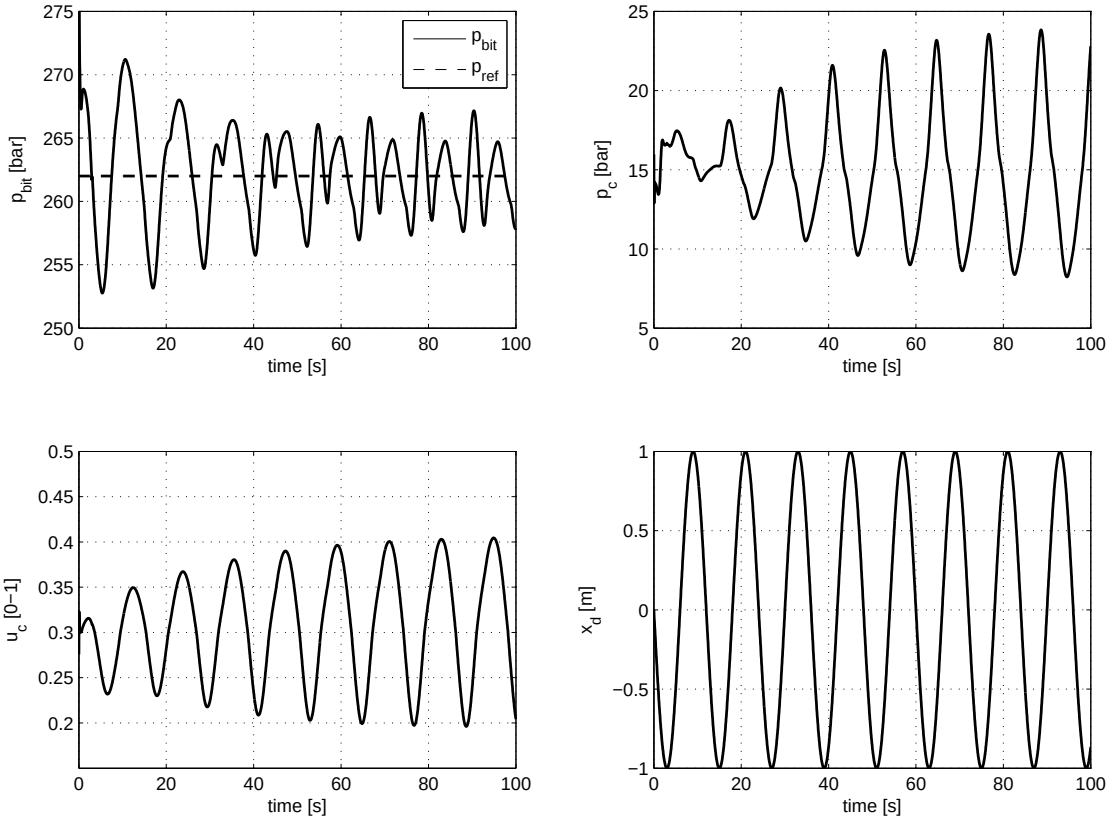

Figure 7.2: Simulation results, internal model controller on IRISDrill. Bottom hole pressure, choke pressure, control signal and drill string movement.

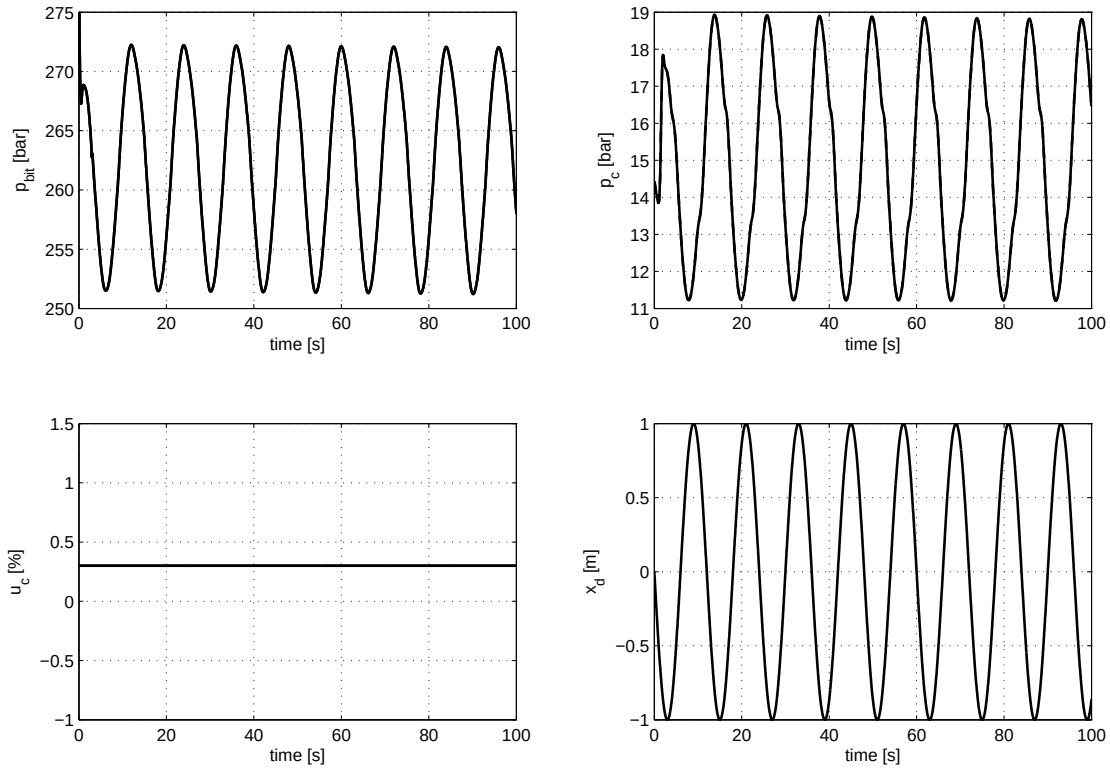

Figure 7.3: Simulation results, "do nothing". Bottom hole pressure, choke pressure, control signal and drill string movement.

We can see that the controller offers a certain amount of attenuation of the pressure oscillations, and in the steady state, the oscillations are bounded to about $\pm 4\,bar$ compared to about $10\,bar$ in the "do nothing" case. This might however not be good enough, and one can suspect that it might be possible to do better using some knowledge of the system dynamics in the controller.

An attempt was also done at using the feedback linearization approach described in Chapter 5.7. The controller, like we presented it, utilizes a full state feedback, so it was necessary to use an observer for the full state of the model (3.11). Since this kind of observer is also used in the output regulation controller, we chose to use the same observer, and thus base it on a 5-volume version of the model. So, the first step in implementing the controller was to fit the observer model to the simulated pressure responses from the IRISDrill simulator. The results from such a model fitting can be seen in Figure 7.4. In this simulation, the drill string is moved up and down following a sinusoidal motion, and the choke opening is also varied according to a sinusoid. This was done in order to adjust the model to the pressure dynamics created by both of these inputs, and turned out to be crucial in order to get the best possible fit.

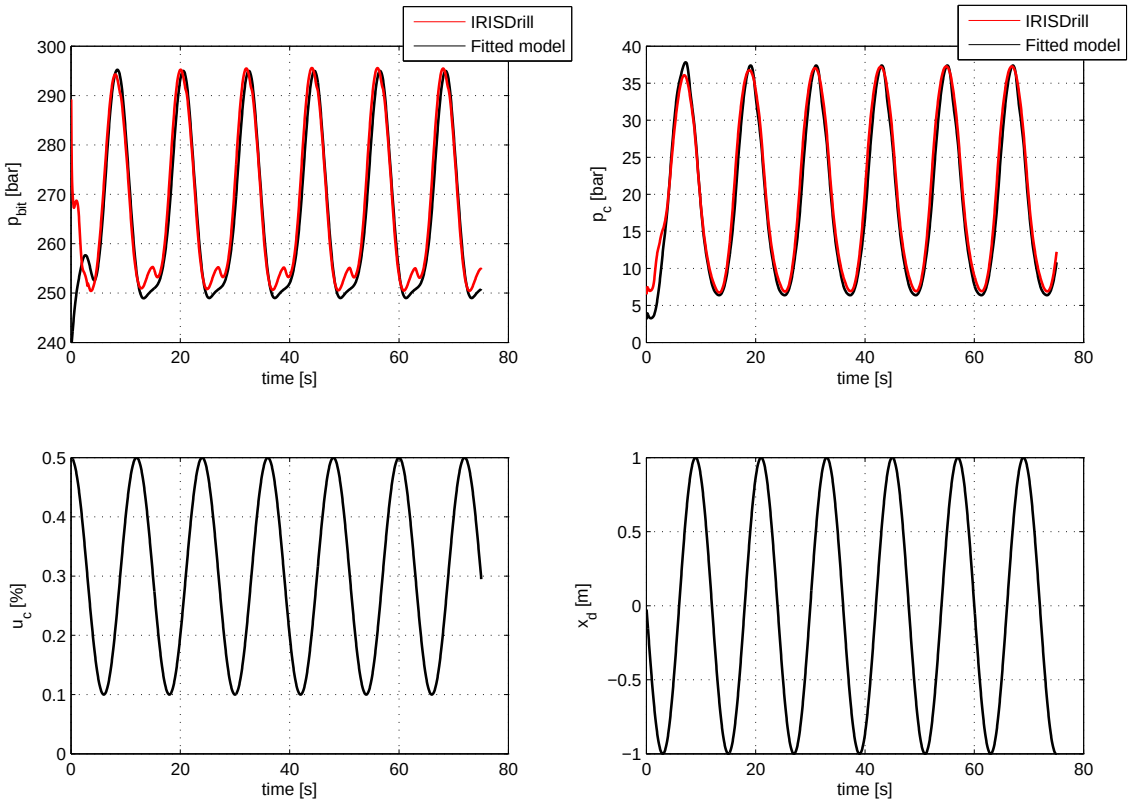

Figure 7.4: Model fitting to the IRISDrill simulation results. Bottom hole pressure, choke pressure, control signal and drill string movement.

This is a very interesting figure that quite nicely shows the major limitation of a low order model in this case: It is very possible to get the amplitude and attenuation of the pressure waves correct, but the lower order model is slower and not completely able to follow the simulator, which we assume is very high order, during the fastest dynamics. It is possible to tune the bulk modulus of the model to adjust the timing and increase the quickness in the pressure responses. This was done here, to a value that is probably much higher than the real value, but increasing it even more will also cause other effects on the estimated pressures that are not desired. The values of the parameters in the fitted model are

$$\begin{aligned} \beta_1 &= \frac{\beta}{Al} = 1.91 * 10^8 \, \frac{Pa}{m^3} \\ \beta_2 &= \frac{A}{l\rho} = 5.1477 * 10^{-8} \, \frac{m^4}{kg} \\ \beta_4 &= \rho g \Delta h = 6.1569 * 10^6 \, Pa \\ Friction\ constant &= 9.1030 * 10^6 \, \frac{sPa}{m^3} \end{aligned}$$

$$k_c = 2900\, m^3 \sqrt{\frac{m}{kg}}$$

Using this observer and measurements of p_c and p_{bit}, the internal model controller was implemented and simulated with the IRISDrill simulator. The parameters of the controller used were:

$$K = \begin{bmatrix} 6, & -2.5*10^8, & 6, & -2.5*10^8, & 6, & -2.5*10^8, & 6, & -2.5*10^8, & 6 \end{bmatrix} \quad (7.3)$$

$$Q_i = 5,\ i = 0, 1, 2 \quad (7.4)$$

The simulation results can be seen in Figure7.5.

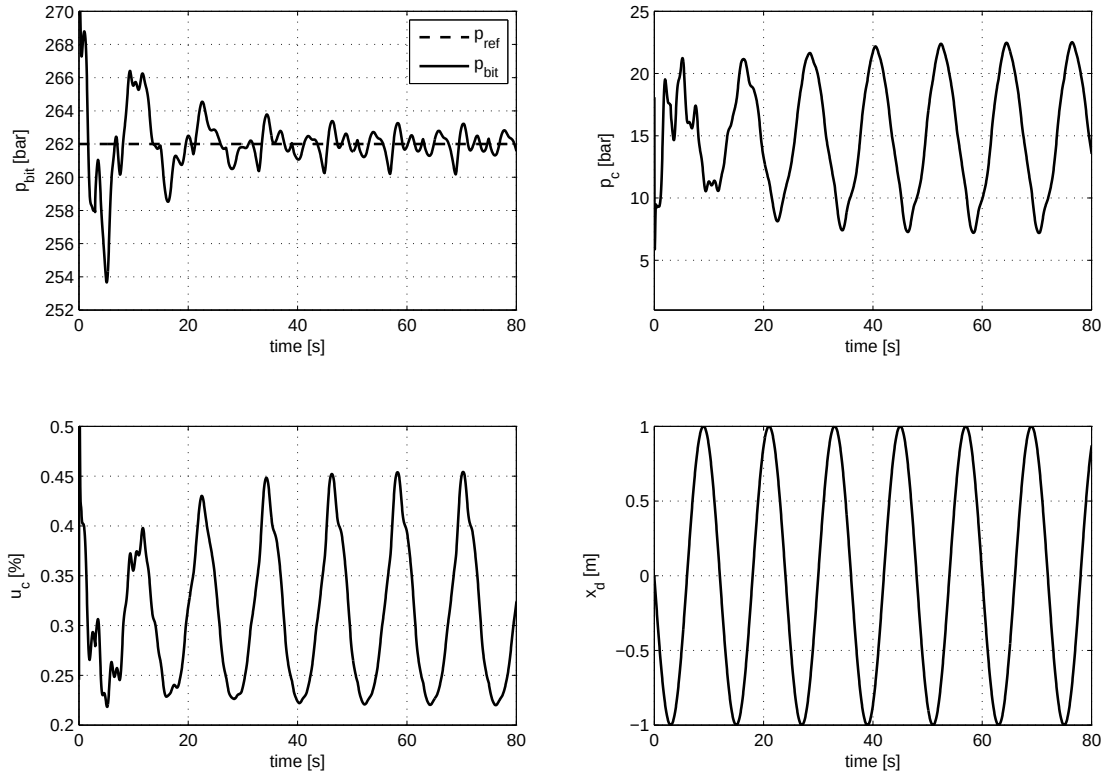

Figure 7.5: Simulation results, internal model controller with feedback linearization. Bottom hole pressure, choke pressure, control signal and drill string movement.

As we can see, the results are surprisingly promising compared to the results from the simulation study in Chapter 6. The differences in the dynamics in this case is not devastating, and after a somewhat rough transient period, the pressure oscillations are actually confined to about $\pm 1.5\, bar$. One can argue that this controller is in many ways very similar to the output regulation controller that we will investigate next, so one might expect similar results. However, this controller is slightly easier to implement, although it does rely on similar knowledge of the system through the observer used.

7.3 Downhole Pressure Regulation by Output Regulation Controller

The output regulation controller also requires the use of an observer, so we used the same observer as that discussed in the previous section. Using this observer and measurements of p_c and p_{bit}, the output regulation controller was implemented and simulated with the IRISDrill simulator. The matrix parameter used in the controller was

$$K = \begin{bmatrix} 10^{-7} & 0 & 0 & 0 & 0 & 0 & 0 & 0 & 10^{-7} \end{bmatrix} \tag{7.5}$$

The simulation results can be seen in Figure 7.6.

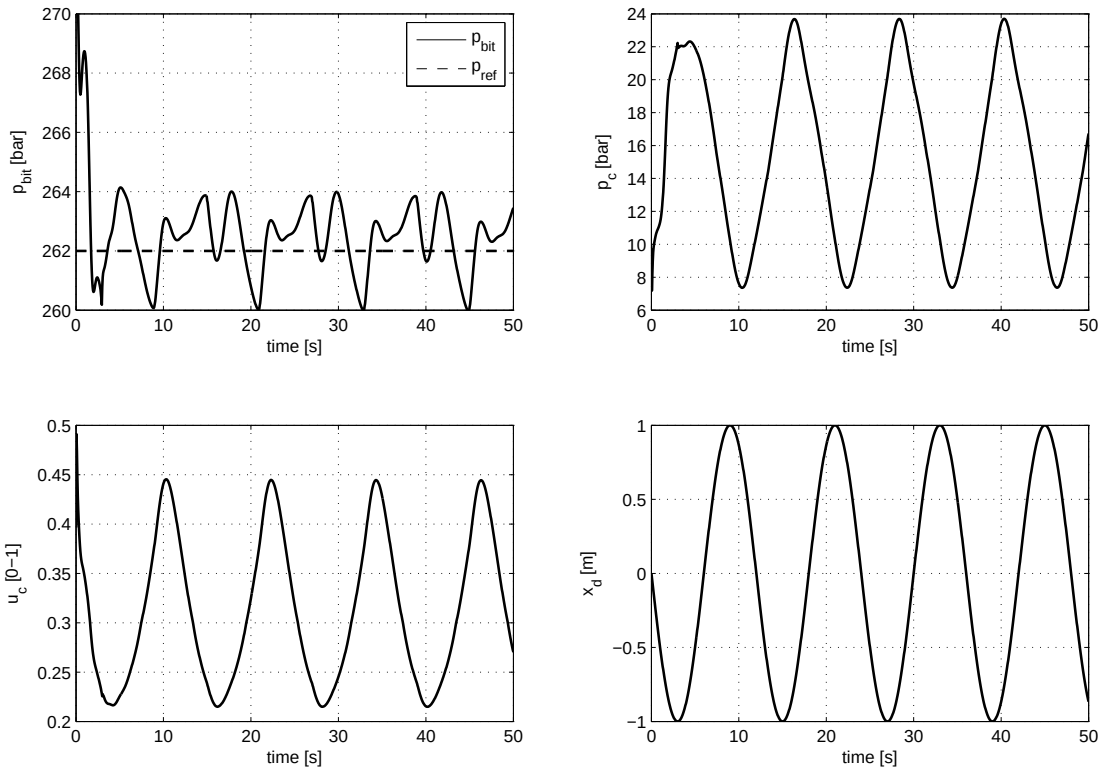

Figure 7.6: Simulation results, output regulation controller on IRISDrill. Bottom hole pressure, choke pressure, control signal and drill string movement.

We can see that the pressure regulation is satisfactory, and quickly confines the oscillations to ± 2 *bar* from the set point. This is slightly worse than the internal model controller, but it is likely that it is possible to improve both these results with better estimation of the choke characteristics as well as with additional tuning of the observer model. The extra implementational complexity does however result in a very good transient response, and an acceptable level for the pressure is reached within a couple of seconds.

7.4 Summary

It is now clear that the conclusion reached after Chapter 6 might not be fully valid when the controllers are applied to an even more accurate and realistic system. It seems that all controllers tested will to a certain degree fulfill the desired pressure tracking property, but it seems to be a pretty even match between the output regulation controller and the internal model controller with feedback linearization for the best performance. As noted, it can be argued that these controllers are the same in many respects, so this might not be very surprising. However, there is some difference in the ease of implementation, with the output regulation controller requiring a bit more calculations, but this does result in a better transient response. In these simulations, the steady state error of the internal model controller with feedback linearization was somewhat smaller than for the output regulation controller, but this is also probably to a certain degree the result of different tuning. In the end, it seems that any of these controllers could be implemented with good performance on a real life system.

Chapter 8

Conclusion and Future Work

To conclude, this thesis has shown several things. First of all, it has shown that the principal reason for the failure of the Ullrigg tests was the control strategy based on an insufficient model. Some discrepancies can also be attributed to time delays in the system and friction in the control choke.

Second, it has been shown that both the uniform output regulation controller and the internal model controller are good control strategies for bottom hole pressure regulation under the influence of heave motion. Both controllers have been tested under model order errors and unknown disturbances. The uniform output regulation controller has the best performance when measured by certain peak and RMS errors, but the internal model controller is superior in terms of ease of implementation. This assessment was confirmed by doing further experiments on a high fidelity drilling simulator provided by IRIS. Using the output regulation controller, it was possible to achieve a pressure regulation within $\pm 2\,bar$ from the set point, and the internal model controller achieved $\pm 4\,bar$. Also, by using a feedback linearization together with the internal model, it was possible to achieve roughly the same performance as the output regulation controller. As a side objective, it was also shown that it is possible to achieve very good tracking for the choke pressure, with a regulation within $\pm 0.4\,bar$ achieved on the IRISDrill simulator.

Finally, two conference papers were written which we plan on submitting to the American Control Conference (ACC) 2012 and The 2012 IADC/SPE Drilling Conference and Exhibition, respectively. These papers aim to show that using overly complicated models of the well hydraulic system is not necessary and that for a large number of applications, very low order models suffice. Also, a goal is to show that it is feasible to design automatic control systems for the challenging scenario of heave induced pressure variations. At the time of submission for this thesis, the ACC was not yet accepting paper submissions for the 2012 conference, but the papers are ready, and the plan is to submit them before the deadline.

There are many interesting questions to be dealt with for any future work on these subjects. In order to implement the output regulation controller on a real system, the next main challenge is to design a sufficiently accurate observer, preferably one that is able to adapt to slowly varying coefficients in the system and also the choke characteristics. There is currently some activity on different state estimation techniques related to the Kaasa model, but it would be most interesting to apply these

techniques to a somewhat higher order model and pair this with the output regulation controller. If this is achieved, my personal belief is that it should be possible to achieve satisfactory heave compensation on drilling rigs even without sufficient bottom hole pressure measurements. If there also is a change in the instrumentation of future drilling installations, the prospects are indeed very bright. A first step towards this could very simply be done by using the already implemented cases on the IRISDrill simulator, but simply removing the use of the down hole pressure measurement. Due to time constraints and very limited time using the simulator, this was not completed and included in this master's thesis, but some initial tests showed promising results and could most likely be improved with more time on hand.

Bibliography

[1] G.-O. Kaasa, O.N. Stamnes, L. Imsland, and O.M. Aamo. Intelligent estimation of downhole pressure using a simple hydraulic model,. In *IADC/SPE Managed Pressure Drilling and Underbalanced Operations Conference and Exhibition*, 2011.

[2] O.N. Stamnes, Jing Zhou, G.-O. Kaasa, and O.M. Aamo. Adaptive observer design for the bottomhole pressure of a managed pressure drilling system. In *Decision and Control, 2008. CDC 2008. 47th IEEE Conference on*, pages 2961 –2966, dec. 2008.

[3] Jing Zhou, G. Nygaard, J. Godhavn, O. Breyholtz, and E.H. Vefring. Adaptive observer for kick detection and switched control for bottomhole pressure regulation and kick attenuation during managed pressure drilling. In *American Control Conference (ACC), 2010*, pages 3765 –3770, 30 2010-july 2 2010.

[4] Jing Zhou, O.N. Stamnes, O.M. Aamo, and G.-O. Kaasa. Switched control for pressure regulation and kick attenuation in a managed pressure drilling system. *Control Systems Technology, IEEE Transactions on*, 19(2):337 –350, march 2011.

[5] J. Zhou, O.N. Stamnes, O.M. Aamo, and G.-O. Kaasa. Observer-based control of a managed pressure drilling system. In *Control and Decision Conference, 2008. CCDC 2008. Chinese*, pages 3475 –3480, july 2008.

[6] J. Zhou, O.N. Stamnes, O.M. Aamo, and G.-O. Kaasa. Adaptive output feedback control of a managed pressure drilling system. In *Decision and Control, 2008. CDC 2008. 47th IEEE Conference on*, pages 3008 –3013, dec. 2008.

[7] O. Breyholtz, G. Nygaard, and M. Nikolaou. Automatic control of managed pressure drilling. In *American Control Conference (ACC), 2010*, pages 442 –447, 30 2010-july 2 2010.

[8] O. Breyholtz, G. Nygaard, J.-M. Godhavn, and E.H. Vefring. Evaluating control designs for co-ordinating pump rates and choke valve during managed pressure drilling operations. In *Control Applications, (CCA) Intelligent Control, (ISIC), 2009 IEEE*, pages 731 –738, july 2009.

[9] John-Morten Godhavn. Control requirements for high-end automatic mpd operations. In *SPE Drilling Conference and Exhibition*, 2009.

[10] E.J. van Riet, D. Reitsma, and B. Vandecraen. Development and testing of a fully automated system to accurately control downhole pressure during drilling operations. In *SPE Middle East Drilling Technology Conference and Exhibition*, 2003.

[11] Alexey Pavlov, Glenn-Ole Kaasa, and Lars Imsland. Experimental disturbance rejection on a full-scale drilling rig. In *Proceedings of IFAC Nonlinear Control Systems Symposium 2009*, 2009.

[12] M. A. A. Shoukat Choudhury, N. F. Thornhill, and S. L. Shah. Modelling valve stiction. *Control Engineering Practice*, 13(5):641 – 658, 2005.

[13] Olav Egeland and Jan Tommy Gravdahl. *Modeling and Simulation for Automatic Control*. Marine Cybernetics, 2002.

[14] W. Kozicki, C. H. Chou, and C. Tiu. Non-newtonian flow in ducts of arbitrary cross-sectional shape. *Chemical Engineering Science*, 21(8):665 – 679, 1966.

[15] Prodromos Daoutidis and Costas Kravaris. Synthesis of feedforward/state feedback controllers for nonlinear processes. *AIChE Journal*, 35(10):1602–1616, 1989.

[16] Alexey Pavlov, Nathan van de Wouw, and Hendrik Nijmeijer. *Uniform Output Regulation of Nonlinear Systems*. Birkhauser Boston, 2006.

[17] Graham Goodwin, Stefan Graebe, and Mario Salgado. *Control System Design*. Prentice Hall, 2000.

[18] Richard Rebarber and George Weiss. Internal model based tracking and disturbance rejection for stable well-posed systems. *Automatica*, 39(9):1555 – 1569, 2003.

[19] Yutaka Yamamoto. Learning control and related problems in infinite-dimensional systems. In *in Essays on Control, eds. H.L.Trentelman and J.C. Willems, Birkhauser*, pages 191–222, 1993.

[20] George Weiss and Martin Hafele. Repetitive control of mimo systems using h[infinity] design. *Automatica*, 35(7):1185 – 1199, 1999.

[21] J. Kasac, B. Novakovic, and V. Milic. On equivalence between internal and external model-based repetitive learning controllers for nonlinear passive systems. *Asian Journal of Control*, 13(1):15–24, 2011.

[22] Thor I. Fossen. *Marine Craft Hydrodynamics and Motion Control*. John Wiley I& Sons Ltd., 2011.

Appendix A

Derivations and Definitions

A.1 Proof of Passivity for Well Model

As stated earlier, the stability of the closed loop system using the internal model controller without any feedback linearization has been proven for passive nonlinear systems. We will now show that the hydraulic well model is in fact passive, so that the stability of this controller is guaranteed. We will do this in the following steps: First, we will show that the system with input $-q_c$ and output p_b is passive by the use of a positive real transfer function. Then, we will show that the memoryless map from v to $-q_c$ is passive, and then show how this implies that the entire system with input v and output p_b is passive. First, let us write down the well model with only two control volumes for simplicity

$$\begin{aligned} \dot{p_c} &= \frac{\beta}{Al}(q+u) \\ \dot{q} &= \frac{A}{L\rho}(p_b - p_c) - \frac{A}{L\rho}Fq - \frac{gA\Delta h}{L} \\ \dot{p_b} &= \frac{\beta}{Al}(-q) \end{aligned} \tag{A.1}$$

where we have chosen $u = -q_c$ and set all other inputs to zero. Without loss of generality, we do a linear transformation of the states, so that the origin is an equilibrium point for the transformed system

$$x_1 = p_c \tag{A.2}$$
$$x_2 = q \tag{A.3}$$
$$x_3 = p_b - \rho g \Delta h \tag{A.4}$$

Then, we find the new system as

$$\dot{x_1} = \beta_1(x_2 + u) \tag{A.5}$$
$$\dot{x_2} = \beta_2(x_3 - x_1 - Fx_2) \tag{A.6}$$
$$\dot{x_3} = \beta_1(-x_2) \tag{A.7}$$
$$\Downarrow \tag{A.8}$$

$$\dot{x} = Ax + Bu \tag{A.9}$$
$$y = \begin{bmatrix} 0 & 0 & 1 \end{bmatrix} x = Cx \tag{A.10}$$

where we have redefined some of the parameters in the original equations for ease of presentation. Then, we find the transfer function $H(s)$ from u to $y = x_3$ as

$$H(s) = C(sI - A)^{-1} B \tag{A.11}$$
$$\Downarrow \tag{A.12}$$
$$H(s) = \frac{\beta_2 \beta_1^2}{s(s^2 + \beta_2 F s + 2\beta_2 \beta_1)} \tag{A.13}$$

Now, since positive realness of $H(s)$ is equivalent to passivity of (A.1), we will consider this property of $H(s)$. (The definition of positive realness for rational transfer functions has been included in the appendix for completeness.)

1. Since $\beta_1, \beta_2, F > 0$ and in general $\beta_1 \gg \beta_2$, all poles of $H(s)$ can readily be seen to have real parts less than or equal to zero.[1]

2. We consider the real part of $H(j\omega)$

$$H(j\omega) = \frac{\beta_2 \beta_1^2}{2\beta_2 \beta_1 + j(\beta_2 F \omega - \omega^3)} \tag{A.14}$$
$$= \frac{\beta_2 \beta_1^2 (2\beta_2 \beta_1 - j(\beta_2 F \omega - \omega^3))}{4\beta_2^2 \beta_1^2 + (\beta_2 F \omega - \omega^3)^2} \tag{A.15}$$
$$\Downarrow \tag{A.16}$$
$$Re(H(j\omega)) = \frac{2\beta_2^2 \beta_1^3}{4\beta_2^2 \beta_1^2 + (\beta_2 F \omega - \omega^3)^2} > 0 \, \forall \omega \tag{A.17}$$

3. Finally, we inspect the residual of the simple pole at $s = 0$

$$Res_{s=0} H(s) = \lim_{s \to 0} sH(s) \tag{A.18}$$
$$= \frac{\beta_1}{2} > 0 \tag{A.19}$$

Thus, we have shown that $H(s)$ is positive real and that the system with input $u = -q_c$ and output p_b is passive. Of course, this was only done for a model with two control volumes, but adding an additional control volume will add two new states to the system, resulting in a new set of complex conjugate poles. All parameters are positive, so this should not affect the passivity of the hydraulic model.
Next, we look at the memoryless mapping from v to $u = -q_c$

$$-q_c = -K_c(-v)\sqrt{p_c - p_0} \tag{A.20}$$
$$\Downarrow \tag{A.21}$$
$$(-q_c)\, v = v^2 K_c \sqrt{p_c - p_0} \tag{A.22}$$

[1] The second order part of the denominator will generate poles at $s = \frac{-\beta_2 F}{2} \pm \frac{\sqrt{\beta_2^2 F^2 - 8\beta_1 \beta_2}}{2}$.

Since $K_c\sqrt{p_c - p_0} \geq 0$, this shows that the mapping from v to $-q_c$ is passive. Finally, we show how this implies that the entire system from v to p_b is passive: We have shown that the system from $-q_c$ to p_b is passive, which implies that there exists some storage function $V_1(x) \geq 0$ and some dissipation function $g_1(x) \geq 0$ such that

$$\dot{V}_1(x) = (-q_c)\, p_b - g_1(x) \tag{A.23}$$

If we then construct a new storage function by assuming that $p_c > p_0$ at all time, we can show the passivity of the entire system

$$\begin{aligned} V &= \int \frac{\dot{V}_1}{K_c\sqrt{p_c - p_0}} dt && \text{(A.24)} \\ &\Downarrow && \text{(A.25)} \\ \dot{V} &= \frac{(-q_c)\, p_b}{K_c\sqrt{p_c - p_0}} - \frac{g_1(x)}{K_c\sqrt{p_c - p_0}} && \text{(A.26)} \\ &= v p_b - \frac{g_1(x)}{K_c\sqrt{p_c - p_0}} && \text{(A.27)} \end{aligned}$$

which implies that the entire system from v to p_b is passive■

A.2 Procedure for Solving the Regulator Equations

Here, it will be shown how the regulator equations are solved for the uniform output regulation controller. The example that will be shown covers a version of the model with five control volumes, the largest which was considered in this thesis. It is trivial to then reduce the order of the model to find the regulator equations for the low order system.

This was originally done for the case where the disturbance was a single harmonic, but it is quite easy to extend this to the case where we consider the sum of an arbitrary number of sinusoids: Let us first define the vector containing the individual frequency components

$$\begin{aligned} X(t) &= \begin{bmatrix} x_1 & x_2 & ... & x_n \end{bmatrix}^T && \text{(A.28)} \\ x_i(t) &= A_i cos(\omega_i t + \epsilon_i),\ i = 1, 2, ..., n && \text{(A.29)} \end{aligned}$$

Then the position of the drill string will be given as

$$\begin{aligned} x_d(t) &= \underline{1} \cdot X(t) && \text{(A.30)} \\ \underline{1} &= \begin{bmatrix} 1 & 1 & ... & 1 \end{bmatrix} && \text{(A.31)} \end{aligned}$$

We then define the speed of the drill string in the same manner

$$\begin{aligned} V(t) &= \begin{bmatrix} v_1 & v_2 & ... & v_n \end{bmatrix} && \text{(A.32)} \\ v_i(t) &= -\omega_i A_i sin(\omega_i t + \epsilon_i) && \text{(A.33)} \\ v_d(t) &= \underline{1} \cdot V(t) && \text{(A.34)} \end{aligned}$$

Then we can write the oscillator in a compact form

$$\dot{x_d}(t) = \underline{1} \cdot V(t) \tag{A.35}$$
$$\dot{v_d}(t) = -\Omega \cdot X(t) \tag{A.36}$$

where the vector of the squared frequencies is defined as

$$\Omega = \begin{bmatrix} \omega_1^2 & \omega_2^2 & ... & \omega_n^2 \end{bmatrix} \tag{A.37}$$

Now we can start to formulate the regulator equations, but first let us just restate the model for five control volumes for reference

$$\dot{p_1} = \beta_1 \left(q_1 + q_{bpp} - K_c u \sqrt{p_1 - p_0}\right) \tag{A.38}$$
$$\dot{q_1} = \beta_2 (p_2 - p_1) - \beta_2 F q_1 - \beta_3 \tag{A.39}$$
$$\dot{p_2} = \beta_1 (q_2 - q_1) \tag{A.40}$$
$$\dot{q_2} = \beta_2 (p_3 - p_2) - \beta_2 F q_2 - \beta_3 \tag{A.41}$$
$$\dot{p_3} = \beta_1 (q_3 - q_2) \tag{A.42}$$
$$\dot{q_3} = \beta_2 (p_4 - p_3) - \beta_2 F q_3 - \beta_3 \tag{A.43}$$
$$\dot{p_4} = \beta_1 (q_4 - q_3) \tag{A.44}$$
$$\dot{q_4} = \beta_2 (p_4 - p_3) - \beta_2 F q_3 - \beta_3 \tag{A.45}$$
$$\dot{p_5} = \beta_1 (-q_3 - v_d A_d) \tag{A.46}$$

Here, some constants have been redefined for simplicity (and β_4 for future sake)

$$\beta_1 = \frac{\beta}{Al} \tag{A.47}$$
$$\beta_2 = \frac{A}{l\rho} \tag{A.48}$$
$$\beta_3 = \frac{gA\Delta h}{l} \tag{A.49}$$
$$\beta_4 = \rho g \Delta h \tag{A.50}$$

and Fq_i represents the friction force. Having this, we can readily formulate the regulator equations

$$\dot{\pi_1} = \beta_1 \left(\pi_1 + q_{bpp} - K_c c \sqrt{\pi_1 - p_0}\right) \tag{A.51}$$
$$\dot{\pi_2} = \beta_2 (\pi_3 - \pi_1) - \beta_2 F \pi_2 - \beta_3 \tag{A.52}$$
$$\dot{\pi_3} = \beta_1 (\pi_4 - \pi_2) \tag{A.53}$$
$$\dot{\pi_4} = \beta_2 (\pi_5 - \pi_3) - \beta_2 F \pi_4 - \beta_3 \tag{A.54}$$
$$\dot{\pi_5} = \beta_1 (\pi_6 - \pi_4) \tag{A.55}$$
$$\dot{\pi_6} = \beta_2 (\pi_7 - \pi_5) - \beta_2 F \pi_6 - \beta_3 \tag{A.56}$$
$$\dot{\pi_7} = \beta_1 (\pi_8 - \pi_6) \tag{A.57}$$
$$\dot{\pi_8} = \beta_2 (\pi_9 - \pi_7) - \beta_2 F \pi_8 - \beta_3 \tag{A.58}$$
$$\dot{\pi_9} = \beta_1 (-\pi_8 - w_2 A_d) \tag{A.59}$$
$$0 = \pi_9 - w_3 \tag{A.60}$$

Here, we have defined the exosystem as the oscillator and the external (constant) reference signal

$$w_1 = x_d \tag{A.61}$$
$$w_2 = v_d \tag{A.62}$$
$$w_3 = p_b^{ref} \tag{A.63}$$

Then, we can start from the bottom of the regulator equations and work our way back up. For simplicity, let us adopt the following notation for the higher order time derivatives

$$x^{(i)} \equiv \frac{d^i}{dt^i}(x) \tag{A.64}$$

First

$$\pi_9 = w_3 \tag{A.65}$$
$$\Downarrow$$
$$\pi_9^{(1)} = 0 \tag{A.66}$$
$$\Downarrow$$
$$\pi_8 = -w_2 A_d \tag{A.67}$$
$$\Downarrow$$
$$\pi_8^{(1)} = (\Omega \cdot X) A_d \tag{A.68}$$
$$\Downarrow$$
$$\pi_7 = \pi_9 - \frac{\pi_8^{(1)}}{\beta_2} - F\pi_8 - \beta_4 \tag{A.69}$$
$$\Downarrow$$
$$\pi_7^{(1)} = -\frac{\pi_8^{(2)}}{\beta} - F\pi_8^{(1)} \tag{A.70}$$
$$\pi_8^{(2)} = (\Omega \cdot V) A_d \tag{A.71}$$
$$\Downarrow$$

Etc, etc. For the sake of sanity (and from the realization that no-one will read all the 40 remaining equations), I will stop this here, but I think it is clear how one can proceed to solve these equations by back substitution. From an implementation point of view, it might be a good idea to store all the time derivatives of the different π_i, just so that the equations look simpler. Proceeding this all the way down to π_1, one can see that the final expression is

$$\pi_1 = \pi_3 - \frac{\pi_2^{(1)}}{\beta_2} - F\pi_2 - \beta_4 \tag{A.72}$$
$$\Downarrow \tag{A.73}$$
$$c = \frac{\pi_2 + q_{bpp} - \frac{\pi_1^{(1)}}{\beta_1}}{K_c\sqrt{\pi_1 - p_0}} \tag{A.74}$$

A warning to be given is that this formulation obscures the fact that one needs to calculate a high number of time derivatives. (This is not a problem in the usual sense: These time derivatives are a result of the disturbance model used and can be calculated.) However, one needs to calculate as far as $\pi_8^{(8)}$ and a large number of the time derivatives of the other variables, so the total number of equations to evaluate is quite large.

A.3 Definitions

Definition 2. [Stability]
A solution $\bar{z}(t)$ of the system from definition 1, which is defined for $t \in (t_*, +\infty)$ is said to be:

- Stable if for any $t_0 \in (t_*, +\infty)$ and $\varepsilon > 0$ there exists $\delta = \delta(\varepsilon, t_0) > 0$ such that $|z(t_0) - \bar{z}(t_0)| < \delta$ implies $|z(t) - \bar{z}(t)| < \varepsilon$ for all $t > t_0$.
- Uniformly stable if it is stable and the δ in the previous definition is independent of t_0.
- Asymptotically stable if it is stable and for any $t_0 \in (t_*, +\infty)$ there exists $\bar{\delta} = \bar{\delta}(t_0) > 0$ such that $|z(t_0) - \bar{z}(t_0)| < \bar{\delta}$ implies $\lim_{t\to\infty} |z(t) - \bar{z}(t)| = 0$.
- Uniformly asymptotically stable if it is uniformly stable and there exists $\bar{\delta} > 0$ (independent of t_0) such that for any $\varepsilon > 0$ there exists $T = T(\varepsilon) > 0$ such that $|z(t_0) - \bar{z}(t_0)| < \bar{\delta}$ for $t_0 \in (t_*, +\infty)$ implies $|z(t) - \bar{z}(t)| < \varepsilon$ for all $t > t_0 + T$.

Definition 3. [Quadratic Stability]
A matrix function $A(\psi) \in \mathbb{R}^{d\times d}$ is said to be quadratically stable over a set Ξ if for some $P = P^T > 0$ and $Q = Q^T > 0$

$$PA(\psi) + A(\psi)^T Q < -Q \ \forall \psi \in \Xi \tag{A.75}$$

Definition 4. [Positive Real Transfer Function]
The rational transfer function $H(s)$ is said to be positive real if and only if the following conditions are met:

1. All the poles of $H(s)$ have real parts less than or equal to zero.
2. $Re(H(j\omega)) \geq 0$ for all ω such that $j\omega$ is not a pole of $H(s)$.
3. If $j\omega_0$ is a pole of $H(s)$, then it is a simple pole and

$$Res_{s=j\omega_0} H(s) = \lim_{s\to j\omega_0} (s - j\omega_0) H(s) \tag{A.76}$$

is real and positive. If $H(s)$ has a pole at infinity, then $R_\infty = \lim_{\omega\to\infty} \frac{H(j\omega)}{j\omega}$ exists and is real and positive.

A.4 Calculating Geometrical Constants for Friction Model

First, define the ratio to the diameters in the annulus as $k = \frac{d_i}{d_o}$. Then, one can find the geometrical constants as

$$a = \frac{(1-k)^2}{4\left(1 - \frac{1-k^2}{2\ln 1/k}\left[1 - \ln\frac{1-k^2}{2\ln 1/k}\right]\right)} \tag{A.77}$$

$$b = \frac{(1-k)^2}{1+k^2-\frac{1-k^2}{\ln 1/k}} - a \tag{A.78}$$

A.5 The Harmonic Addition Theorem

The harmonic addition theorem states that the sum of an arbitrary number of sinusoids with the same frequency can be written as one single sinusoid with that frequency. In fewer words

$$\sum_{i=1}^{n} A_i cos\left(\omega t + \delta_i\right) = A cos\left(\omega t + \delta\right) \tag{A.79}$$

The amplitude and phase shift are given by

$$A^2 = \sum_{i=1}^{n}\sum_{j=1}^{n} A_i A_j cos\left(\delta_i - \delta_j\right) \tag{A.80}$$

$$tan\left(\delta\right) = \frac{\sum_{i=1}^{n} A_i sin\left(\delta_i\right)}{\sum_{i=1}^{n} A_i cos\left(\delta_i\right)} \tag{A.81}$$

Appendix B

Conference Papers

These conference papers were submitted to the American Control Conference, and a response is awaited on the time of delivery of this thesis. The first paper is more or less a summary of the fall project "Advanced Modeling for Managed Pressure Drilling," and includes the work on model reduction techniques. The second paper is a brief view on heave compensation on the bottom hole pressure.

Developments in drilling process modeling for MPD operations: A case study of Ullrigg drilling rig

Ingar Skyberg Landet, Hessam Mahdianfar, Alexey Pavlov, Ole Morten Aamo
Engineering Cybernetics, Faculty of Information Technology, Mathematics and Electrical Engineering
Norwegian University Of Science and Technology (NTNU)
Trondheim, Norway
Email: ingarsky@stud.ntnu.no, hessam.mahdianfar@itk.ntnu.no, alepav@statoil.com, aamo@ntnu.no

***Abstract*—In this paper, a mathematical model that describes the distribution of flow and pressure in a drilling fluid is derived. The model is based on a hydraulic transmission line, and is discretized through a finite volumes method. Furthermore, three new scenarios are added to this model: circulating in a new type of drilling fluid, vertical motion of the drill string and rotation of the drill string. In addition, a new friction model is also explored based on the non-Newtonian characteristics of the drilling fluid together with available experimental data. Finally, this model is verified through simulations, compared and tuned to available experimental data from UllRigg tests. In the last part of the paper, reducing the complexity of model via decreasing the number of control volumes and balanced order reduction technique are compared and it is shown that the latter performs significantly better, and it can be considered as an alternative for simplifying the model for control design purposes.**

I. Introduction

In drilling operations, a drilling fluid called mud is pumped down the drill string and flows through the drill bit in the bottom hole of the well (See Figure 1 taken from [1]). Then it flows up the well annulus carrying cuttings out of the well. It is also used to keep the pressure in the annulus at a desired level. This pressure control is crucial in all drilling operations, as the pressure has to be between certain boundaries. Specifically, it has to be above the pore pressure to prevent unwanted inflow from the surrounding formations into the well. Moreover, it has to be below the fracture pressure of the surrounding formations to prevent the well from fracturing.

Managed pressure drilling (MPD) is an adaptive drilling process used to precisely control the annular pressure profile throughout the well-bore. The objectives are to ascertain the down-hole pressure environment limits and to manage the annular hydraulic pressure profile accordingly [2]. Controlling the annulus pressure in an oil well during drilling can be a challenging task, due to the very complex dynamics of the multiphase flow potentially consisting of drilling mud, oil, gas and cuttings. By allowing manipulation of the topside choke and pumps, MPD provides a means of quickly affecting pressure to counteract disturbances, and several control schemes are found in the literature [2].

Since down-hole pressure measurements are unreliable due to slow sampling or transmission delays, the core component in the control schemes is an estimator for the down-hole pressure. In [3], an unscented Kalman filter exploiting down-hole measurements is used to tune the predicted pressure loss due to friction in both the drill string and the annulus. In [4]–[6], nonlinear adaptive observers were developed based on a simple dynamic model, consisting of only three ordinary differential equations. In [7], nonlinear model predictive control in combination with an unscented Kalman filter was used to control the bottom-hole pressure based on a two-phase flow model in [8] and [9]. In [10] a switched control scheme for regulation of

the annular pressure in a well during drilling is presented. There is still a significant potential to improve existing control and estimation schemes. To accurately control mud pressure in a given position inside the well, one needs to have an accurate model of pressure distribution along the well in various operational procedures. The objective of this paper is to further extend and analyze the existing model for various operational scenarios including

1) Circulation of different muds (changes in viscosity, density and bulk modulus)
2) Vertical motion of the drill string
3) Rotational motion of the drill string
4) Mud gelling (viscous friction with stiction).

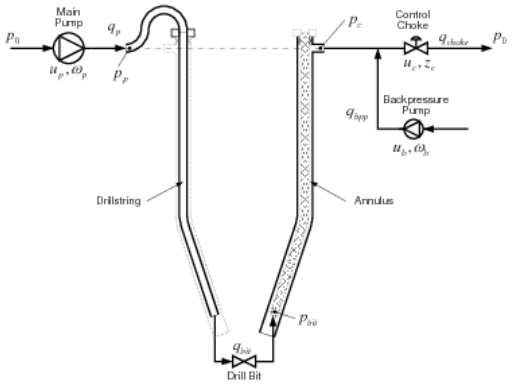

Figure 1. Schematic representation of drilling set up

II. Mathematical Modeling

A. Hydraulic Transmission Line

This derivation follows that from [11], pages 429-430. The hydraulic transmission line model is derived from the mass and momentum balances for a differential control volume Adx where $A[m^2]$ is the cross section area and $x[m]$ is the spatial coordinate along the volume. The volume contains a compressible fluid with density $\rho(x,t)[\frac{kg}{m^3}]$, and by looking at the average velocity of the fluid over the cross section, we can find the mass balance for the volume. First, the mass flow $w[\frac{kg}{s}]$ is

$$w(x,t) = \int_A \rho v dA = \rho \bar{v} A \tag{1}$$

where $\bar{v}$ is the average velocity. Thus, for this simple one-dimensional problem, the mass balance is found to be

$$\frac{\partial \rho}{\partial t} = -\frac{1}{A}\frac{\partial w}{\partial x} \tag{2}$$

This is now in the form of a differential equation that describes the dynamics of the density in the volume. Instead, we would like to make a change of variables to pressure, and this is achieved by considering the equation, $dp = (\beta/\rho)d\rho$ where $\beta[Pa]$ is bulk modulus. This gives:

$$\frac{\partial p}{\partial t} = -\frac{\beta}{A}\frac{\partial q}{\partial x} \tag{3}$$

To find an equation for the flow rate, q, we consider the momentum balance for the same control volume, which reduces to:

$$\frac{\partial w}{\partial t} = -A\frac{\partial p}{\partial x} - A\frac{\partial}{\partial x}\int_A \rho v^2 dA - F + A\rho g\cos(\alpha) \tag{4}$$

where the term α is defined as the angle between the positive flow direction and gravity $g[\frac{m}{s^2}]$. Fdx is the friction force acting on the volume. Now, assuming that the change $\frac{\partial}{\partial x}\int_A \rho v^2 dA$ is small, we neglect this term and, as before, treat the density as a constant, we get the equation for the volumetric flow rate:

$$\frac{\partial q}{\partial t} = -\frac{A}{\rho_0}\frac{\partial p}{\partial x} - \frac{F}{\rho_0} + Ag\cos(\alpha(x)) \tag{5}$$

To summarize, the continuous differential equations describing the hydraulic transmission line are given by equations (3) and (5).

B. Discretized Simulation Model With Variable Complexity

The transmission line model found in the previous subsection is in the form of two coupled partial differential equations. For simulation this has to be discretized in both time and space, so we choose a simple finite volumes method and apply the differential equations to the average pressures and flows of each control volume. To make this work out, we define the volumes in a staggered manner, interpreting the average pressures and flows to exist in the center of their own volumes.

1) Boundary Conditions: Boundary conditions for the model are the different external inputs; the mud pump flow q_p, the back pressure pump flow q_{bpp}, the influx from the surroundings q_f and the control choke opening z_c. The flow from the different pumps is modeled by q_p. The choke flow is modeled simply by the orifice equation, $q_c = K_c g_c(z_c)\sqrt{\frac{\Delta p}{\rho}}$, where K_c is some constant and $g_c(z_c)$ gives the choke opening as a function of the control signal. The influx q_f is seen as a disturbance and should be zero for most operations.

2) Parameterization of Physical Quantities: All physical quantities on the right hand side of (3) and (5) have to be parameterized as a function of the spatial coordinate x, so that control volume i has its own cross section A_i, density ρ_i, bulk modulus β_i, height difference Δh_i and frictional pressure loss $F_i = F(q_i, d_i, l_i, \rho_i, \mu_i)$ where $d_i[m]$ is the diameter of the drill string (or hydraulic diameter of annulus) in cross section i, $l_i[m]$ is the length of volume i and μ_i $[\frac{kg}{sm}]$ is the viscosity in volume i.

3) Complete Simulation Model: Combining all of these, we can now write down the entire simulation model for an arbitrary number of control volumes N:

$$
\begin{aligned}
\dot{p}_{1d} &= \frac{\beta_{1d}}{A_{1d} l_{1d}}(q_p - q_{1d}) \\
\dot{p}_{2d} &= \frac{\beta_{2d}}{A_{2d} l_{2d}}(q_{1d} - q_{2d}) \\
&\vdots \\
\dot{p}_{Nd} &= \frac{\beta_{Nd}}{A_{Nd} l_{Nd}}(q_{(N-1)d} - q_{bit}) \\
\dot{q}_{1d} &= \frac{A_{1d}}{l_{1d}\rho_{1d}}(p_{1d} - p_{2d}) - \frac{F_{1d}A_{1d}}{\rho_{1d} l_{1d}} \\
&\quad + Ag\frac{\Delta h_{1d}}{l_{1d}} \\
&\vdots \\
\dot{q}_{(N-1)d} &= \frac{A_{(N-1)d}}{l_{(N-1)d}\rho_{(N-1)d}}(p_{(N-1)d} - p_{Nd}) \\
&\quad - \frac{F_{(N-1)d}A_{(N-1)d}}{\rho_{(N-1)d} l_{(N-1)d}} + Ag\frac{\Delta h_{(N-1)d}}{l_{(N-1)d}} \\
\dot{q}_{bit} &= \frac{2A_{Nd}A_{1a}}{A_{1a}\rho_{Nd} l_{Nd} + A_{Nd}\rho_{1a} l_{1a}}\Big((p_{Nd} - p_{1a}) \\
&\quad - F_{bit} + \frac{g(\rho_{Nd}\Delta h_{Nd} - \rho_{1a}\Delta h_{1a})}{2}\Big) \\
\dot{p}_{1a} &= \frac{\beta_{1a}}{A_{1a} l_{1a}}(q_{bit} - q_{1a} + q_f) \\
&\vdots \\
\dot{p}_{Na} &= \frac{\beta_{Na}}{A_{Na} l_{Na}}(q_{(N-1)a} - q_c + q_{bpp}) \\
\dot{q}_{1a} &= \frac{A_{1a}}{l_{1a}\rho_{1a}}(p_{1a} - p_{2a}) - \frac{F_{1a}A_{1a}}{\rho_{1a} l_{1a}} \\
&\quad - Ag\frac{\Delta h_{1a}}{l_{1a}} \\
&\vdots \\
\dot{q}_{(N-1)a} &= \frac{A_{(N-1)a}}{l_{(N-1)a}\rho_{(N-1)a}}(p_{(N-1)a} - p_{Na}) \\
&\quad - \frac{F_{(N-1)a}A_{(N-1)a}}{\rho_{(N-1)a} l_{(N-1)a}} - Ag\frac{\Delta h_{(N-1)a}}{l_{(N-1)a}}
\end{aligned}
\tag{6}
$$

Here, the subscripts a, d refer to annulus and drill string, respectively. We also define the influx from the surroundings to enter into volume 1 on the annulus side. This is because the rest of the annulus is usually cased in concrete so there should be no influx into the other volumes. Finally, the equation for the drill bit flow q_{bit} is described in a similar manner to what was done in [1]. Here however, we use only the lower-most volumes on each side of the bit to calculate the pressure and weight difference.

C. Friction Model

The drilling mud is a highly complex fluid that does not exhibit the classical Newtonian behavior. It is known to exhibit a so called yield stress, meaning that it takes a certain pressure gradient to initiate flow. We consider the implications of the non-Newtonian behavior in this paper.

1) Bingham Plastic Rheological Model: In this paper, the Bingham plastic model is used to describe drilling mud flow model, which incorporates a yield stress:

$$\tau = \tau_0 + \mu\frac{\partial v}{\partial y} \tag{7}$$

where $\tau_0[Pa]$ is the yield stress and μ is the consistency.

2) Frictional Pressure Losses in Steady, Laminar Flow: A classical friction model including a static break-away force is used to model the yield stress behavior of the system. This model takes the following form:

$$F = \begin{cases} F(v) & v \neq 0 \\ F_e & v = 0 \, and \, |F_e| < F_s \\ F_s sgn(F_e) & otherwise \end{cases} \quad (8)$$

The idea is that we look at the pressure difference over a control volume, $F_e = \Delta p - \rho g \Delta h$, and see if this is larger than the yield pressure, F_s. If it is not, the friction force will exactly match the external pressure force. If it is larger however, there will be a non-zero flow, and we can calculate the pressure loss as $F(v)$, given by constant yield pressure plus a term proportional to flow rate for viscous friction; $F(v) = k_1 + k_2 v$. This model provides enough damping for low flow rates. Figure 2 shows the pressure difference from mud pump to control choke and the mud pump flow for the same experiment. These pressures are at approximately the same height, so the difference should be mostly given by friction alone. From this experiment, we can also find the pressure drops in the annulus and drill string alone by looking at the down hole measured pressure and correcting for the height difference. These pressure losses as a function of flow rate can be seen in Figure 3. Notice that the pressure drops in the drill string also include the valve at the drill bit, which typically has a high pressure drop.

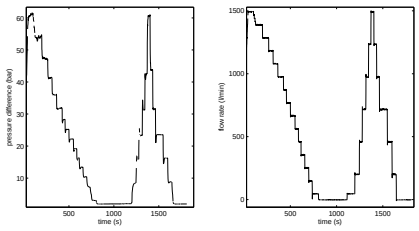

Figure 2. Pressure difference and flow rate for experimental data.

Now, analyzing this, we can see that the pressure losses seem to be a linear function of the flow rate for a large range of flows, something that fits well with the standard theory on friction factors for laminar flow regime. What is more important is that we do not see a build up in pressure difference that is needed to overcome a static break-away force. Instead, one might think of this as the pump pushing the solid gel with a constant force until the gel yields and begins to flow. This is what inspired the final model of the mud as a substance that can change between different phases dependent on external influence, governed by the simple state diagram in Figure 4.

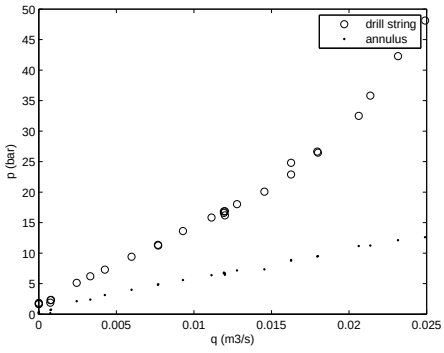

Figure 3. Pressure drops in drill string and annulus, UllRigg data.

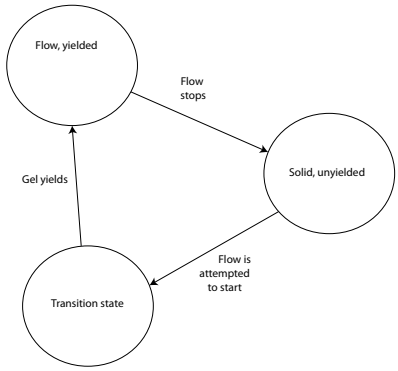

Figure 4. State diagram for gel/liquid behavior.

To conclude, the influence of the friction can be expressed in the following way. In the zero flow state, there is no change anywhere in the system, we are in a steady state. When flow is initiated,

there is a resistance against the flow, but this is due to the solid state of the gel and does not lead to an increased pressure anywhere in the system. When the gel breaks down and starts to flow as a fluid, in the laminar flow regime there would be a friction force that is linear in the flow rate, $F(v) = k_1 + k_2 v$. To model this linear friction force, we add a quite small constant k_1 to increase the damping and stability of the system for low flow rates. The second part, $k_2 v$, can be modeled using standard Newtonian friction factor correlation $f = \frac{16}{Re}$ where the Fanning friction factor and Reynolds number are defined as above. The tuning parameters will then be the physical properties of the mud, especially the viscosity, which can be obtained by substituting the Reynolds number and friction factor into the equation for the pressure loss to give the following linear expression:

$$\Delta p = \frac{32 \mu L v}{R^2} \tag{9}$$

3) Effects of Different Geometries: In this paper we are interested in taking a unified approach towards different geometries in friction factor similar to what is done in [12]. The paper finds a unified solution by letting the friction factor for the laminar case to be $f = \frac{16}{Re^*}$, where Re^* is a generalized Reynolds number defined by $Re^* = \frac{\rho v^{2-n^*} r_h^{n^*}}{2^{n^*-3} K^*}$. Here, r_h is the hydraulic radius and is given by

$$r_h = \begin{cases} \frac{d}{4} & cylinder \\ \frac{(d_2 - d_1)}{4} & concentric\, annulus \end{cases}$$

n^* and K^* have very specific meaning, but in the simple case of the Newtonian model, it suffices to say that they reduce to $n^* = 1$ and $K^* = \mu(a+b)$ where a and b are constants defining the geometry of the cross section. For a cylinder, $a + b = 1$, and it is easy to show that Re^* reduces to the familiar Re for Newtonian flow in a circular pipe. But for the concentric annulus $a + b = \frac{(1-k)^2}{1 + k^2 - \frac{1-k^2}{ln 1/k}}$, $k = \frac{R_1}{R_2}$, and $Re^* = \frac{4 \rho v r_h}{\mu(a+b)}$.

4) Transition to Turbulent Flow: Following the simplification and using the model from the previous subsection, it makes sense to use the generalized Reynolds number as an indicator of laminar flow and expect laminar flow whenever $Re^* < 2300$. However, by examining Figure 3, we can see that there is a transition in the friction losses in the drill string, possibly due to a transition to turbulent flow. This seems to happen at a flow rate of around $q = 0.0175 \frac{m^3}{s}$. Using the density and estimated viscosity for the mud used in this experiment, this can be translated into a critical Reynolds number for the end of laminar flow. However, the critical Reynolds number is probably quite empiric and subject to other conditions of the flow, especially the inlet conditions. During the transition phase, the friction factor is highly uncertain, and neither equations for laminar nor turbulent flow will be accurate. One proposed approach is to use a linear function, $f = a_f Re + b_f$, to describe the friction factor in this phase, where $f(Re_{crit}) = \frac{16}{Re_{crit}}$ and $f(Re_{fully\, turbulent})$, given in the next section, are used to find the constants a_f, b_f. Still, one would have to determine the Reynolds number at which the flow is fully turbulent.

5) Fully Turbulent Flow: For the case of fully turbulent flow, one usually relies on empirical or semi-empirical models for calculating the friction factor. The most celebrated one is the Colebrook equation:

$$\frac{1}{\sqrt{f_D}} = -2 log_{10}\left(\frac{\delta/d_h}{3.7} + \frac{2.51}{Re\sqrt{f_D}}\right) \tag{10}$$

This equation takes into account the roughness of the pipe through the constant δ. Notice that the subscript D refers to the fact that this is the Darcy friction factor, which is easily related to the Fanning friction factor by $f = 4 f_D$. This is an implicit equation and can be solved by a simple iterative procedure. However, there are several explicit approximations to this equation, in particular the one due to Haaland:

$$\frac{1}{\sqrt{f_D}} = -1.8 log_{10}\left[\left(\frac{\delta/d_h}{3.7}\right)^{1.11} + \frac{6.9}{Re}\right] \tag{11}$$

The Haaland equation is accurate enough and better suited for the implementation in a simulator program. To calculate the frictional pressure losses, the state diagram Figure 4 is first consulted. If we are in the transition state, in the simulations presented here, we just wait for the gel to yield. If,

on the other hand, we are in the flowing state, the Reynolds number is first calculated to indicate the flow regime. Then, the friction factor is calculated as described in the previous subsections, and via this friction factor, we find the pressure drop.

D. New Mud Circulation

To model the scenario of circulating in a new type of mud to the system, we approach it by keeping track of the distance traveled by the front between the two types of mud. This front divides a control volume into two parts, so that we do not consider mixing the properties of the two types of mud. We can then use the correct two-volumes model described in the previous section to propagate the front and the pressure changes in the system.

The following model is proposed as two-volumes model:

$$\begin{aligned}\dot{p}_{v1} &= \frac{\beta_1}{Al_1}(q_1 - q_f) + \frac{q_f \rho_1 g}{2A} - F\frac{q_f}{2lA} \\ \dot{q_f} &= \frac{2A}{l\bar{\rho}}(p_{v2} - p_{v1}) - F\frac{A}{\bar{\rho}l} + gA \\ \dot{p}_{v2} &= \frac{\beta_2}{Al_2}(q_f - q_2) + \frac{q_f \rho_2 g}{2A} - F\frac{q_f}{2lA}\end{aligned} \tag{12}$$

Here, again, F is the pressure drop due to friction, and has also been included to reflect the fact that when the midpoint of the control volume shifts, there is also a pressure change due to a different friction drop. The multiplication by $\frac{1}{2}$ reflects the fact that for a certain expansion of the length of a control volume, the midpoint is shifted by half of this expansion. $\bar{\rho}$ is an average density defined by $\bar{\rho} = \frac{\rho_1 l_1 + \rho_2 l_2}{l}$ and q_f describes the speed of the front by $q_f = v_f A$. l_1 and l_2 are described by the dynamic variable $\dot{x_f} = q_f/A$ so that $l_1 = mod(x_f, l)$ and $l_2 = l - l_1$ where x_f is the position of the front. Notice that in this case, there is actually no flow going out of volume one and no flow going into volume two, so the terms q_f actually describe the changes in volumes one and two, $q_f = \dot{V}_1 = -\dot{V}_2$.

Care must also be taken to ensure that we calculate q_1 and q_2 correctly. The issue here is just to get the right size of the control volumes where these flows are defined, and this is solved by introducing the new lengths $\bar{l_1}, \bar{l_2}$ defined by $\bar{l_1} = \frac{l_1 + l}{2}$ and $\bar{l_2}$ in the same way.

E. Vertical Motion of Drill String

The scenario of moving the drill string vertically in the well is something that might arise in two different ways; heave and tripping. Tripping is the operation of pulling the drill string out of the well, and heave is encountered when the drilling vessel is subjected to waves on the sea surface.

To model the vertical motion of the drill string, an additional dynamic variable, x_d is considered. This variable keeps track of the current position of the drill bit, and is governed by the dynamic equation $\dot{x_d} = v_d$ where v_d is the speed of the drill bit, taken as an exogenous signal. Using v_d and x_d, we can modify the frictional pressure losses as well as the dynamics of the pressures and flows surrounding the actual drill bit.

1) Changes in Drill String Dynamics: The control volumes are moving with the speed of the drill string, so the transport of any quantity over the cross sections is the same as before, as in equations (3), and (5).

2) Changes in Annulus Dynamics: If we consider the control volumes containing the mud in the annulus region, they will consist of the fixed walls of the well, which are not moving, as well as the moving inner cylinder. Although there is no transport of any quantity over this moving boundary, the relative velocity between the fluid inside and the walls of the inner cylinder changes, which causes the pressure drop due to friction to change as well. To include this in the model, we look at the described friction factor in II-C3.

In this paper, all derivations are actually done by introducing a slip velocity $v_0 = \frac{1}{h}\int_h v_w ds$, where h is the contour of the cross section and v_w is the slip velocity at the wall. Now, interpreting this in a slightly different way by assuming no slip, but letting the actual wall of the inner cylinder move with a constant speed v_d, we can find v_0 as $v_0 = \frac{R_1}{R_2} v_d$, reflecting the fact that only the inner cylinder is moving. Using this, we can now find the Reynolds number as $Re^* = \frac{4\rho(v - u_0)r_h}{\mu(a+b)}$, and calculate the pressure losses as before.

Another issue that needs to be addressed is what happens to the control volume in which the bottom of the drill string is currently in. As the drill string moves up and down, this control volume will change size, and the pressure directly outside of the drill bit will change, affecting the flow through the drill bit, q_{bit}. The first issue is solved by keeping track of the distance moved by the drill bit and then calculating the pressure change as:

$$\dot{p} = \frac{\beta}{V}(q_{in} - q_{out} - v_d A_d) \tag{13}$$

Here, q_{in} refers to the sum of all flows into the volume, i.e. $q_{\text{in}} = q_{bit} + q_f + q_a(i-1)$ and v_d is defined positive upwards so that $v_d A_d = \dot{V}$. The second issue is also solved by keeping track of the distance moved by the drill bit and calculating the pressure at the current bit position. This pressure will then determine the dynamics of q_{bit}.

F. Rotation of Drill String

Rotating the drill string has a positive effect on cleaning the borehole and effectively moving cuttings out of the way. For our purposes we need a model that is only concerned with the change in frictional pressure losses. Using the empirical and semi-empirical relationships, we can calculate the new pressure losses in both the drill string and the annulus given the rotational speed of the drill string.

1) Changes in Drill String Pressure: For laminar flow, [13] found the empirical relationship

$$f_D = 31\frac{Re_\omega^{0.16}}{Re} \tag{14}$$

where the rotational Reynolds number is defined as $Re_\omega = \frac{d\rho v_\omega}{\mu}$, in which v_ω is the azimuthal speed of the rotating pipe, $v_\omega = \omega R$, and ω is the rotational speed of the pipe. This expression for the friction factor is claimed to be valid for $500 < Re < 1500$ and $500 < Re_\omega < 5000$.

2) Changes in Annulus Pressure: Ahmed et al [14] used extensive data from four different wells during actual drilling operations together with dimensional analysis techniques to find the following model:

$$\begin{aligned}\text{PLR} &= \frac{(dP/dL)_\omega}{(dP/dL)_{\omega=0}} \\ &= 0.36\big(13.5 + \frac{\tau_0}{\rho v^2}\big)^{0.428} \times \epsilon_{av}^{0.158} \times Ta^{0.0319} \\ &\quad \times n^{0.054} \times Re_{eff}^{0.042} \times k(\frac{1}{k} - 1)^{-0.0152}\end{aligned} \tag{15}$$

stated in words, the ratio of the pressure loss with rotation to the pressure loss without rotation is defined as a function of several physical and geometrical properties. Here, τ_0 is the yield stress of the fluid, ϵ_{av} $[\frac{1}{m}]$ is the average eccentricity of the well, Ta is the Taylor number, n is fluid behaviour index, Re_{eff} the effective Reynolds number and k the ratio of the diameters. These quantities are defined by:

$$\epsilon_{av} = \frac{2E}{d_2 - d_1}\frac{L}{\Delta h} \tag{16}$$

Here, E is the eccentricity and is recommended to be 50% for a straight well, and larger for an inclined one. Δh is the change in elevation, equal to L for a straight well.

$$Ta = \frac{d_1\,(d_2 - d_1)^3}{16}\left(\frac{\rho\omega}{\mu}\right)^2 \tag{17}$$

$$Re_{eff} = \frac{8\rho v^2}{\tau_{wall}} \tag{18}$$

where τ_{wall} is the wall shear stress.

III. Simulation Results and Accuracy Analysis

In this part, simulation results are presented. For most of the simulations, specific scenarios are recreated for which experimental data from Ull-Rigg tests were available. In these data sets, there were normally measurements of choke flow, choke opening, mud pump flow, back pressure pump flow, mud pump pressure, choke pressure as well as a down-hole pressure sensor. In addition, there were measurements of the position of the drill string as well as rotation rate which are used for the scenarios of heave and rotation. Normally, the mud pump flow and control choke opening are considered as external signals for the simulations; and the pressure estimates from the simulated model are compared to the measured pressures.

A. *Friction Model*

The frictional pressure losses are normally a function of the fluid velocity, so for purposes of verifying, and tuning our model, one of the experimental data sets in which the velocity varied over a large region is used. In this data set, the mud pump flow is stepped up and down between $1500\frac{l}{min}$ and $0\frac{l}{min}$ while the control choke is kept open at 100%. Using these two signals from the data set, the scenario was simulated, and the resulting pressure estimates are shown in Figure 5. The applied mud pump flow rate, $q_p = \omega_p V_{lps}$, is illustrated in Figure 2. We can see that the steady state pressures match the data fairly well.

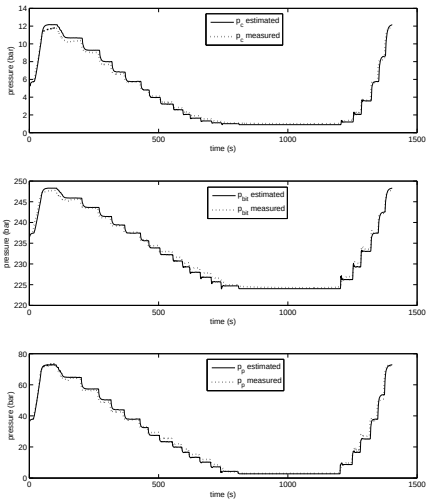

Figure 5. Measured and estimated pressure for stepping of mud pump flow.

The number of control volumes is not important for capturing the steady state pressures or the restart of mud flow, but it does play a role when it comes to the speed of pressure waves traveling the system. As we can see from Figure 6, a lower order system reacts more slowly, and during the fast transients, the estimated pressure is somewhat erroneous. Moreover, it is evident that the difference between $N = 10$ and $N = 50$ is small, and even the lowest order, $N = 2$, is capable of reasonably well reproducing the dynamics, although it lags and introduces a small time delay in the estimate of the pressure.

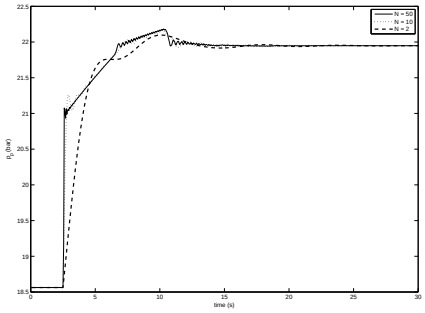

Figure 6. Step in input mud flow rate, different number of control volumes.

B. *Vertical Motion of Drill String*

For this scenario, heave emulation data from UllRigg experiments are used. For these experiments, the drill string was moved periodically up and down with relatively high frequency while the mud pump flow was kept constant and the choke fully opened. A measurement of the relative drill string position was then taken, which is used to estimate the velocity of the drill string. A plot of the measured relative position together with estimated velocity is given in Figure 7.

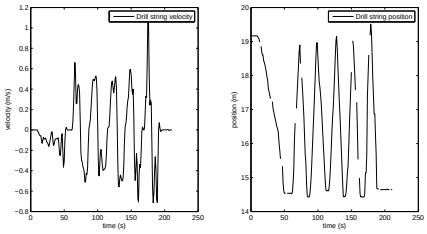

Figure 7. Position and velocity for heave emulation, UllRigg.

Simulation results compared to UllRigg data are shown in Figure 8. A note to these simulations is that the mud pump is actually turned off and the back pressure pump is turned on, thus the pressure dynamics of the drill string are really not

interesting. In other words, there is no externally forced flow through the entire system, just around the choke.

As we can see, the main dynamics are captured

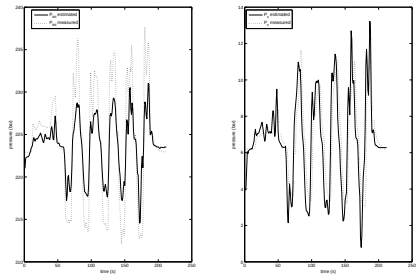

Figure 8. Pressure estimates compared to UllRigg data, heave emulation.

through the described model. The phase of the pressure fluctuations is correct and the timing of the fluctuations is very good for the drill bit pressure.

Figure 9 shows how the number of control volumes affects the simulations. We can see that for $N = 10$ and $N = 50$ the differences are small; but in this case, the lowest order model is not performing well. Therefore, using a model with higher number of control volumes is recommended for pressure control design subject to the heave motion.

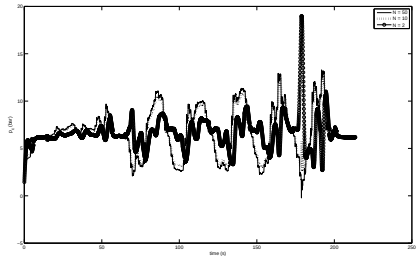

Figure 9. Heave simulation, different number of control volumes.

C. Rotation of Drill String

For this scenario the available experimental data from UllRigg is used. An experiment was done running the system with constant mud pump flow and fully open choke, while the drill string was rotated with different rotation rates. A measurement of this rotation rate was taken, which is used as an input signal for the simulations. Simulation results compared to UllRigg data are presented in Figure 10. We can see that the semi-empirical models give a fairly good estimate of the actual dynamics. In this simulation, the first pressure peak corresponds to a rotation rate of $100RPM$ whereas the second and third correspond to a rotation rate of $150RPM$, see Figure 11.

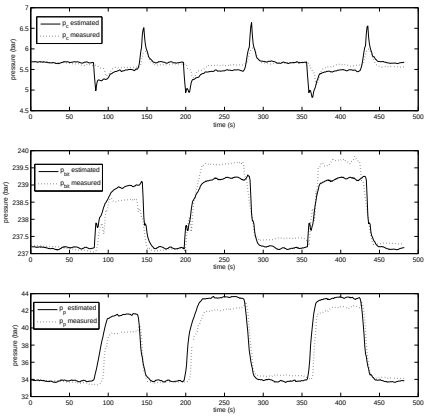

Figure 10. Estimated and measured pressure for rotating drill string.

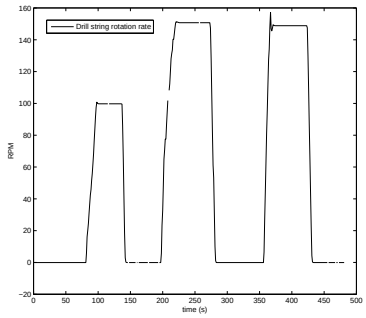

Figure 11. Drill string rotation rate.

To see how the number of control volumes af-

fect the results, this scenario was simulated with different order models, and the results can be seen in Figure 12. It is clear that the lowest order model has quite a large error when compared to the higher order models.

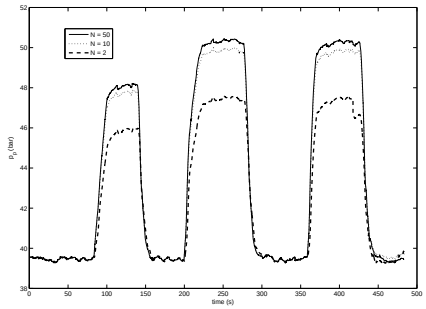

Figure 12. Rotating drill string, different number of control volumes.

D. Model Reduction by Balanced Truncation

Balanced truncation method is used for model order reduction in this paper. To find a reasonable truncation size, one can look at how the Hankel singular values decay and truncate at a point where there is a significant drop in the magnitude of these values. The peak error in the magnitude of the transfer function of the reduced order system is no more than twice the sum of the truncated Hankel singular values [15], however this error bound can be quite conservative.

To apply this to the described system, it is necessary to have it in a linear form. Our friction model might cause problems for this formulation, but as we have seen at least in the laminar case, the friction loss is actually a linear function of the flow rate.

Now, by defining $u = \begin{bmatrix} q_p & q_c & v_d \end{bmatrix}^T$ and disregarding the disturbances q_f, q_{bpp}, this is in the form of an affine system:

$$\dot{x} = Ax + Bu + a_p \tag{19}$$

To get it in the more standard linear form, we follow the approach from [16] and redefine the input vector to be $w = [u, a_p]^T$, thus making the new system:

$$\dot{x} = Ax + B_w w \tag{20}$$

where $B_w = [B, I]$. Using this system, we can calculate the Hankel singular values and determine the reduced order systems. For this work, a measurement equation $y = Cx$ was used, where C picks out only the lowermost pressure in the annulus, assuming that this is the most important pressure to estimate. This makes the system have a single output and thus easier to analyze.

By looking at the Hankel singular values, shown in Figure 13, we can see that it makes sense to truncate to 5 states for a certain amount of accuracy. Moreover, 40 states would yield a high degree of accuracy.

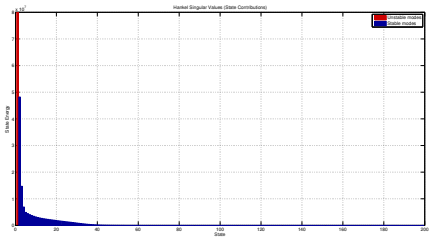

Figure 13. Hankel singular values of the system

Several simulations has been done for this part. Here only the most important one is presented. Simulation results for the different models can be seen in Figure 14. In this simulation, the frequency of the drill string oscillation is $v_d(t) = -30sin(30t)$. It is clear that the 40th order model is a considerably better approximation as compared to the 5th order model.

At the end, we want to compare simplification of the drilling model using two methods: balanced truncation method and decreasing the number of control volumes in discretizing the nonlinear PDE model. Two experiments are done in this respect. First a two control volume approximation, which is a 7th order differential equation, is compared to a 7th order model obtained by truncated model order reduction from a 50 control volume model. The outcome is illustrated in Figure 15.

Next, a 10 control volume model, which is a 39th order model, is compared to a 39th order model obtained using model reduction by balanced

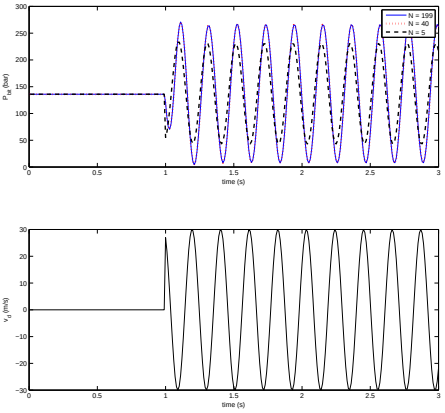

Figure 14. Oscillating drill string.

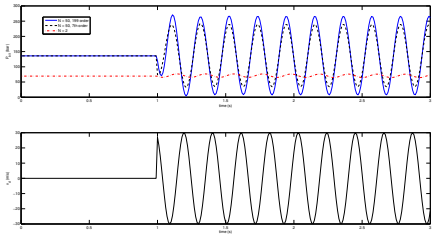

Figure 15. Comparison of control volume method and model reduction by balanced truncation, 7th order models.

truncation method on a 50 control volume model. The result is shown in Figure 16. The amplitude and frequency of the drill-string in this experiment is the same as before.

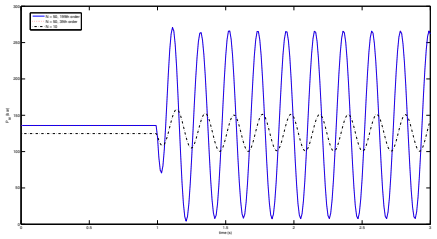

Figure 16. Comparison of control volume method and model reduction by balanced truncation, 39th order models.

As it is clear in both experiments the model reduction method by balanced truncation for simplifying the model works much better that simplification by reducing the number of control volumes.

IV. Conclusions

In this paper, first a dynamical model that describes the distribution of flow and pressure in a drilling fluid is derived. Next, it has been shown that a friction model based on standard, Newtonian friction factor correlations gives a simple and accurate way of describing the pressure losses during flow, with the viscosity of the fluid as a tuning parameter. This is also suitable for a simulator program, as opposed to the non-Newtonian correlations. Still, care must be taken for zero flow, and in this case, the yield stress of the non-Newtonian drilling fluid has to be modeled. This is done by integrating the applied external forces over time until the yield boundary is achieved.

Next, three different drilling scenarios are modeled and simulated. The results are compared to actual responses from UllRigg drilling experiments. The new fluid circulation problem is solved by adding an extra control volume, the vertical motion is described as a piston motion and the rotation of the drill string is modeled using semi-empirical relationships between rotation rate and pressure drop. The complexity of the model versus the accuracy is inspected in different scenarios, and it is shown that for the case of heave motion, a low order model is not sufficient. However, for all other scenarios, a low order model is sufficiently accurate after some tuning.

Finally, simplification of the model is done through reducing the number of control volumes and a balanced model reduction technique and it is shown that the latter could be considered as an alternative for reducing the complexity of the model for control system design purposes.

References

[1] G.-O. Kaasa, "A simple dynamic model of drilling for control," Statoil Research Centre Porsgrunn, Tech. Rep., 2007.

[2] B. Rehm, J. Schubert, A. Haghshenas, A. S. Paknejad, and J. Hughes, *Managed Pressure Drilling*. Gulf Publishing Company, 2008.

[3] J. E. Gravdal, R. J. Lorentzen, K. K. Fjelde, and E. H. Vefring, "Tuning of computer model parameters in managed-pressure drilling applications using an unscented-kalman-filter technique," *SPE Journal*, vol. 15, no. 3, pp. 856–866, 2010.

[4] Ø. N. Stamnes, J. Zhou, G.-O. Kaasa, and O. M. Aamo, "Adaptive observer design for the bottomhole pressure of a managed pressure drilling system," in *IEEE Conference on Decision and Control*, 2008, pp. 2961–2966.

[5] J. Zhou, . Stamnes, O. Aamo, and G.-O. Kaasa, "Adaptive output feedback control of a managed pressure drilling system," in *2008 47th IEEE Conference on Decision and Control*, Piscataway, NJ, USA, 2008, pp. 3008–3013.

[6] J. Zhou, Ø. N. Stamnes, O. M. Aamo, and G.-O. Kaasa, "Pressure regulation with kick attenuation in a managed pressure drilling system," in *IEEE Conference on Decision and Control*, Shanghai, 2009, pp. 5586–5591.

[7] G. Nygaard, L. Imsland, and E. A. Johannessen, "Using nmpc based on a low-order model for control pressure druing oil well drilling," in *8th International Symposium on Dynamics and Control of Process Systems*, vol. 8, no. 1. IFAC, 2007.

[8] O. G. H. Nygaard, "Multivariable process control in high temperature and high pressure environment using non-intrusive multi sensor data fusion," Ph.D. dissertation, Norwegian University of Science and Technology (NTNU), 2006.

[9] B. Fossli and S. Sangesland, "Managed pressure drilling for subsea applications; well control challenges in deep waters," in *SPE/IADC Underbalanced Technology Conference and Exhibition, number SPE 91633*, 2004.

[10] J. Zhou, Ø. N. Stamnes, O. M. Aamo, and G.-O. Kaasa, "Switched control for pressure regulation and kick attenuation in a managed pressure drilling system," *IEEE Transactions on Control Systems Technology*, vol. 19, no. 2, pp. 337–350, 2011.

[11] O. Egeland and J. T. Gravdahl, *Modeling and Simulation for Automatic Control*. Marine Cybernetics, 2002.

[12] W. Kozicki, C. H. Chou, and C. Tiu, "Non-newtonian flow in ducts of arbitrary cross-sectional shape," *Chemical Engineering Science*, vol. 21, no. 8, pp. 665–679, 1966.

[13] S. Imao, M. Itoh, Y. Yamada, and Q. Zhang, "The characteristics of spiral waves in an axially rotating pipe," *Experiments in Fluids*, vol. 12, no. 4-5, pp. 277–285, 1992.

[14] R. Ahmed, M. Enfis, H. Miftah-El-Kheir, M. Laget, and A. Saasen, "The effect of drillstring rotation on equivalent circulation density: Modeling and analysis of field measurements," *SPE Annual Technical Conference and Exhibition*, vol. 135587-MS, 2010.

[15] G. Dullerud and F. Paganini, *A Course in Robust Control Theory, A Convex Approach*. Springer, 1999.

[16] H. R. Shaker and R. Wisniewski, "On exact/approximate reduction of dynamical systems living on piecewise linear partition," *IMACS IFAC Symposium on Mathematical Modelling - 6th MATHMOD*, 2009.

Control of Heave-Induced Pressure Fluctuations in Managed Pressure Drilling

Ingar Skyberg Landet, Alexey Pavlov, Ole Morten Aamo*

***Abstract*—Managed pressure drilling is a sophisticated pressure control method which is intended to meet increasingly high demands in drilling operations in the oil and gas industry. With this method, the well is pressurized and the drilling mud is released through a control choke which can be used to actively control/reject pressure variations. Such a control system needs to handle several disturbances, and in particular vertical motion of the drill string causes severe pressure variations that need to be compensated by active use of the control choke. In this paper we present and apply two different disturbance rejection strategies based on discretized partial differential equations for the well hydraulic system. The performance of both controllers are shown through simulations both under idealized conditions as well as by simulations on a high fidelity drilling simulator.**

I. Introduction

In drilling operations performed in the oil and gas industry, one of the most important challenges is to control the pressure in the drilling fluid, often called drilling mud. This drilling fluid is pumped at high pressure into the drill string at the top of the well, flows through the drill bit in the bottom hole of the well, and continues up the well annulus carrying cuttings out to the surface (See Figure 1 taken from [1]). At the surface, the mud is cleaned for cuttings and reinjected through the main pump. In addition to transporting cuttings, the mud is needed to keep the pressure in the annulus at a desired level. This pressure control is crucial in all drilling operations, as the pressure has to be between certain boundaries. Specifically, it has to be above the pore pressure to prevent unwanted inflow from the surrounding formations into the well. Also, it has to be below the strength of the rocks of the surrounding formations to prevent the well from fracturing. Another issue is the possibility of the well to collapse on itself if the pressure becomes too low. All of these issues could result in costly and time consuming repair, loss of mud, a lost well and drill or even great environmental damage from oil spills or blow outs. Conventionally, pressure control is done by circulating in new mud with different density whenever the pressure needs to be changed, i.e. when the drilling reaches into an area with different pore or fracture pressures, as specified by geophysical data. For example, if the required down hole pressure should increase, one could change to drilling with a heavier mud, since the pressure is mainly a function of the mud density (hydrostatic pressure) and the pressure loss due to friction. However, a new method for pressure control that has received some attention is called Managed Pressure Drilling (MPD). With this method, the well annulus is sealed off and a control choke is installed to release the mud at the top of the well. By manipulating the choke opening, it is possible to significantly influence the annulus pressure profile. To further increase the controllability of the annulus pressure in case of a shut down of the main pump, a back pressure pump is installed at the control choke. (See again Figure 1). This type of active pressure control allows for the drilling of wells that would not have been possible using the conventional pressure control methods.

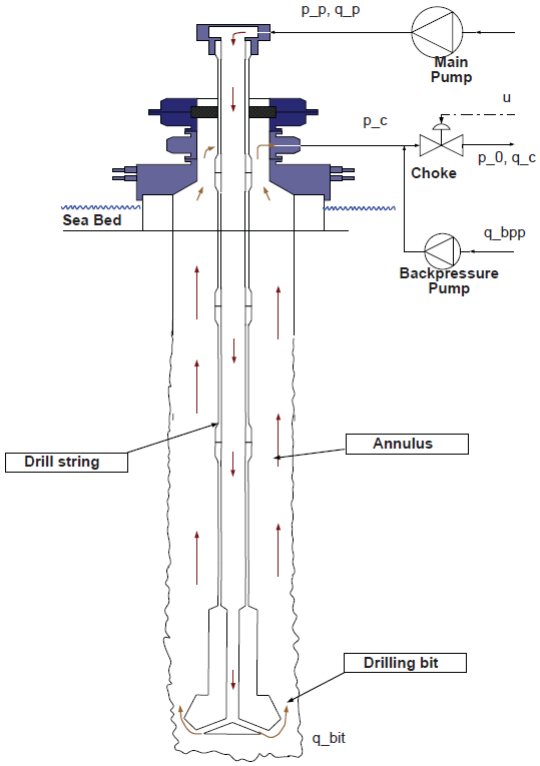

Figure 1. Well and hardware configuration in managed pressure drilling system.

When designing such a manged pressure drilling control system, there are several disturbances affecting the pressure that need to be accounted for. Specifically, we will focus on the pressure fluctuations due to the vertical motion of the drill string in the well annulus. This could arise from several different operational procedures, but in particular, this is an

Ingar Skyberg Landet is a graduate student at the Institute for Engineering Cybernetics at the Norwegian University of Science and Technology (NTNU). Email: ingarsky@stud.ntnu.no.

Alexey Pavlov is a principal researcher at the intelligent drilling group at Statoil ASA R&D. Email: alepav@statoil.com.

Ole Morten Aamo is a professor at the Institute for Engineering Cybernetics at NTNU. Email: aamo@ntnu.no.

issue when drilling from a floating rig. In this case, waves will affect the entire rig causing it to move vertically, so called heave motion. For most of the time spent drilling, this motion will not have a large effect on the pressure in the well, because of other heave compensation techniques decoupling the drill string from the heave motion. However, from time to time it is necessary to extend the drill string by a drill string connection, and in this case the drill string is rigidly connected to the floating vessel. This will in turn lead to the drill string acting like a piston down into the well, causing relatively large pressure fluctuations due to volume changes.

Results on MPD control systems design and implementation can be found in a number of papers, where such aspects as bottom hole pressure observer design [2], pressure control [3], [4], gas kick attenuation [5], [6] and implementation aspects [7], [8], [9] are considered. Still, there are not a lot of published results on the issue of heave generated pressure fluctuations.

An attempt at making an automatic control system for this scenario together with experimental results can be found in [1]. Here, a simple model of the well hydraulics developed in [10] was used for controller design. This worked well in simulations, but failed in full scale testing under realistic conditions. To the authors knowledge, there are no other published results on heave induced pressure fluctuation attenuation in MPD systems.

The hypothesis made now is that the heave induced pressure fluctuations can be compensated by designing an automatic control system based on a higher order model of the well hydraulics and using sophisticated nonlinear control techniques. The goal is to show the efficiency of the proposed controllers by using simulations and comparison to existing measurement data from earlier full scale tests presented in [1]. A sub goal is to add to the number of applications of the nonlinear output regulation theory, see e.g. [11], which in the last 15 years have undergone major theoretical developments.

This paper is organized in the following way: Section 2 presents the higher order model of the well hydraulic system with friction; sections 3 and 4 present two different control strategies, and; sections 5 and 6 present simulation results under ideal and non-ideal circumstances, respectively.

II. Hydraulic Well Model With Friction and Waves

A. Hydraulic Transmission Line

We will model the well annulus with the drilling mud as a hydraulic transmission line, and a common way of doing this is by the following partial differential equations (See e.g. [12], Chapter 11)

$$\frac{\partial p}{\partial t} = -\frac{\beta}{A}\frac{\partial q}{\partial x} \quad (1)$$

$$\frac{\partial q}{\partial t} = -\frac{A}{\rho}\frac{\partial p}{\partial x} - \frac{F}{\rho} + Agcos\left(\alpha\left(x\right)\right) \quad (2)$$

Here, p is pressure, q is volumetric flow rate, β is the compressibility or bulk modulus, A is the cross section area, ρ is the (constant) mass density, F is the friction force per unit length, x is the positive flow direction, g is the gravitational constant and $\alpha\left(x\right)$ is the angle between gravity and the positive flow direction. Considering the well system during the drill string connection, the main mud pump is turned off (see again Figure 1), the back pressure pump is turned on and the drill string travels with a speed v_d up and down the annulus region. Thus, we can disregard the flow in the drill string and continue by dividing the annulus region into an arbitrary number of control volumes. We discretize (1) and (2) using a finite volumes method to get a set of ordinary differential equations describing the dynamics of the pressures and flows at different positions in the well profile.

To incorporate the important pressure dynamics created by the drill string movement, there are two things to bear in mind: First, the volume of the annulus will continuously change by $v_d(t)A_d$, where A_d is the drill string cross section area, due to the top of the drill string moving in and out of the well. Second, one also has to consider the fact that the cross section of the drill bit will in general be larger than that of the rest of the drill string. This will cause the generated flow to be "squeezed" in over a smaller cross section, increasing the velocity and thus also the friction around the drilling bit. (See also Figure 2.) The final equations are then given by

$$\begin{aligned}
\dot{p_1} &= \frac{\beta_1}{A_1 l_1}\left(-q_1 - v_d A_d\right) \\
\dot{p_i} &= \frac{\beta_i}{A_i l_i}\left(q_{i-1} - q_i\right),\ i = 2, 3, .., N-1 \\
\dot{p_N} &= \frac{\beta_N}{A_N l_N}(q_{(N-1)} - q_c + q_{bpp}) \\
\dot{q_i} &= \frac{A_i}{l_i \rho_i}(p_i - p_{i+1}) - \frac{F_i\left(q_i\right) A_i}{\rho_i l_i} - A_i g \frac{\Delta h_i}{l_i}\ i = 1, 2, ..N-1
\end{aligned} \quad (3)$$

Here, the numbers $1...N$ refer to control volume number, with 1 being the lower most control volume representing the down hole pressure ($p_1 = p_{bit}$), and N being the upper most volume representing the choke pressure ($p_N = p_c$). The length of each control volume is denoted l, and the height difference is Δh. To our disposal for control are the back pressure pump flow q_{bpp} and the choke flow q_c. The choke flow is modeled by an orifice equation

$$q_c = K_c\sqrt{p_c - p_0}\, g\left(u\right) \quad (4)$$

Here, K_c is some constant regarding the area of the choke (and also the density of the drilling fluid, with reference to the general orifice equation), p_0 is the (atmospheric) down stream pressure and g is a strictly increasing and invertible function relating the control signal to the actual choke opening, taking its values on the interval $[0, 1]$.

B. Friction Model

To model the friction force acting on each control volume, we propose to use standard, Newtonian friction factor correlations. This is due to the observations from measurement data from full scale tests that suggests the friction force in the annulus is a linear function of flow rate, at least for the modest flow rates that can be expected without externally forced flow. (Zero main mud pump flow.) This corresponds well to Newtonian

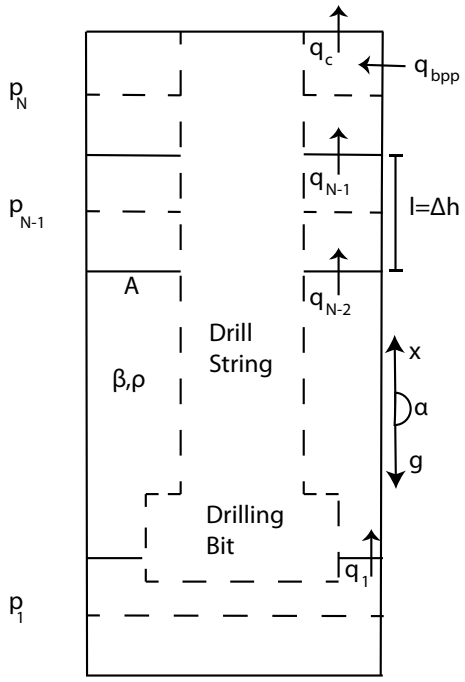

Figure 2. Control volumes of annulus hydraulic model.

friction factors for laminar flow. See Figure 3 for the measured steady state friction drops.

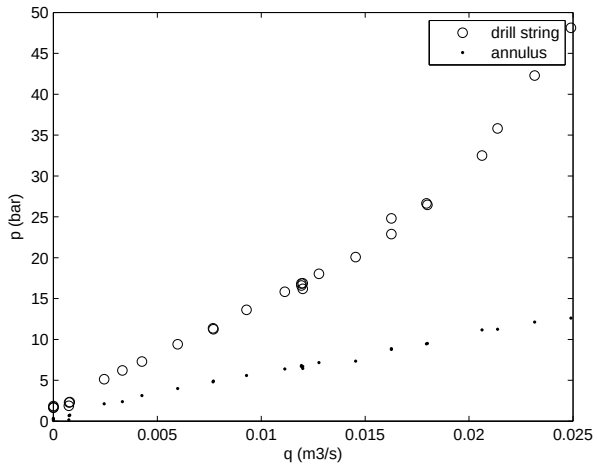

Figure 3. Friction losses from observed, full scale testing data

Taking the special geometry of the annulus region into account, it has been proposed [13] to use a modified Reynolds number to calculate the friction factor. However, to keep the detail level manageable, we will in this paper lump the entire friction model into a constant (or, more likely, slowly varying) friction coefficient k_{fric}, giving the resulting friction force on control volume i

$$F_i(q_i) = \frac{k_{fric} q_i}{A_i} \tag{5}$$

To see the validity of this model for the scenario of interest, consider Figure 4 and Figure 5. Here, we have compared the pressure as estimated by our model for different number of control volumes to measured pressures taken from full scale tests at Ullrigg located at International Research Institute of Stavanger (IRIS). Most of the parameters, like the bulk modulus, mass density and geometry was either available from specifications of the well or measurements taken during the tests, but the friction coefficients were identified from measurement data.

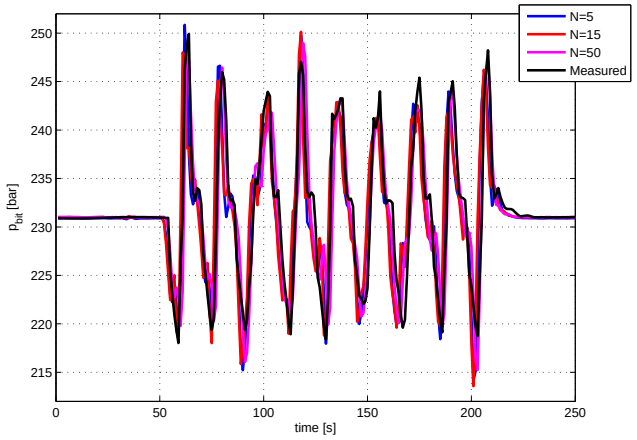

Figure 4. Simulation results compared to measured data, p_{bit}, different number of control volumes.

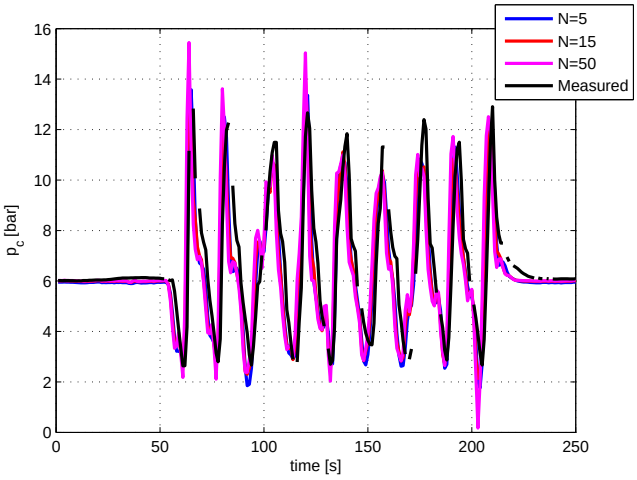

Figure 5. Simulation results compared to measured data, p_c, different number of control volumes.

As we can see, the main dynamics of the heave induced fluctuations are reproduced. There might be some large, instantaneous errors, but these are quickly corrected and are mostly due to timing issues. The error in the amplitude of the oscillations is never more than a couple of bar. Also, there seems to be little to be gained by increasing the number of control volumes beyond 5.

C. Wave Model

We will model the motion of the drill string as an oscillatory motion driven by the waves on the open sea. To this end, we

have consulted the JONSWAP spectrum, which is the result of a large measurement project designed to find the frequency spectrum of the waves in the north atlantic. It seems that the peak of this spectrum is at the frequency $\omega_{waves} = \frac{2\pi}{12}\ \frac{rad}{s}$, so we choose to consider the speed of the drill string v_d to be the output of the harmonic oscillator

$$\dot{w_1} = w_2 \quad (6)$$

$$\dot{w_2} = -\omega_{waves}^2 w_1 \quad (7)$$

$$v_d = w_2 \quad (8)$$

If we wish to be a bit more sophisticated in our wave model, it is quite simple to generate a signal v_d spanning more of the frequency range of the JONSWAP spectrum by adding several such harmonic oscillators with different frequencies and amplitudes according to the spectrum. (See for instance [14]).

D. Problem Statement

The main control problem in managed pressure drilling is to keep the pressure at some point in the annulus (usually the bottom hole pressure p_1) at a specified set-point. In this paper we are concerned with the problem of the pressure tracking ($p_1(t)$ following a reference $p_1^{ref}(t)$) in the situation when the main mud pump is turned off, the back pressure pump is turned on and the vertical position of the drill string follows a wave-like motion due to the heave motion of the drilling rig. This corresponds to the described scenario of a drill string connection on a floating rig. That is, we wish to develop control algorithms such that $\left|p_1^{ref}(t) - p_1(t)\right| \leq \epsilon$ as $t \to +\infty$ despite the drill string vertical motion. Ideally, $\epsilon = 0$, but we might also settle for some non-zero error.

III. Output Regulation Controller

When we consider the total system model (3) with linear friction, it is clear that the only nonlinearity is in the choke flow. Thus it should be simple to find a feedback linearizing control and then apply some linear control strategy to the linearized input-output map. However, we will try to utilize the nonlinear output regulation theory on the full, nonlinear system. For a thorough treatment of the nonlinear output regulation theory, see e.g. [11]. This theory considers a general nonlinear system on the form

$$\dot{x} = f(x, w, u) \quad (9)$$

$$e = h_r(x, w) \quad (10)$$

$$y = h_m(x, w) \quad (11)$$

Here, $x \in \mathbb{R}^n$ is the state vector, $u \in \mathbb{R}^k$ is the control input, $e \in \mathbb{R}^{l_r}$ is the regulated output and $y \in \mathbb{R}^{l_m}$ is the measured output. The external input $w \in \mathbb{R}^m$ is generated by a so called exosystem on the form

$$\dot{w} = Sw \quad (12)$$

This exosystem is written here as a linear system, but could in general be nonlinear as well. It could include any number of harmonic disturbances on the form (7) and also a large range of reference signals for the regulated output. Now, the theory tells us that a controller solving the output regulation problem will, for certain boundedness assumptions on w, both stabilize the system and make the regulated output $e(t)$ tend to zero. This controller can be written as

$$u = c(w) + K(x - \pi(w)) \quad (13)$$

Here K is an appropriate matrix which ensures quadratic stability of a certain matrix function on the system matrices, and $c(w), \pi(w)$ are the solutions to the so-called regulator equations

$$\dot{\pi} = f(\pi(w(t)), w(t), c(w(t))) \quad (14)$$

$$0 = h_r(\pi(w(t)), w(t)) \quad (15)$$

We can then define the regulated output to be $e = p_1^{ref} - p_1 = w_3 - p_1$ and postulate that the wave motion of the floating rig is the output from the harmonic oscillator (7). Then it is a simple (though large) task to solve the regulator equations by back substitution from (15) for any number of control volumes. Also, the disturbance model can be extended to include any number of harmonic oscillators. This will increase the complexity of the regulator equations, but they are still straight forward to solve. This controller will clearly solve the pressure tracking problem as we posed it in this paper, as $\left|p_{bit} - p_{bit}^{ref}\right| \to 0$ as $t \to +\infty$ under the boundedness assumption on $w(t)$.

IV. Internal Model Controller

The internal model principle is a popular linear control design tool for tracking or disturbance rejection, and for a basic introduction, see e.g. [15]. The idea is that if one can find the so-called disturbance generating polynomial and include it in a stable closed loop error feedback control system, the disturbance will vanish asymptotically. If we consider the same harmonic disturbance (7), one can readily find the disturbance generating polynomial as

$$\Gamma(s) = s^2 + \omega_{waves}^2 \quad (16)$$

A very simple way of creating an asymptotically rejecting controller is then

$$C(s) = Q_0 + \frac{Q_1}{s} + \frac{Q_2 s}{s^2 + \omega_{waves}^2} \quad (17)$$

which includes a PI controller in addition to the disturbance generating polynomial. Here, Q_i are appropriate constants and could for instance be tuned by classical frequency domain methods. Again, this is easily extended to any number of frequencies. Of course, this is mostly seen in the scope of linear systems, and it is definitely a possibility to use a feedback linearizing approach together with this internal model. However, stability has also been proven for a controller on the form (17) for passive nonlinear systems [16], and we will take advantage of this to design a very simple and low maintenance yet effective controller. Notice however that the nonlinearity in the system might induce other harmonics that we do not in general compensate with the proposed controller, thus it is difficult to guarantee asymptotic rejection.

To implement this controller, we need to consider how we should influence the system. The paper [16] proves the passivity of the controller (17) and the closed loop stability of the error feedback system with this controller and a passive nonlinear system. The hydraulic transmission line is quite clearly dissipative due to the friction force, but to ensure passivity from the output of the controller, named v, to the bottom hole pressure, p_1, we must be careful with the polarity of the input to the choke opening. Let us suggest the following

$$u = g^{-1}(-v) \tag{18}$$

The polarity $-v$ must be enforced to ensure that the transmission line is passive with input v and output p_1[1]. Thus we actually have a controller that is totally independent on the system parameters, and the only information needed is the frequency of the wave disturbance. Of course, the guarantees on rejection are weaker than for the output regulation controller, but this might be offset by the low demand for information about the system.

V. Simulation Results Under Perfect Conditions

To show the effectiveness of the proposed controllers, we will show simulation results for the two controllers with the described disturbance (7) assuming perfect information. That is, we can measure both the full state of the model (3) and both states of the oscillator (7). The output regulation controller was developed for a model with 5 control volumes due to the large job of solving the regulator equations, but in general, there is no limit to the number of control volumes one can solve them for. Simulation results can be seen in Figure 6 and Figure 7. In this scenario, the well model is also made up of 5 control volumes due to the assumption of perfect information. The harmonic disturbance is such that $x_d = cos\left(\frac{2\pi}{12}t\right)$, where $\frac{2\pi}{12}$ corresponds closely to the most dominant wave frequency in the North Atlantic, with reference to the JONSWAP spectrum.

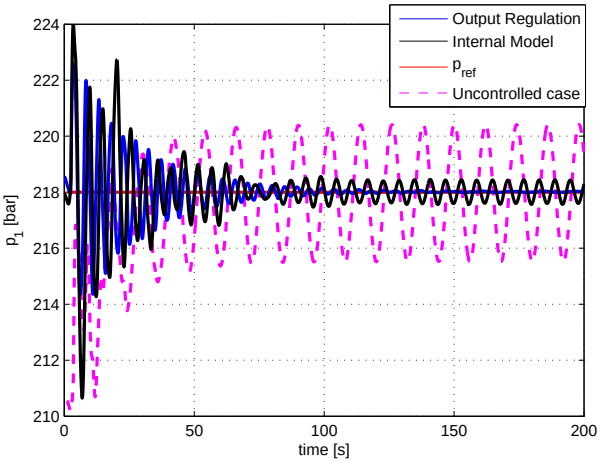

Figure 6. Simulated performance of the proposed controllers under perfect information.

[1]The proof of this is omitted for space requirements. It can be shown by the use of a positive real transfer function with $-q_c$ as input and p_1 as output, and then showing passivity from v to p_1 by using the memoryless mapping from v to $-q_c$ and assuming $p_c > p_0$.

Parameter	Value
$\beta_1 = \frac{\beta}{Al}$	$1.91 * 10^8 \frac{Pa}{m^3}$
$\beta_2 = \frac{A}{l\rho}$	$5.1477 * 10^{-8} \frac{m^4}{kg}$
$\beta_4 = \rho g \Delta h$	$6.1569 * 10^6 Pa$
k_{fric}	$9.1030 * 10^6 \frac{sPa}{m^3}$

Table I
Parameters identified from the IRISDrill simulator.

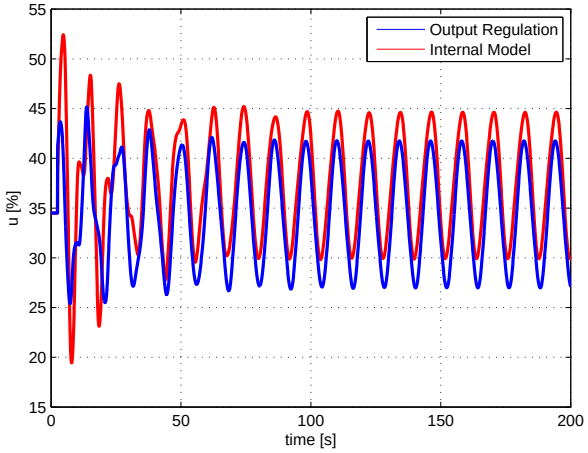

Figure 7. Applied control signal to choke, simulations with perfect information.

We can see that the output regulation controller achieves the promised asymptotic rejection under these circumstances, and that the internal model controller is stable and confines the pressure fluctuations to a quite narrow band around the pressure set point. This is also compared to the uncontrolled case, where one would simply keep the choke at the opening required to reach the pressure set point without waves.

VI. Simulation Results Under Non-Ideal Conditions

To assess the performance of the proposed controllers under more realistic and non-ideal conditions, we will present simulation results using a high fidelity drilling simulator program named "IRISDrill for MATLAB", developed by IRIS. The same controllers as in the last section were used, but this time the output regulation controller had to rely on an observer for the unmeasured states of the hydraulic model and the wave disturbance. The necessary parameters had to be identified through initial tests with the simulator program, and their values can be found in Table I. One of the main limitations in using a lower order model for controller design, is that it is not as fast as the real system during some of the pressure dynamics. This was compensated by increasing the bulk modulus to a larger value than what is likely the case, however, this can also change other aspects of the dynamics in unwanted ways, so the low order model is still not quite as fast as the IRISDrill simulator. The simulator was run with the same disturbance as in the last section, and simulation results can be seen in Figure 8 and 9.

We can see that both controllers give a certain amount of attenuation of the pressure oscillations. The output regulation

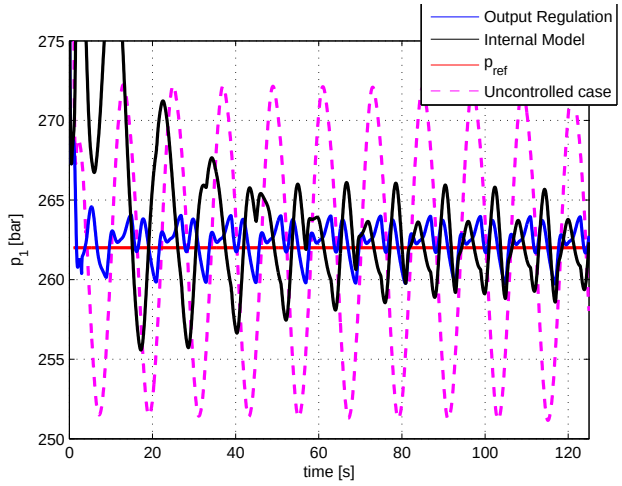

Figure 8. Simulated performance of the two controllers on the IRISDrill simulator.

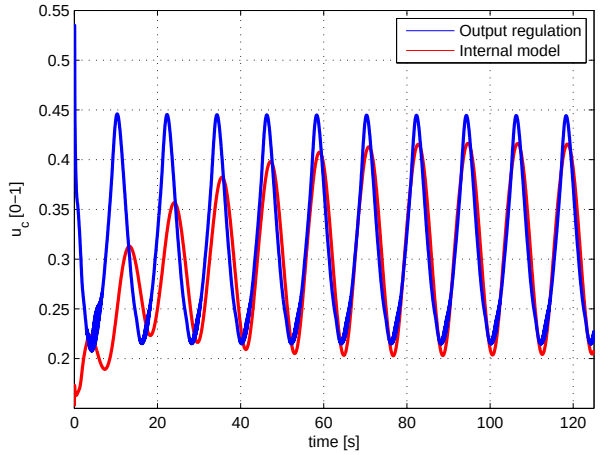

Figure 9. Applied control signal to choke, IRISDrill simulations.

has a much shorter transient period, and the resulting pressure oscillations are also confined to $\pm 2\ bar$, while the internal model controller, in the steady state, confines the oscillations to $\pm 4\ bar$. This is the result of the trade-off between system knowledge and ease of implementation.

VII. Acknowledgments

The authors wish to thank Statoil ASA for providing the test data from previous heave compensation tests. Also, we wish to thank Gerhard Nygaard and Lars Næsheim at the International Research Institute of Stavanger for the access and guidance to the IRISDrill for MATLAB simulator.

References

[1] A. Pavlov, G.-O. Kaasa, and L. Imsland, "Experimental disturbance rejection on a full-scale drilling rig," in *Proceedings of IFAC Nonlinear Control Systems Symposium 2009*, 2009.

[2] O. Stamnes, J. Zhou, G.-O. Kaasa, and O. Aamo, "Adaptive observer design for the bottomhole pressure of a managed pressure drilling system," in *Decision and Control, 2008. CDC 2008. 47th IEEE Conference on*, dec. 2008, pp. 2961 –2966.

[3] J. Zhou, O. Stamnes, O. Aamo, and G.-O. Kaasa, "Observer-based control of a managed pressure drilling system," in *Control and Decision Conference, 2008. CCDC 2008. Chinese*, july 2008, pp. 3475 –3480.

[4] ——, "Adaptive output feedback control of a managed pressure drilling system," in *Decision and Control, 2008. CDC 2008. 47th IEEE Conference on*, dec. 2008, pp. 3008 –3013.

[5] J. Zhou, G. Nygaard, J. Godhavn, O. Breyholtz, and E. Vefring, "Adaptive observer for kick detection and switched control for bottomhole pressure regulation and kick attenuation during managed pressure drilling," in *American Control Conference (ACC), 2010*, 30 2010-july 2 2010, pp. 3765 –3770.

[6] J. Zhou, O. Stamnes, O. Aamo, and G.-O. Kaasa, "Switched control for pressure regulation and kick attenuation in a managed pressure drilling system," *Control Systems Technology, IEEE Transactions on*, vol. 19, no. 2, pp. 337 –350, march 2011.

[7] J.-M. Godhavn, "Control requirements for high-end automatic mpd operations," in *SPE Drilling Conference and Exhibition*, 2009.

[8] O. Breyholtz, G. Nygaard, J.-M. Godhavn, and E. Vefring, "Evaluating control designs for co-ordinating pump rates and choke valve during managed pressure drilling operations," in *Control Applications, (CCA) Intelligent Control, (ISIC), 2009 IEEE*, july 2009, pp. 731 –738.

[9] E. van Riet, D. Reitsma, and B. Vandecraen, "Development and testing of a fully automated system to accurately control downhole pressure during drilling operations," in *SPE Middle East Drilling Technology Conference and Exhibition*, 2003.

[10] G.-O. Kaasa, O. Stamnes, L. Imsland, and O. Aamo, "Intelligent estimation of downhole pressure using a simple hydraulic model,," in *IADC/SPE Managed Pressure Drilling and Underbalanced Operations Conference and Exhibition*, 2011.

[11] A. Pavlov, N. van de Wouw, and H. Nijmeijer, *Uniform Output Regulation of Nonlinear Systems*. Birkhauser Boston, 2006.

[12] O. Egeland and J. T. Gravdahl, *Modeling and Simulation for Automatic Control*. Marine Cybernetics, 2002.

[13] W. Kozicki, C. H. Chou, and C. Tiu, "Non-newtonian flow in ducts of arbitrary cross-sectional shape," *Chemical Engineering Science*, vol. 21, no. 8, pp. 665 – 679, 1966.

[14] T. I. Fossen, *Marine Craft Hydrodynamics and Motion Control*. John Wiley I& Sons Ltd., 2011.

[15] G. Goodwin, S. Graebe, and M. Salgado, *Control System Design*. Prentice Hall, 2000.

[16] J. Kasac, B. Novakovic, and V. Milic, "On equivalence between internal and external model-based repetitive learning controllers for nonlinear passive systems," *Asian Journal of Control*, vol. 13, no. 1, pp. 15–24, 2011.

Appendix C

MATLAB Code

This appendix includes the implementation of the output regulation controller, since this is the most extensive. All the other controllers are very straight forward to implement. All other MATLAB code is included on the accompanying CD.

```
function [z_c,q_bpp] = outputRegulationHO(x_d,v_d,p_ref,pc,y,param,q_bpp,pb)
%Implements the output regulation controller for a 5-volum version of the
%hydraulic model.
%Written by Ingar Landet, 2011

% Read parameters for controller
beta = param.beta;
A = param.A;
l = param.l;
k_c = param.k_c;
p0 = 1.0131*10^5;
do = param.do;
d_a = param.d_a;
rho = param.rho;
g = param.g;
dh = param.dh/4;
omega = param.omega;
mju = 0.5;
a_an = 0.49;
b_an = 0.99;
p2a = 5.0909e+04;
k1 = 1.3;
k2 = 0.3;
Ao = pi*do^2/4;
beta1 = beta/(l*A);
beta2 = A/(l*rho);
beta4 = rho*g*dh;
kf1 = (1/4.5)*p2a;
kf2 = 32*mju*(a_an+b_an)*l/(A*(d_a^2-do^2));

%Initialize controller variables
p = [0;0;0;0;0;0;0;0;0];
x = [pc;y(9);y(4);y(8);y(3);y(7);y(2);y(6);pb];

% Solve the regulator equations
p(9) = p_ref;
p(8) =  -k1*v_d*Ao;
p8D = k1*omega^2*x_d*Ao;
p(7) = p(9) - p8D/(beta2*k2) - kf1 - kf2*p(8)/k2 - beta4;
p82D = k1*omega^2*v_d*Ao;
p7D = -p82D/(beta2*k2) -kf2*p8D/(k2);
p(6) = p(8) - p7D/beta1;
p83D = -k1*omega^4*x_d*Ao;
p72D = -p83D/(beta2*k2) - kf2*p82D/k2;
```

```
p6D = p8D - p72D/beta1;
p(5) = p(7) - p6D/beta2 - kf1 - kf2*p(6) - beta4;
p84D = -k1*omega^4*v_d*Ao;
p73D = -p84D/(beta2*k2) - kf2*p83D/k2;
p62D = p82D - p73D/beta1;
p5D = p7D - p62D/beta2 - kf2*p6D;
p(4) = p(6) - p5D/beta1;
p85D = k1*omega^6*x_d*Ao;
p74D = -p85D/(beta2*k2) -kf2*p84D/k2;
p63D = p83D - p74D/beta1;
p52D = p72D - p63D/beta2 - kf2*p62D;
p4D = p6D - p52D/beta1;
p(3) = p(5) - p4D/beta2 - kf1 -kf2*p(4) - beta4;
p86D = k1*omega^6*v_d*Ao;
p75D = -p86D/(beta2*k2) -kf2*p85D/k2;
p64D = p84D - p75D/beta1;
p53D = p73D - p64D/beta2 - kf2*p63D;
p42D = p62D - p53D/beta1;
p3D = p5D - p42D/beta2 -kf2*p4D;
p(2) = p(4) - p3D/beta1;
p87D = -k1*omega^8*x_d*Ao;
p76D = -p87D/(beta2*k2) -kf2*p86D/k2;
p65D = p85D - p76D/beta1;
p54D = p74D - p65D/beta2 - kf2*p64D;
p43D = p63D - p54D/beta1;
p32D = p52D - p43D/beta2 -kf2*p42D;
p2D = p4D - p32D/beta1;
p(1) = p(3) - p2D/beta2 - kf1 -kf2*p(2) - beta4;
p88D = -k1*omega^8*v_d*Ao;
p77D = -p88D/(beta2*k2) -kf2*p87D/k2;
p66D = p86D - p77D/beta1;
p55D = p75D - p66D/beta2 - kf2*p65D;
p44D = p64D - p55D/beta1;
p33D = p53D - p44D/beta2 -kf2*p43D;
p22D = p42D - p33D/beta1;
p1D = p3D - p22D/beta2 - kf2*p2D;


% Calculate the control signal
if p(1) <= p0
    u = 10^-4;
else
    c = (p(2) + q_bpp - p1D/beta1)/(k_c*sqrt(1400/rho)*sqrt((p(1)-p0)*10^-5)
      *0.001/60);
    K = 10^-1*[10^-6 0 0 0 0 0 0 0 10^-6];
    u = c + K*(x-p);
end


% Choke characteristics
Z_c = (1/100)*[0 4 9 10 15 20 30 40 50 70]';
G_c = 1/700*[0 1 35 45 80 125 200 300 400 700]';
g_cInv=@(g) interp1( G_c, Z_c, max(0, min(g, 1)) );

z_c = g_cInv(u);

end
```